Institutional Adaptations to Climate Change Project:

Future Climate Change Scenarios for the South Saskatchewan River Basin

Suzan Lapp, Dave Sauchyn and Elaine Wheaton

November 2008

Abstract

This report describes scenarios of climate change constructed to assess vulnerability of communities to future conditions in the South Saskatchewan River Basin (SSRB). Five Global Climate Models (GCMs) that best captured the full range of uncertainty are used to construct future climate scenarios of temperature and precipitation (e.g. warmest-wettest, warmest-driest, coolest-wettest, and coolest-driest) over the SSRB. Using the stochastic weather generator, LARS-WG, scenarios were downscaled for Lethbridge, Alberta and Swift Current, Saskatchewan and results were compared to future scenarios derived using the coarse resolution grid-box GCMs solely. The results between the GCM and LARS-WG scenarios were comparable; both showing increases in monthly temperatures, increases in winter precipitation, and typically decreasing summer precipitation but with amplified variability compared to the winter season. Drought scenarios based on the climate moisture index (CMI) of precipitation – potential evapotranspiration (P-PET) were also derived annually and for the May-July (MJJ) season.

Table of Contents

List of Tables

List of Figures

Introduction

A key component of the conceptual framework, and associated research methodology, of the Institutional Adaptations to Climate Change (IACC) project is the assessment of future vulnerability to climate change. The river basins, the Elqui in Chile and South Saskatchewan in Canada, are arid and semi-arid, respectively. Dry environments have the most variable hydroclimate. In the southern part of Canada, the highest year to year variation in precipitation is in the prairies. The only region with a coefficient of variation (standard deviation / mean) above 25% nearly coincides with the South Saskatchewan River basin (SSRB) (Schoney et al. 1990).

Achieving the project objective "To examine the effects of climate change risks on the identified vulnerabilities" requires that we develop future scenarios for climate risks identified by the studied communities. In the SSRB, the climate risks most often identified in the studied communities of Hanna, Taber, Outlook, Cabri, Stewart Valley and Blood Indian Reserve were drought, extreme weather events such as intense thunderstorms and associated hail and flash floods, and low river flows affecting potable water (Young and Wandel 2007; Pittman 2008; Prado 2008; Matlock 2007; and Magzul 2007). The vulnerability of these rural communities to climate change will depend on the extent to which these regional climate risks are affected by global warming.

Objectives

This report presents both climate change scenarios and future climate scenarios of temperature, precipitation and climate moisture indices of the SSRB and communities studied. Results are presented on an annual basis for three future time periods (2020s, 2050s, and 2080s) and also on a seasonal basis for the 2050s using output from runs of GCMs forced with anthropogenic greenhouse gases to simulate global warming. A further analysis was conducted using the LAWS-WG downscaling method to compare the results at the five stations between the climate scenarios developed directly from GCM output and those downscaled, with the hypothesis being that downscaling will provide little improvement to narrow down the range of uncertainty. Also, initial results are presented that compare the historical climate variability of P-PET and scenarios of future climate variability using CGCM3.1/T63 model for three SRES emission scenarios. This report goes beyond other climate change reports for the Canadian Prairie region by comparing future scenarios derived using direct GCM output and developing 30-year average changes but also to develop scenarios using a downscaling technique and compare the results. To date

the future scenarios for this region have not attempted to incorporate any climate variability within the future 30 year time periods or even for the 2000-2100 period.

Climate Change Scenarios

A climate change scenario is a plausible representation of a future climate that is constructed from consistent assumptions about future emission of greenhouse gases (GHGs) and other pollutants, for explicit use in investigating the potential impacts of anthropogenic climate change (IPCC 2001a). Scenarios are not forecasts of future climate but rather are intended to provide adequate quantitative measures of uncertainty that are represented with a range of plausible future paths (IPCC 2001a). Future greenhouse gas concentrations are an unknown because we cannot predict what activities humans will engage in that will reduce or increase them

Three main types of climate scenarios provide input to hydrological, agricultural, socio-economic, and biophysical models for impact and sensitivity studies: (1) synthetic; (2) analogue (temporal and spatial) and, (3) derived from Global Climate Models (GCMs). Synthetic and analogue scenarios capture a wide range of possible future climates and are useful for identifying thresholds or discontinuities of response beyond which effects are no longer beneficial or are detrimental (Parry and Carter 1998; Barrow et al. 2004). Synthetic scenarios apply an arbitrary change to a particular variable of an observed time series, for example, adding 2^{o}C to the monthly average temperature. However, this new time series maintains the variability of the original time series. Analogue scenarios represent potential future climate by using the observed climate regime at a previous (typically warmer) period or spatial location as an anticipated future climate. Temporal analogues are derived from either instrumental or paleoclimatic records. As these scenarios represent real historical climate states, they are physically possible and can be constructed for various climate variables. One weakness with spatial analogues is often the lack of correspondence between climatic and non-climatic features between regions; therefore, these scenarios may not represent physically plausible scenarios for conditions in the study region. Also, most drivers of the analogue climates are likely natural variations rather than a response to greenhouse gas (GHG)-induced warming.

Global Climate Models (GCMs)

Global climate models “are the only credible tools currently available for simulating the response of the global climate system to increasing greenhouse gas concentrations" (IPCC-TGCIA 2007); therefore, they

will be used in this study for the construction of future climate scenarios. GCMs are fully coupled mathematical representations of the complex physical laws and interactions between ocean/atmosphere/sea-ice/land-surface (Smith and Hulme 1998). They simulate the behaviour of the climate system on a variety of temporal and spatial scales using a three-dimensional grid over the globe. A high level of confidence can be placed in climate models based on the fact that they are (Randall et al., 2007): (1) fundamentally based on established physical laws, such as conservation of mass, energy and momentum, along with numerous observations; (2) able to simulate important aspects of the current climate; and, (3) able to reproduce features of past climates and climate changes. Climate models have accurately simulated ancient climates, such as the warm mid-Holocene of 6000 years ago and trends over the past century combining both human and natural factors that influence climate.

GCM experiments simulate future climate conditions based on estimated warming effects of carbon dioxide (CO_2) and other GHGs and the regional cooling effects of increasing sulphate aerosols, beginning in the late 19th century or early 20th century using scenarios of future radiative forcing. The Intergovernmental Panel on Climate Change Third Assessment Report (IPCC-TAR) (IPCC 2001b) published forty different emission scenarios provide a range of future possible GHG emissions and atmospheric concentrations from socio-economic scenarios labelled SRES (Special Report on Emission Scenarios) (Nakicenovic et al. 2000). The SRES describes 4 narrative storylines (i.e. A1, A2, B1 and B2) which represent different demographic, social, economic, technological, and environmental and policy future, as emission drivers. The SRES emissions scenarios are the quantitative interpretations of these qualitative storylines. Typically of interest are the pre-industrial control experiments, which run for long periods holding the forcing agents at fixed levels of the year 1850. They are used assess the GCMs ability to reproduce historical natural climate variability and also provide reference for the 20th Century and SRES experiments. The 20th Century experiment begins in the middle of the 19th century continuing to the end of the 21st century with the forcing agents representing the historical (or estimated) record. The future SRES A1b, A2 and B1 scenarios begin in the year 1990 of the respective 20th Century experiment run and extend until 2100. Some stabilization experiments extend until 2300 holding the concentrations fixed at the 2100 levels. The latest IPCC Fourth Assessment Report (AR4) (IPCC 2007) describes the latest vintage of GCMs and experiments currently available developed from advances in technology and a better understanding of the global climate system. Most GCM experiments also consist of multiple (or ensemble) simulations for each of these experiments representing different initial boundary conditions of the GCM at the beginning of the experiment. The combination of scenarios

based on ensemble simulations and scenarios reproducing multi-decadal natural climate variability from long GCM control simulations are being adopted for impact studies (Hulme et al. 1999).

Limitations of GCMs as Sources of Climate Change Scenarios

One of the limitations of GCMs for constructing climate change scenarios are the differences in climate sensitivity between models. Due to the parameterization and simplification of modeling processes and feedbacks, different GCM simulations may also respond quite differently to the same forcing (Barrow et al. 2004). Parameters derived by the parameterization and simplification process that must be used with caution directly as output from the GCM are precipitation, cloud formation, fog etc. Conversely, tropospheric quantities like temperature and geopotential height are intrinsic parameters of the GCM physics and are more skillfully represented by GCMs. Despite differences in numerical methods, parameterization schemes, and grid-box resolution, past and current models do a reasonable job of simulating the large-scale feature of the climate system (Schlesinger & Mitchell 1987; McFarlane et al. 1992). All of the recent GCM predictions project similar warming trends for 2090-2099 relative to 1980-1999 temperatures when averaged globally (IPCC et al. 2007b).While GCMs probably capture a large part of the uncertainty range in dealing with modeling responses, they certainly do not encapsulate the range of uncertainties in future emission scenarios. By choosing an array of GCMs and several future emission scenarios (SRES), a broad range of future climate scenarios (e.g. warmest-wettest, warmest-driest, coolest-wettest, and coolest-driest) can be generated to capture much of the uncertainty. Each scenario is as likely as another scenario, therefore greater certainty of a climate change scenarios is achieved when the majority of model output agree on similar climate.

While climate models are “the only credible tools” currently available for simulating future climate scenarios, there are limitations that apply in general to impact studies and specifically to our attempt to link future climate to current climate risks in the SSRB. The coarse spatial resolution (100s km) is a commonly cited drawback of GCM derived climate scenarios. This problem is particularly acute for a study like the IACC where the aim is to evaluate the vulnerability of individual rural communities by providing climate and water scenarios. Fortunately much of the SSRB, beyond the eastern slopes of the Rocky Mountains, has relatively low relief and homogenous land cover. Even so, we are applying single values of climate variables for GCM grid boxes (hundreds of kilometres) to small rural communities. Other methods have been developed to overcome this spatial resolution limitation through a technique called “downscaling” that further refines local and regional scale monthly or seasonal climate scenarios

from GCMs using relationships between observed large-scale atmospheric information and station-scale data. Downscaling provides information required for water resources management at scales much finer than the current resolution of any GCM for the interpretation of impacts related to climate change or climate variability (Venugopal et al. 1999).

Downscaling

The two common approaches to the downscaling of climate scenarios are dynamic and statistical. The confidence that may be placed in downscaled climate change information is foremost dependent on the validity of the large-scale fields from the GCM (IPCC 2001b).

Regional Climate Models (RCMs)

Dynamical downscaling involves the use of high-resolution (regional) climate models (RCMs) to obtain finer resolution climate information from large-scale GCMs (IPCC 2001a). RCMs are "nested" within a GCM that provides the initial and lateral boundary driving conditions. The RCM is run at a finer resolution than the large-scale climate models and thus incorporates better parameterization schemes and a direct representation of some small-scale processes such as topographical features and land cover inhomogeneity (IPCC 2001b). RCMs are more computationally demanding than global-scale models (Hay and Clark, 2003); therefore, RCM data are typically available only for one run of a single model for limited time spans. The latest version of the CRCM.4.2.0 (Canadian Regional Climate Model) has output available for the CGCM3 SRES A2 and the time period of 2041-2070 with a 45-km horizontal grid-size (www.cccma.ec.gc.ca); previous versions of CRCMs provided data for a twenty-year window (2046-2065). As illustrated in Figure 2, on the other hand, there are numerous runs of various GCMs providing a range of future climates or scenarios.

Statistical Downscaling

Statistical downscaling methods are much more popular than dynamical downscaling techniques for deriving future climate scenarios; they are a cheap way of obtaining climate change data at higher temporal or spatial resolution than can be provided by the GCM. The statistical downscaling of GCM data is based on the statistical model linking the climate simulated by the GCM and the current climate characterized by instrumental data. This technique has been widely applied to derive daily and monthly precipitation at higher spatial resolution for impact assessments (Semenov and Barrow 1997; Wilby et al. 2002). SDSM (Statistical Downscaling Model) (Wilby et al. 2002) and LARS-WG (Weather Generator) (Semenov and Barrow, 2002) are two popular methods of statistical downscaling.

SDSM relies upon empirical relationships between large-scale predictors and local scale processes. The main strength of this technique is its simple application and computational straightforwardness; however a relationship must first exist and be developed at a particular locality between the predictor-predictand. One major weakness is that this technique assumes that the full range of variability is captured within the calibration period, but often-extreme events lie outside this range (Wilby 1994). The assumption that the predictor-predictand relationship will remain valid under future climate conditions is another weakness. Data stationarity during the calibration period is also required. When tested for this study precipitation failed this assumption, suggesting non-stationarity (Wilby 1997), making it difficult to design and calibrate this model for downscaling. It was concluded that this model was unable to accurately simulate the historical climate and therefore was felt unsuitable for deriving future climate simulations.

LARS-WG stochastic weather generator simulates high-resolution temporal (daily) and spatial (site) climate change scenarios for a number of climate variables (e.g., precipitation amount, maximum/minimum temperature, and solar radiation) which are all conditioned on whether the day is wet or dry. Scenarios incorporate changes in climatic variability such as duration of dry and wet spells or temperature variability derived from daily output from GCMs (Semenov 1997). Future climate scenarios are stochastically generated by adjusting the parameters in direction proportion to the changes projected by a GCM. Further details of the LARS-WG can be found in the user manual (Semenov and Barrow, 2002). The main advantage of weather generators is their ability to produce multiple climate scenarios of daily climate variables at local station, making them very useful for risk assessment studies.

Droughts are natural reoccurring phenomena that are highly variable in both time and space. Historically the Canadian Prairies have been highly susceptible to drought events, particularly those that occur during the growing season of May to August, when most of the precipitation is received (Bonsal & Wheaton 2005). Many drought-monitoring programs throughout the world strive to understand how climate change will impact the occurrence and duration of drought. These initiatives monitor the relationship between precipitation, temperature and potential evapotranspiration and the overall impact on soil moisture and surface water (Keyantash & Dracup 2002). Although a lack of precipitation is the main driver of severe meteorological drought conditions, anomalously high temperatures increase

evaporation often enhancing droughts, therefore, “It is critical that any assessment of future drought take into account changes to temperature, as well as, precipitation” (Bonsal & Regier 2007).

Climate Moisture Index (CMI)

The Climate Moisture Index (CMI), the difference between annual precipitation (P) and annual potential evapotranspiration (PET), is a fairly simple indicator of soil moisture (Willmott and Feddema 1992; Hogg 1997).

In 1996 the Ecological Stratification Working Group released “A National Ecological Framework Report for Canada” (Marshall & Schut 1999) presenting the ecological framework maps that divide the country into ecozones, ecoregions and ecodistricts. For each ecodistrict they calculated the CMI (P-PET) using the Thornthwaite Method and Penman methods. Hogg (Hogg 1994; Hogg 1997) was able to reproduce the present distribution of vegetation for the Prairie Provinces using the same CMI of P-PET for the 1951-1980 period using the Jenson-Haise, Priestley-Taylor and the simplified Penman-Monteith (SPM) methods for calculating PET. The Jenson-Haise and Priestley-Taylor methods are more complex equations that require monthly solar radiation and is rarely available. Sauchyn et al. (2002) derived future climate scenarios of CMI (P/PET) using the Thornthwaite method using three emission scenarios (cool-wet, warm-dry and median), since very few stations have recorded solar radiation and wind data. Their analysis projects a higher frequency of dry years over a larger area for the Canadian Prairies.

Tree Ring Analysis

Until recently an extensive network of moisture-sensitive tree-ring chronologies has been lacking for western Canada. In recent years, researchers at the University of Regina Tree-Ring Lab (www.parc.ca/urtreelab) have collected tree rings at 110 sites, extending from island forests of northeastern Montana through the forested regions of Alberta and Saskatchewan and across the southern Northwest Territories. At most of these sites, tree growth is limited by available soil moisture and therefore is a proxy of summer and annual precipitation, soil moisture and runoff (Beriault and Sauchyn 2006; Sauchyn *et al.*, 2003; Girardin and Sauchyn, 2008).

The trees with the greatest age and moisture sensitivity are concentrated in southwestern Alberta. Nine tree-ring records from this region have a strong common signal, such that when we apply principal

components analysis (PCA) the leading principal component (PC1) accounts for 73% of the total variance in the tree-ring data. The values of the leading PC (*i.e.* loadings of the individual tree-ring chronologies) highly correlate with July-June and May-July (MJJ) P-PET throughout southern Alberta and the SSRB (Figure 1). Therefore, these two seasons (July-June and MJJ) will be used for reconstructing CMI from tree rings and for producing future CMI climate change scenarios.

Further studies will use the tree-rings ability to capture moisture variability on a large spatial scale, test the ability of GCMs to simulate similar hydroclimate variability, and apply the results to future scenario development.

a.

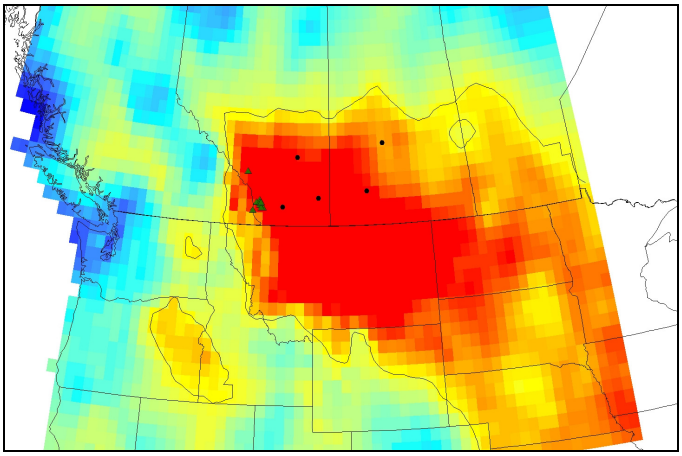

b.

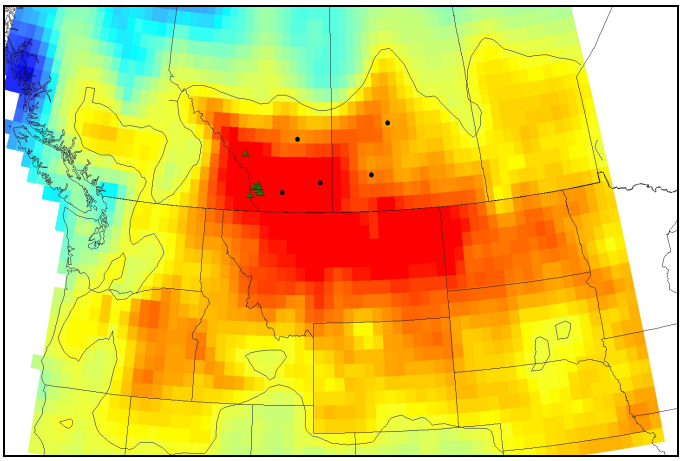

Figure 1. Spatial correlation between PC1 and CMI (1901-2000), the area outlined is significant at p=0.05. A) July-June season, B) May-July season.

Data and Methods

The Fourth Assessment Report (AR4) of the IPCC (2007) lists 24 climate models that were screened for daily maximum/minimum temperature and precipitation for both the 1961-90 historical and future 2040-69 period, and only seven met the criteria (Table 1). The SRES (Nakicenovic et al. 2000) experiments A1B, A2 and B1 were available for the AR4 models. Outputs from the HadCM3 TAR (Third Assessment Report) also were used because the AR4 did not provide the required variables for this model, the A2 and B2 experiments were available for various runs of the HadCM3 TAR model, and this GCM has been used for previous climate change research in western Canada (Bonsal and Prowse 2006; Bonsal, et al. 2003; Toyra et al. 2005; etc.). GCM output for the AR4 models (daily and monthly) was obtained from the World Climate Research Programme's (WCRP's) Coupled Model Intercomparison Project phase 3 (CMIP3) multi-model dataset (Program for Climate Model Diagnosis and Intercomparison 2008). Monthly and daily HadCM3 TAR output was available, respectively, from the IPCC Data Distribution Center (IPCC-DDC: http://www.ipcc-data.org/) and the Climate Impacts LINK Project (UK Met office, 2003: http://badc.nerc.ac.uk/browse/badc/link). The 20^{th} Century experiment (20CM) from each GCM provided the baseline period (1961-1990) output from the AR4 models and the SRES scenario experiments for the HadCM3 model.

Baseline observed historical gridded (0.5^{o}) climate data (monthly precipitation, maximum and minimum temperature), covering North America from 1901-2000, were recently generated, using a thin plate smoothing spline by ANUSPLINE, by the Canadian Forest Service (McKenney et al. 2006). There a number of observed historical data sets available (Climatic Research Unit (www.cru.uea.ac.uk/), CANGRID (www.cics.uvic.ca/climate/data.htm), NCEP/NCAR (www.cdc.noaa.gov/cdc/reanalysis/)). An analysis conducted by Meinert et al. (2008) between station data, CRU and the Canadian Forest Service gridded data sets found that the Canadian Forest Service data were more accurate. The CANGRID data set is available only for the 1961-1990 time period and the NCEP/NCAR for the 1947-current time period but on a 2.5^{o} spatial resolution which is much too large for analyzing the SSRB. The GCM output was interpolated to the historical data 0.5 degree grid, using the linear interpolation routine in Matlab 7.1, and mapped to illustrate future climate scenarios for the basin. This allows for direct comparison of both the baseline periods and the future scenarios with historical events.

Table 1. Information about each climate models chosen for this study; the country of origin, SRES simulations available, grid cell size and dimensions of the area from each model used in this analysis. Output available from the IPCC Fourth Assessment Report (2007) for all models except the HadCM3 from the Third Assessment Report (2001) at the IPCC Data Distribution Centre (http://www.ipcc-data.org/) and Program for Climate Model Diagnosis and Intercomparison (http://www-pcmdi.llnl.gov).

Climate Modeling Centre	Model	SRES Simulation	Grid Cell Size (degrees)	Dimensions
Canadian Centre for Climate Modelling and Analysis **Canada**	CGCM3 (T47)	A1B*, A2*, B1*	3.75^{o} x 3.75^{o}	238.125 – 256.875W 44.52 – 55.77N
	CGCM3 (T63)	A1B,A2,B1	2.81^{o} x 2.81^{o}	241.8725 – 258.7475W 46.04 – 57.29N
Met Office Hadley Centre **UK**	HadCM3	A2*, B2 (TAR)	3.75^{o} x 2.55^{o}	241.885 – 260.625W 46.25 – 56.25N
National Institute for Environmental Studies **Japan**	MIROC3.2-MEDRES	A1B*, A2*, B1*	2.8125^{o} x 2.8^{o}	240.468– 257.343 W 44.64 – 55.84N
Geophysical Fluid Dynamics Laboratory **USA**	GFDL 2.0	A1B, B1	2.5^{o} x 2.0^{o}	241.875 – 259.375W 46 - 56N
Max-Planck-Institut for Meteorology **Germany**	ECHAM5-OM	A1B,A2,B1	1.875^{o} x 1.87^{o}	240.9375 – 257.8125W 46.629 – 55.979N
Australia's Commonwealth Scientific and Industrial Research Organization A**ustralia**	CSIRO-MK3.0	A1B,A2,B1	1.875^{o} x 1.87^{o}	240.9375 – 257.8125W 46.6312 – 55.637N

*More than one experiment was carried out for these emission scenarios.

Constructing Climate Change Scenarios

Developing a climate scenario for an impact study requires that data for the relevant climate variable(s) be available from both the GCMs and the 'climatological' record, for two time periods typically each of 30 years: some future time period such as the 2020s, 2050s or the 2080s (i.e., 2010-2039, 2040-2069 and 2070-2099) and the baseline climate (1961-1990)[1]. A climate change scenario constructed using GCM output is typically expressed as a percentage change in precipitation or temperature change in degrees relative to a mean baseline of 1961-90 for a future 30-year period. These differences or ratios are then used to adjust the observed climatological baseline dataset to develop a future climate scenario. A 30-year time period is used to differentiate between the climate change signal and the inter-decal variability within the time series.

Thornthwaite Method of Calculating PET

The Thornthwaite PET method was derived from water balance studies in valleys of east-central USA (Jensen et al. 1990) affected by changes in mean monthly air temperature and shortwave radiation (number of sunlight hours per month, adjusted according to latitude). The Thornthwaite formula is:

$PET=1.6C_f(T/I)^a$
PET= potential evaportranspiration (cm/month);
T= monthly mean air temp (C);
C_f=latitude dependent correction factor for day length.
$a=0.49 + 0.0179\ I - 7.71 \times 10^{-5}\ I^2 + 6.75 \times 10^{-7}\ I^3$
I=annual heat index
$I=\text{sum}\ (i=1:12)\ (Ti/5)^{1.5}$

The heat index is the summation of the 12 monthly index values. This heat index helps satisfy the difference between cold climates and hot climates, where using the mean annual temperature of areas with below-freezing is unrepresentative (Thornthwaite 1948). The annual heat index generally increases from high to low latitudes corresponding to monthly mean temps above 0^oC and the day-length correction factor. The annual range in mean monthly temperatures above 0^oC closely matches seasonal day-length changes and generally increases from low to high latitudes up to approximately 50^o. For latitudes greater than 50^o the relationship between increasing day length and increasing seasonal mean sensible temperature tends to diverge resulting in greater lag time between increase in seasonal

[1] The baseline dataset or "normal" period is representative of the observed, present-day meteorological conditions and describes the average conditions, spatial and temporal variability and anomalous events. The current 30-year "normal" period as identified by the WMO (World Meteorological Organization) is 1961-1990 (IPCC-TGCIA, 2007).

sensible heat as estimated by temperature and increasing seasonal day-length change. This method relies on day length rather than solar radiation in calculating PET.

PET values were calculated using the Thornthwaite equation because of its relatively simple routine; only mean monthly temperature and day length are required and data for limited variables are available from the GCMs.

Results

Climate Change Scenarios for SSRB

GCMs were chosen using a similar method as Barrow and Yu (2005) by plotting the seasonal changes of precipitation and mean temperature for the 2050s. The 2020s and 2080s time periods were not plotted as we are approaching the 2020s and for the 2080s we have less confidence in GCM projections; therefore, the middle time frame of 2050s was examined. The scatter plots for the four seasons in the 2050s were analyzed and model experiments used for this analysis were chosen using the summer season as this provided the greatest range in results.

Figure 2 shows a climate change scenario scatter plot for the 2050's (2040-69) of summer season average temperature (degrees C) and precipitation (%) relative to the 1961-1990 period for the 7 GCMs and experiments. Five model experiments were chosen to represent the range of possible climates: MIROC3.2 MEDRES A2(1) (warm/dry: +3.3^{o}C/-17.3%), HadCM3 TAR a2(1) (warm/wet: +2.9^{o}C/+4%), CGCM3.1/T47 B1(1) (cool/dry: +2.1^{o}C/-6.5%), CSIRO MK3.0 A1B(1) (cool/wet: +1.3^{o}C/+10.3%), and CGCM3.1/T47 B1(2) (median: +2.2^{o}C/+2.2%). These model experiments were used to develop future seasonal temperature, precipitation and CMI climate change and climate scenarios for the SSRB and for five climate stations that were located at or nearby the study sites.

Figure 2. **Scatter plots indicating mean temperature (^{o}C) and precipitation (%) change for SSRB for the 2050s summer. The models were chosen based on the availability of the required climate variables: daily minimum and maximum temperature and daily precipitation. The colours correspond to the GCM and the symbol the scenario. MIROC Medres A2(1) (warm/dry), HadCM3 TAR A2(a) (warm/wet), CGCM3.1/T47 B1(1) (cool/dry), CSIRO MK3.0 A1B(1) (cool/wet), CGCM3/T47 B1(2) (median) are all circled. (Value in brackets identifies the run number).**

Annual Mean Temperature Climate Change Scenarios

Figures 3-5 show the annual mean temperature (^{o}C) climate change scenarios for the 2020s, 2050s and 2080s periods, respectively, for the five climate models and relative to the 1961-90 baseline period. Temperature increases for the 2020s average between +1 to +3^{o}C. Greater increases in annual mean temperature are visible for the 2050s, with temperature increases ranging from +2 to +5^{o}C with the greatest temperature increase projected in the eastern part of the basin. Larger temperature increases are expected further inland, away from the influence of the cooler ocean waters. The 2080s temperature increases range from +2 to +3^{o}C for the cool and median GCMs. The warm GCMs project increases ranging from +4 to +7 ^{o}C, again with the greatest warming towards the eastern region of the basin.

MIROC3.2 MEDRES A2(1) (warm/dry)

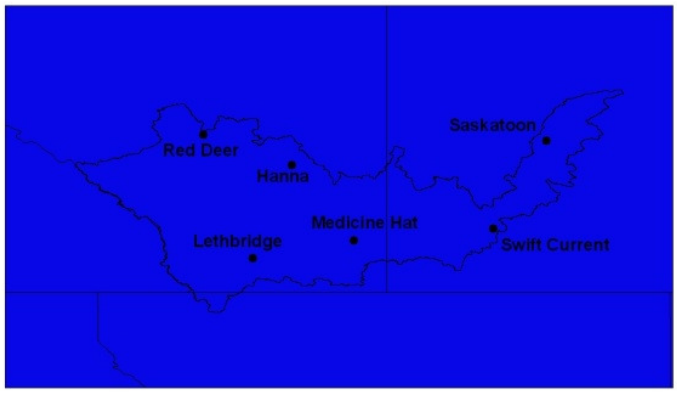

HadCM3 TAR A2(a) (warm/wet)

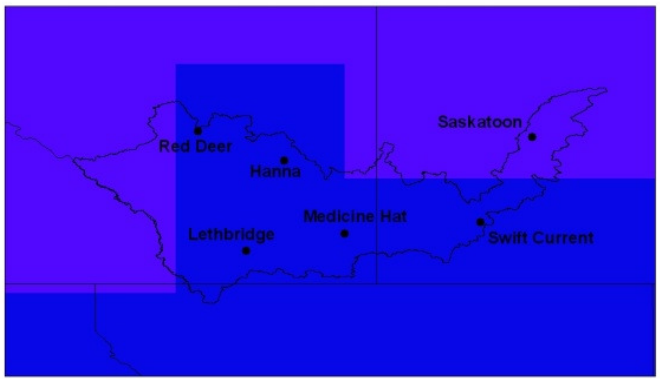

CGCM3.1/T47 B1(1) (cool/dry)

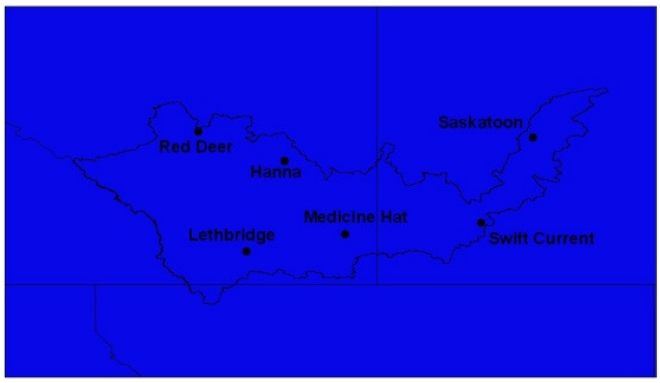

CSIRO MK3.0 A1B(1) (cool/wet)

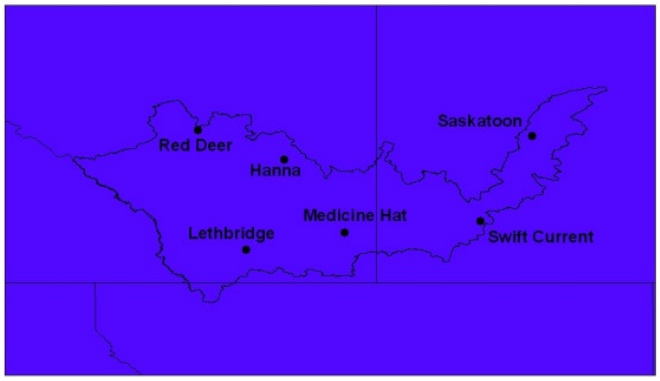

CGCM3.1/T47 B1(2) (median)

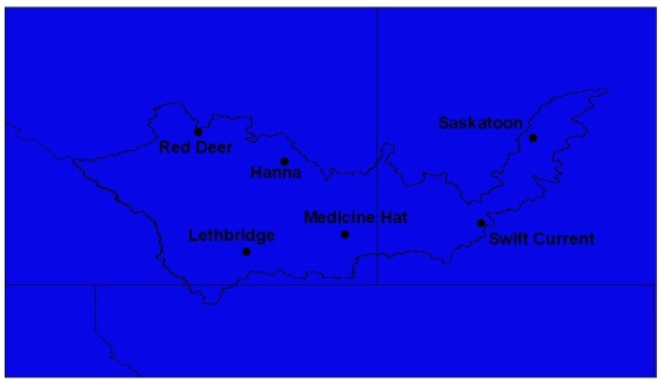

Figure 3. Annual mean temperature (°C) climate change scenario for the 2020s.

MIROC3.2 MEDRES A2(1) (warm/dry)

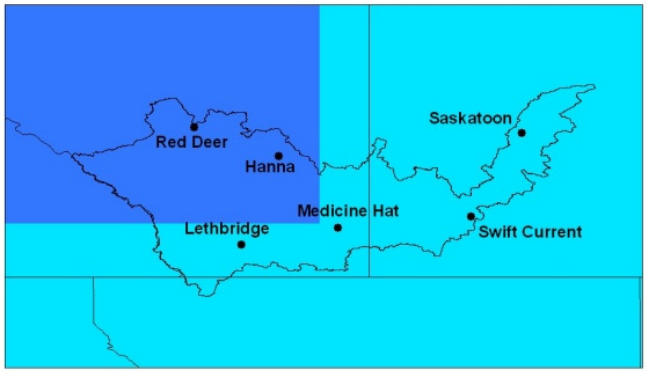

HadCM3 TAR A2(a) (warm/wet)

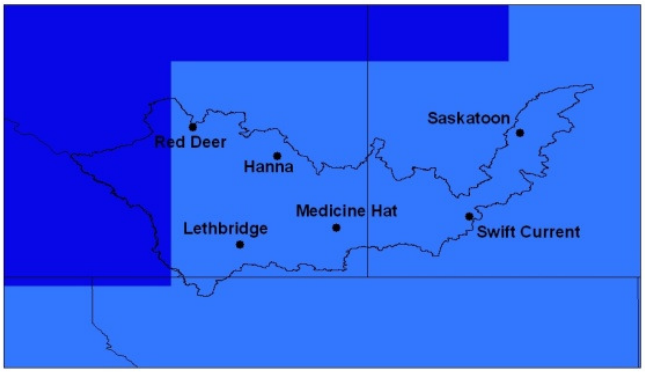

CGCM3.1/T47 B1(1) (cool/dry)

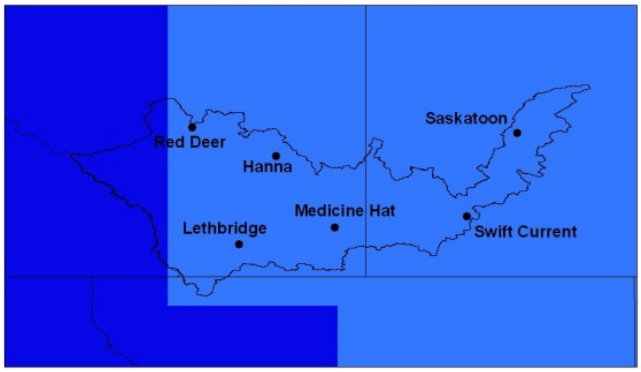

CSIRO MK3.0 A1B(1) (cool/wet)

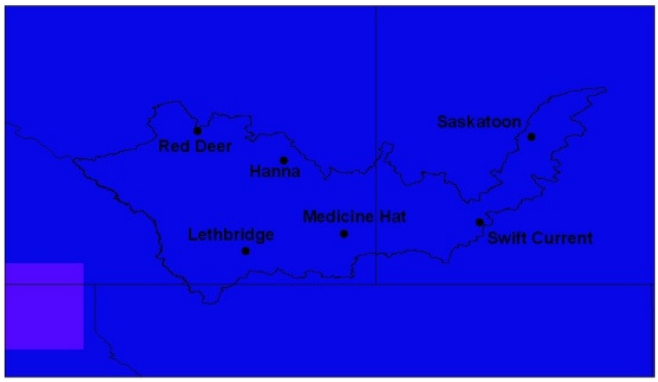

CGCM3.1/T47 B1(2) (median)

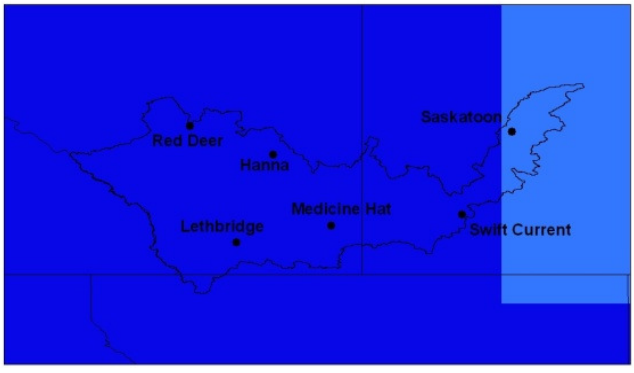

Figure 4. Annual mean temperature (°C) climate change scenario for the 2050s.

MIROC3.2 MEDRES A2(1) (warm/dry)

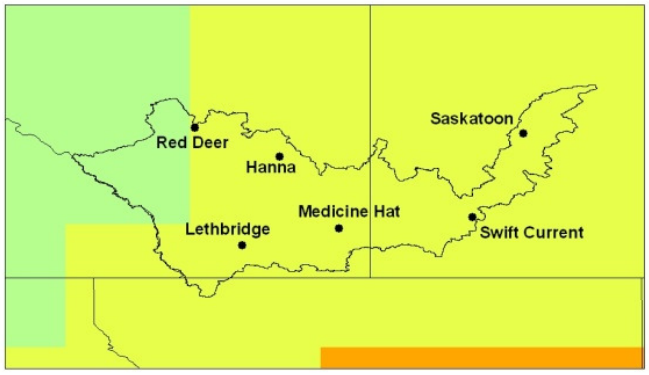

HadCM3 TAR A2(a) (warm/wet)

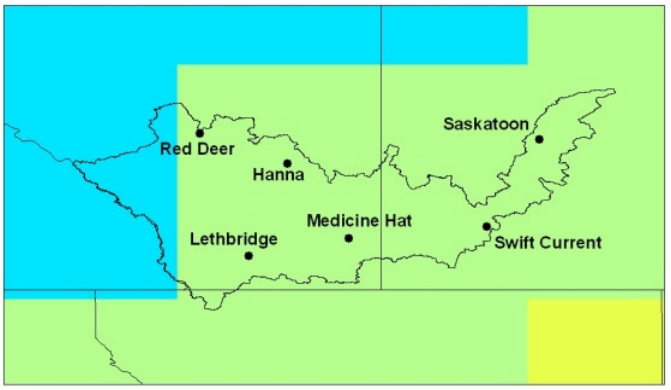

CGCM3.1/T47 B1(1) (cool/dry)

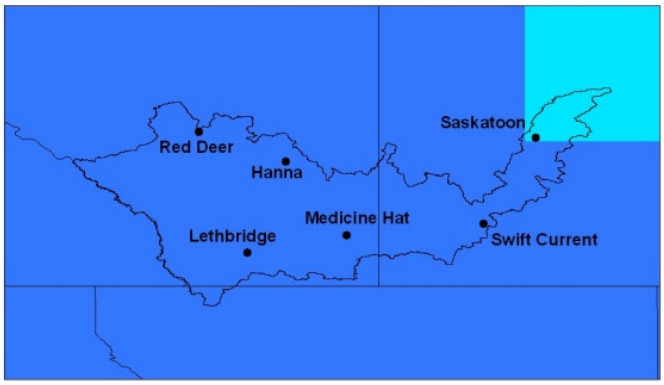

CSIRO MK3.0 A1B(1) (cool/wet)

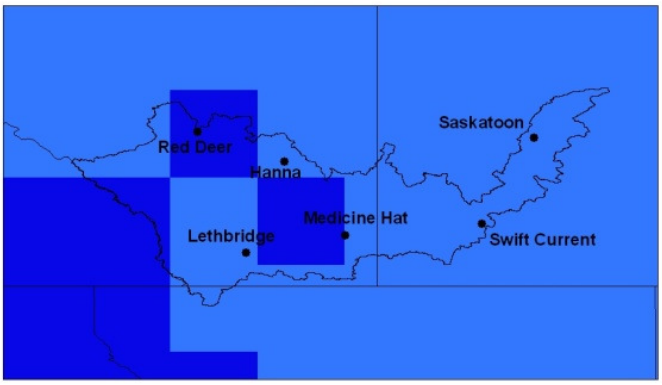

CGCM3.1/T47 B1(2) (median)

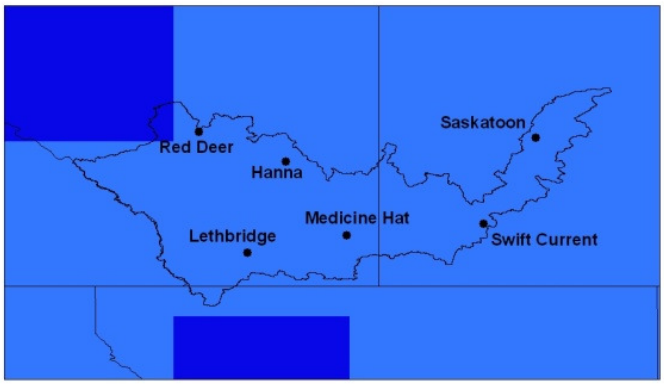

Figure 5. Annual mean temperature (°C) climate change scenario for the 2080s.

Annual Average Maximum Temperature Climate Change Scenarios

Annual average maximum temperature (^{o}C) climate change scenarios for the 2020s, 2050s and 2080s are shown in Figures 6-8, respectively, for the 5 climate models. Temperature increases for the 2020s period range from +1 to +3^{o}C. For the 2050s the models project increases between +2 to +5^{o}C and for the 2080s increases ranging between +2 and +8^{o}C. The MIROC3.2 MEDRES A2(1) (warm/dry) and the HadCM3 TAR A2(a) (warm/wet) models project the greatest increase in maximum temperature for all future time periods.

MIROC3.2 MEDRES A2(1) (warm/dry)

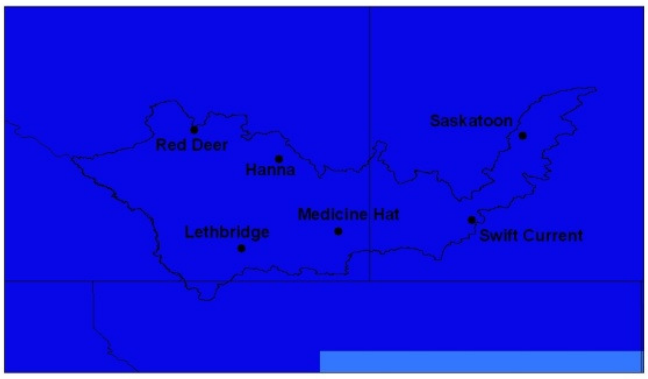

HadCM3 TAR A2(a) (warm/wet)

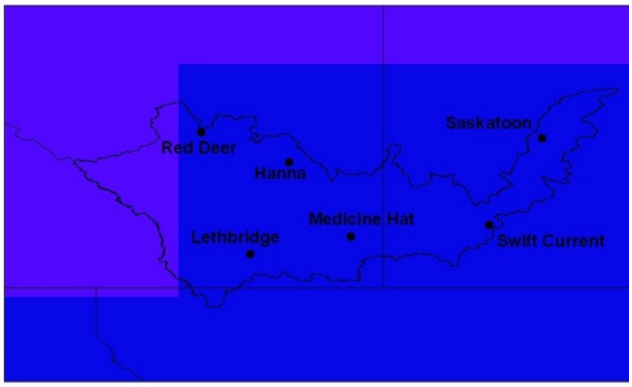

CGCM3.1/T47 B1(1) (cool/dry)

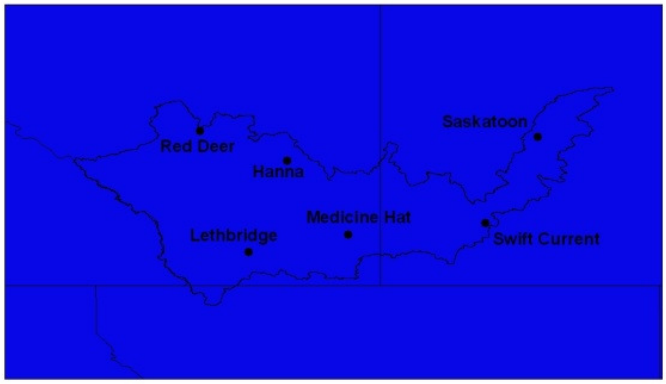

CSIRO MK3.0 A1B(1) (cool/wet)

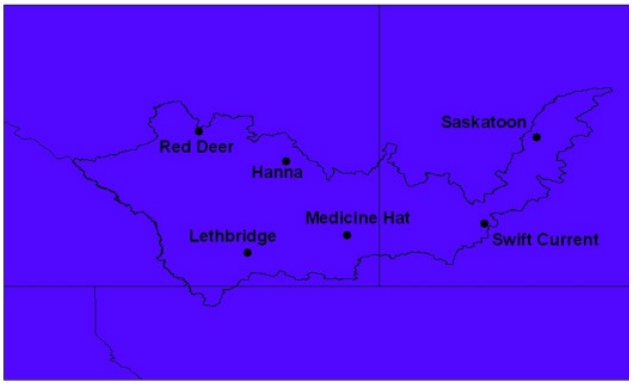

CGCM3.1/T47 B1(2) (median)

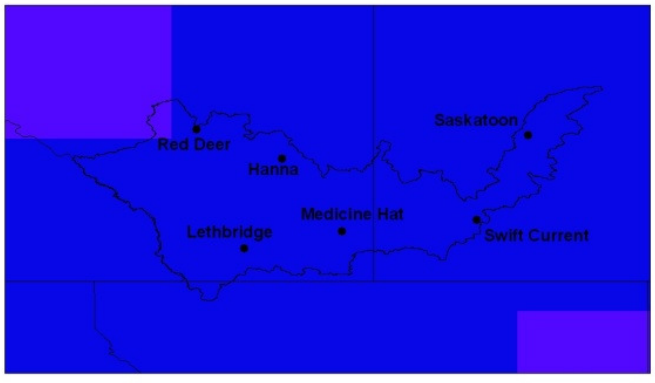

Figure 6. Annual maximum temperature (°C) climate change scenario for the 2020s.

MIROC3.2 MEDRES A2(1) (warm/dry)

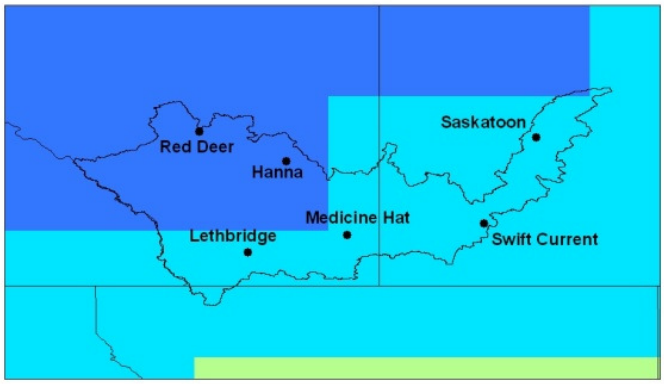

HadCM3 TAR A2(a) (warm/wet)

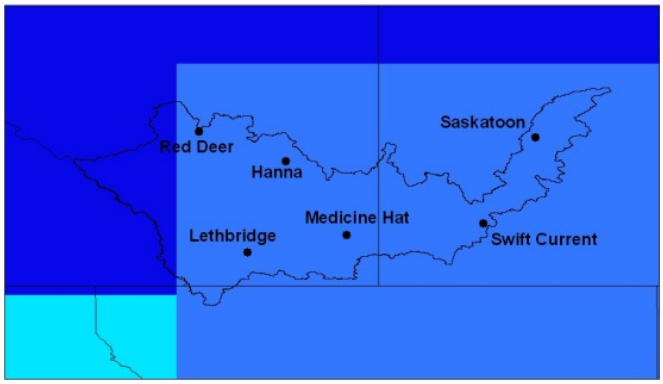

CGCM3.1/T47 B1(1) (cool/dry)

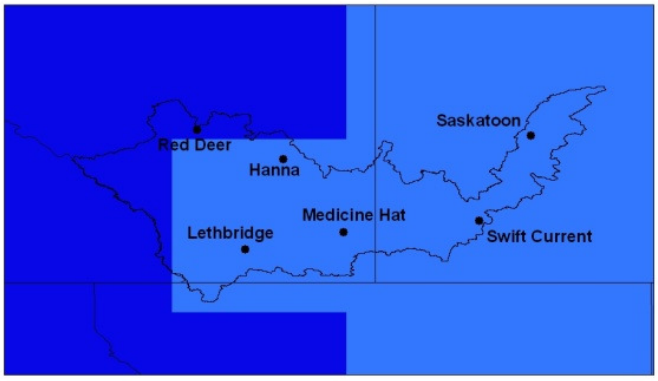

CSIRO MK3.0 A1B(1) (cool/wet)

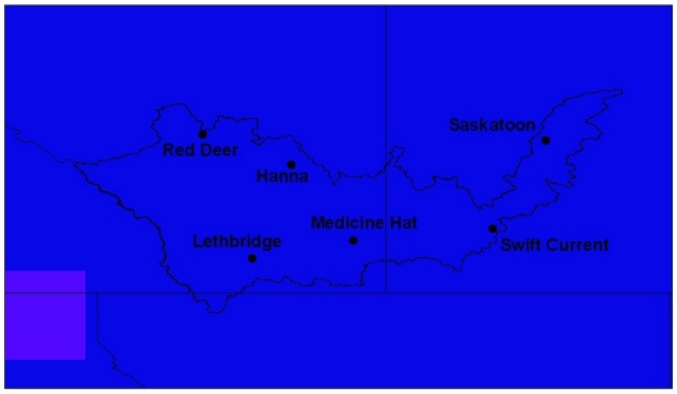

CGCM3.1/T47 B1(2) (median)

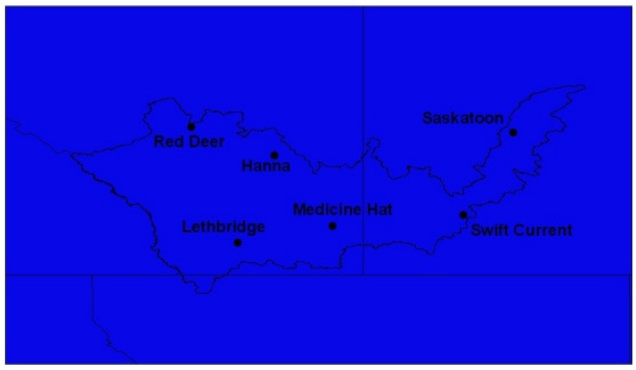

Figure 7. Annual maximum temperature (°C) climate change scenario for the 2050s.

MIROC3.2 MEDRES A2(1) (warm/dry)

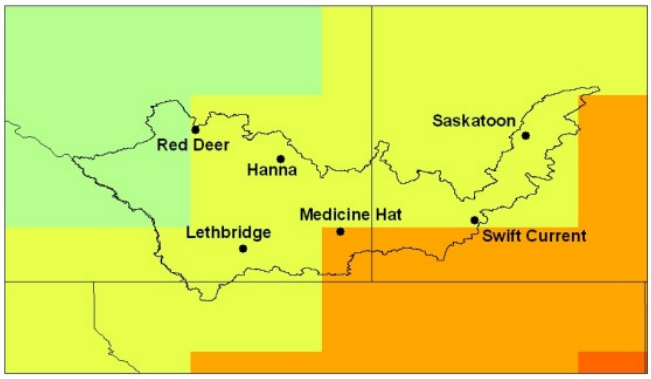

HadCM3 TAR A2(a) (warm/wet)

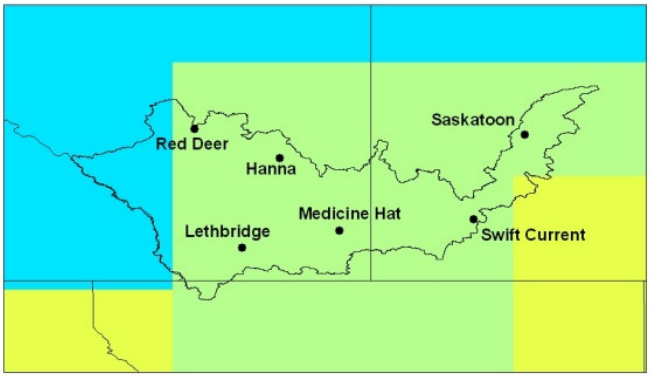

CGCM3.1/T47 B1(1) (cool/dry)

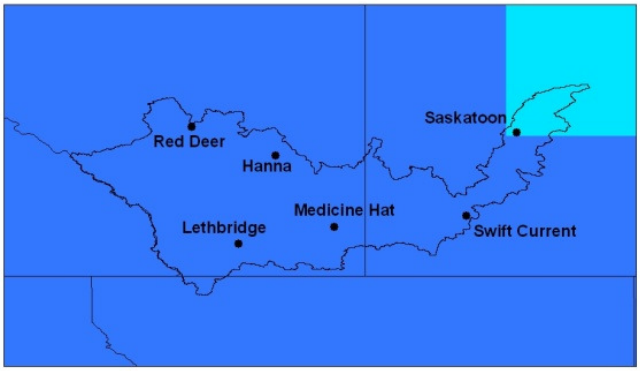

CSIRO MK3.0 A1B(1) (cool/wet)

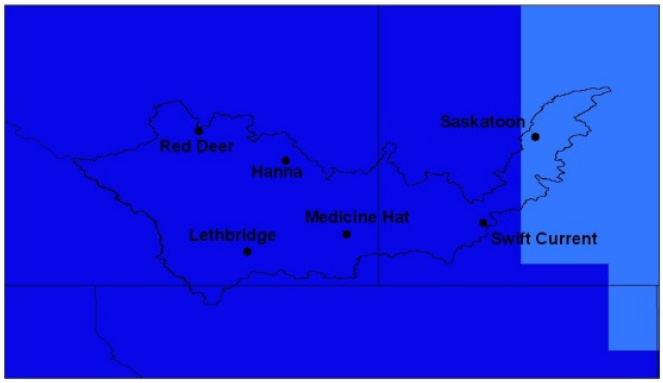

CGCM3.1/T47 B1(2) (median)

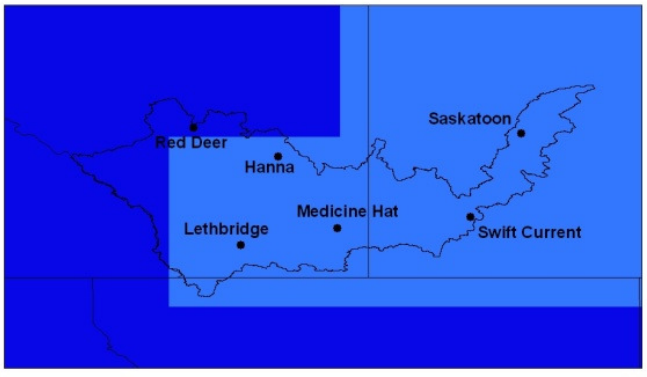

Figure 8. Annual maximum temperature (°C) climate change scenario for the 2080s.

Annual Average Minimum Temperature Scenarios

Figures 9-11 show annual average minimum temperature climate change scenarios for the 2020s, 2050s, and 2080s, respectively, for the 5 climate models. Temperature increases are similar to that of maximum temperature increases throughout the basin for the 2020s. The 2050s minimum temperature increases are about 1^{o}C greater than for the 2020s over the basin. Minimum temperatures are projected to increase more than maximum temperatures and this is reflected in the figures comparing the maximum and minimum temperature climate change scenarios, with the overall basin experiencing increased warming. This increase in minimum temperatures continues through the 2080s with temperature increases ranging between +3 to +7^{o}C.

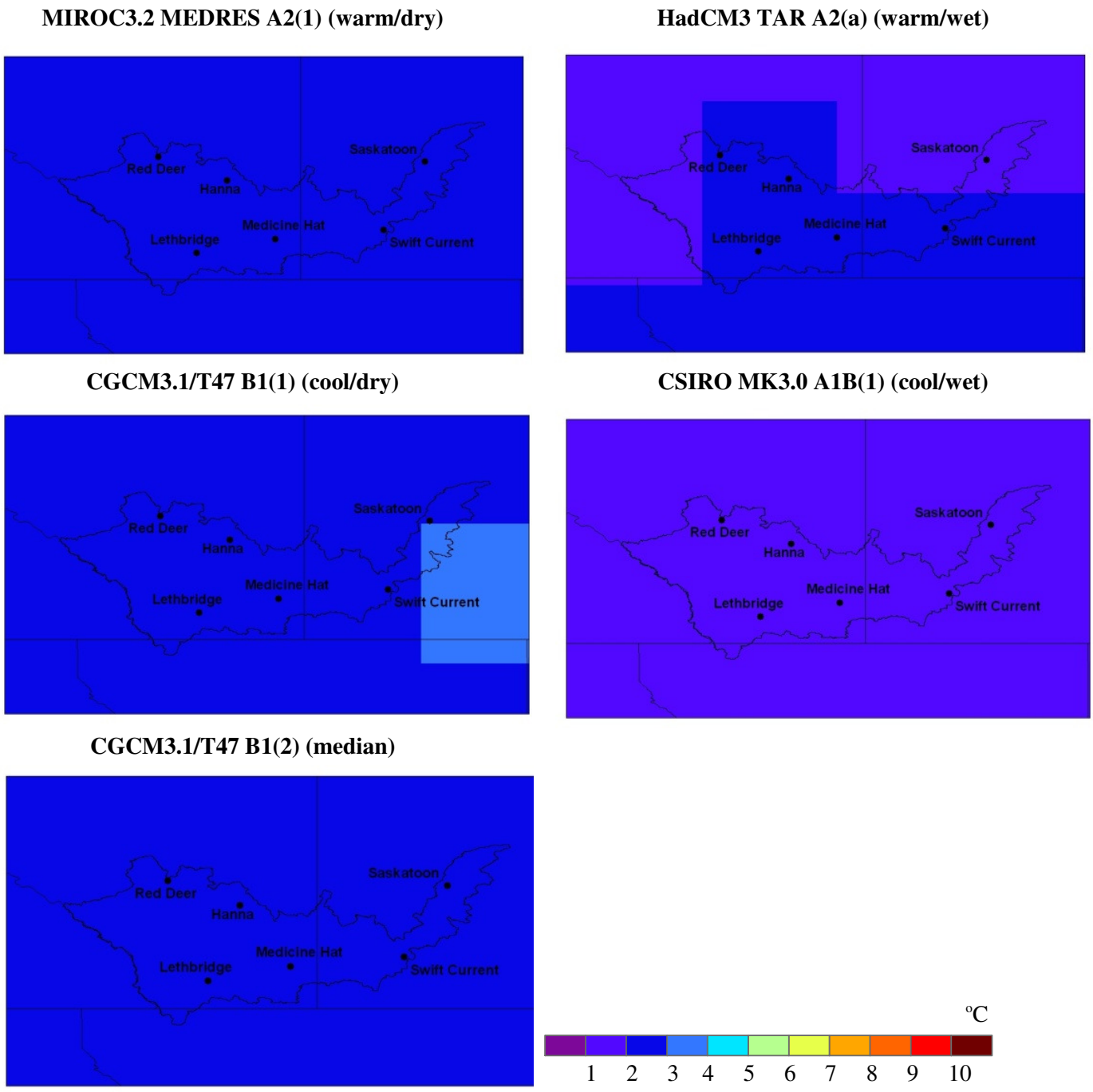

Figure 9. Annual minimum temperature (°C) climate change scenario for the 2020s.

MIROC3.2 MEDRES A2(1) (warm/dry)

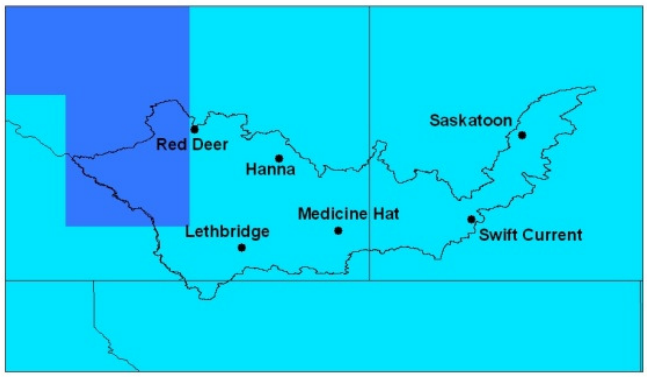

HadCM3 TAR A2(a) (warm/wet)

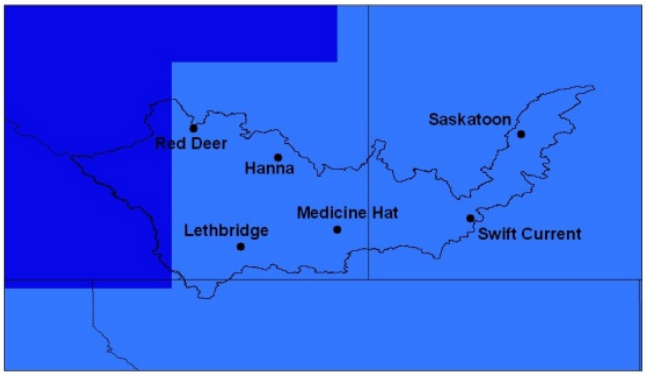

CGCM3.1/T47 B1(1) (cool/dry)

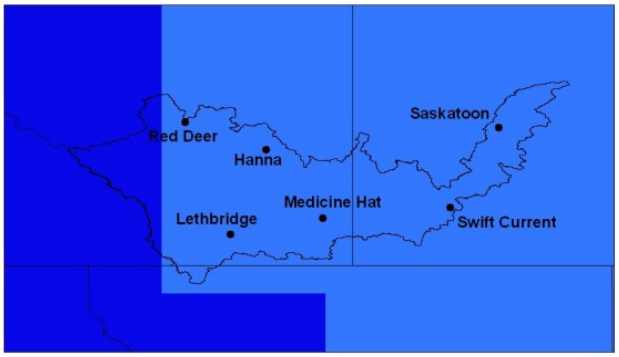

CSIRO MK3.0 A1B(1) (cool/wet)

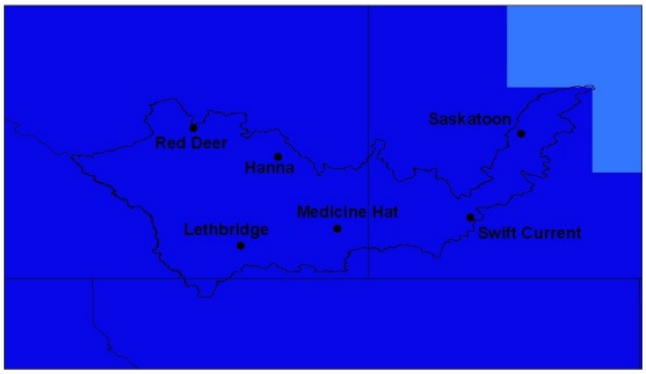

CGCM3.1/T47 B1(2) (median)

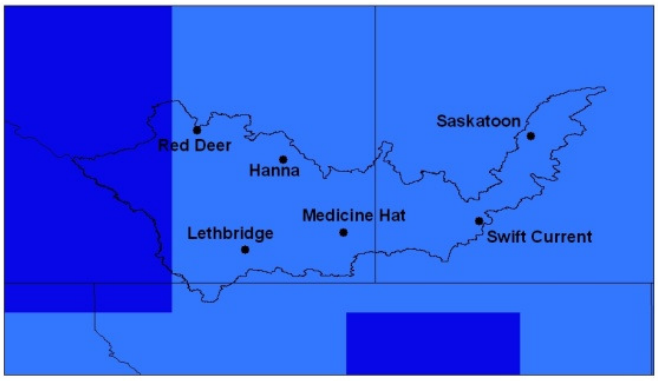

Figure 10. Annual minimum temperature (°C) climate change scenario for the 2050s.

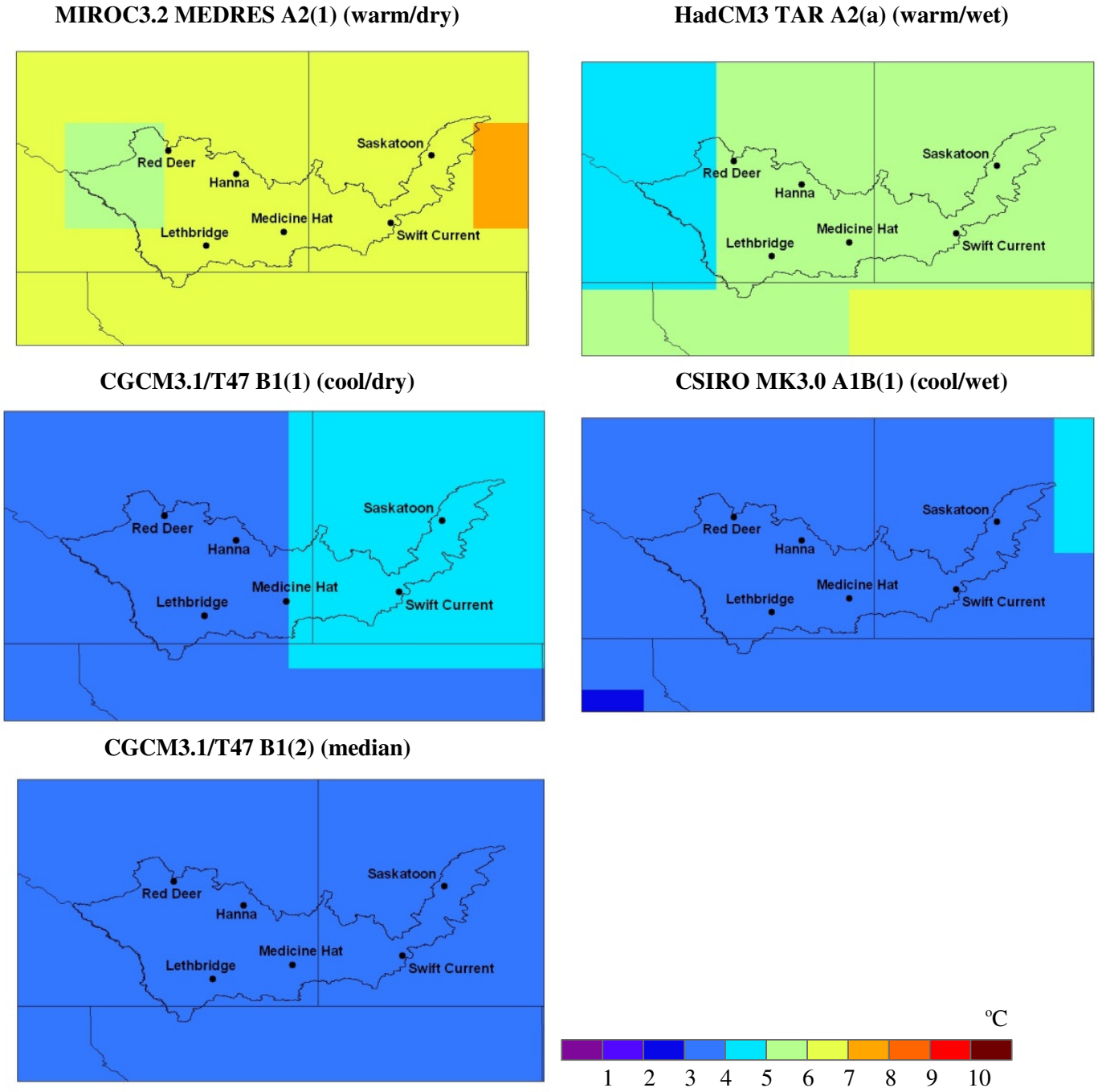

Figure 11. Annual minimum temperature (°C) climate change scenario for the 2080s.

Annual Average Precipitation Climate Change Scenarios

Figures 12-14 show the annual average precipitation change scenario (%) throughout the basin for the 2020s, 2050s, and 2080s period, respectively, relative to the baseline for the 5 climate models. During the 2020s the MIROC3.2 MEDRES A2(1) is the only model projecting precipitation decreases (0 to -10%) throughout most of the basin. The HadCM3 TAR A2(a) projects a small decrease (0 to -5%) over the foothills and Rocky Mountains, which could have significant downstream impacts. Over the rest of the basin, precipitation is projected to increase up to +5%.

The remaining models project increases up to +10 to +15% over the basin for the 2020s (Figure 12). Precipitation changes increase over the basin for the MIROC3.2 MEDRES A2(1), HadCM3 TAR A2(a) and CGCM3.1/T47 B1(1) (cool/dry) during the 2050s (Figure 13) compared to the 2020s projections. The CSIRO MK3.0 A1B(1) (cool/wet) and CSIRO MK3.0 A1B(1) (cool/wet) are still projecting increased precipitation relative to the 1961-90 baseline but less than the 2020s scenario. Annual precipitation changes projections for the 2080s (Figure 14) shows an even greater increase in precipitation over the basin relative to the 2050s.

MIROC3.2 MEDRES A2(1) (warm/dry)

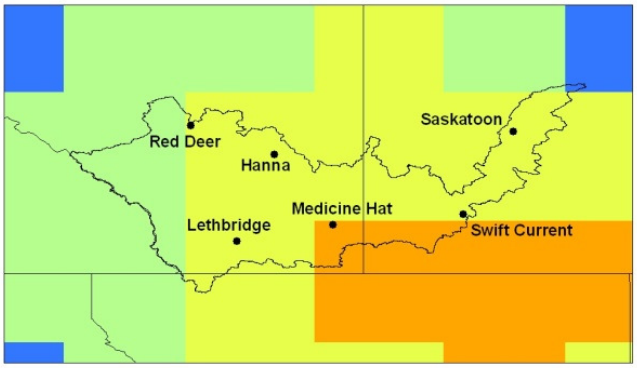

HadCM3 TAR A2(a) (warm/wet)

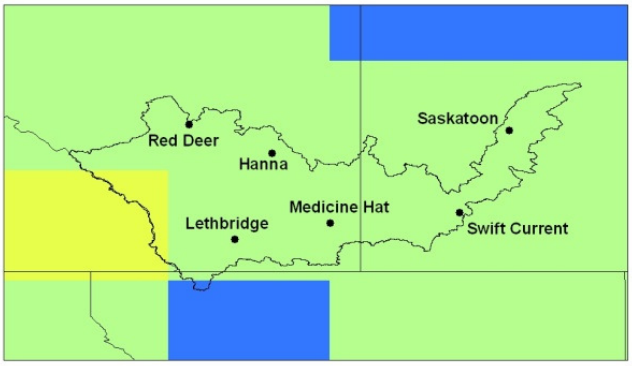

CGCM3.1/T47 B1(1) (cool/dry)

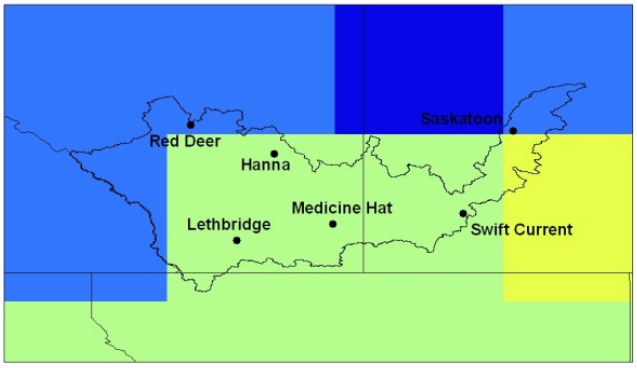

CSIRO MK3.0 A1B(1) (cool/wet)

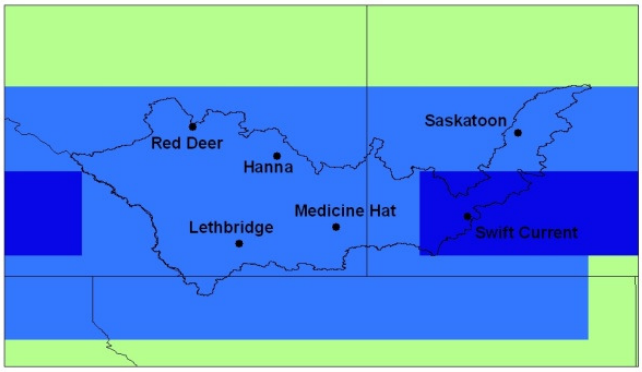

CGCM3.1/T47 B1(2) (median)

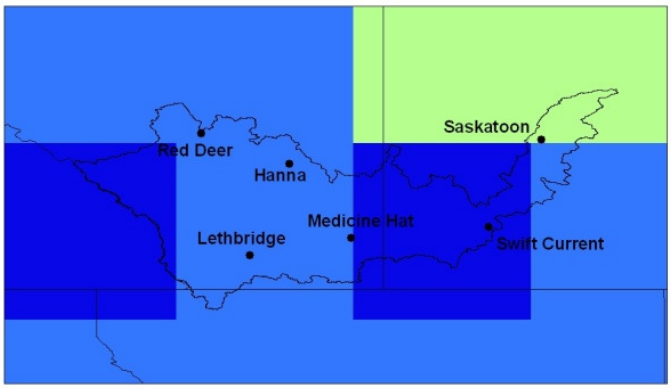

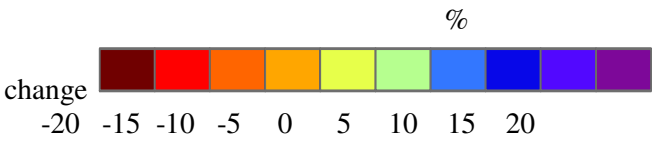

Figure 12. Annual precipitation (% change) climate change scenario for the 2020s.

MIROC3.2 MEDRES A2(1) (warm/dry)

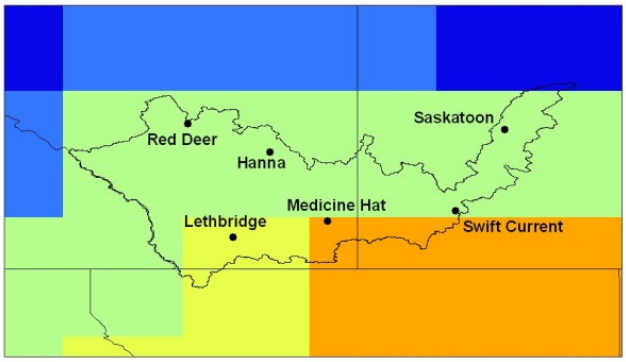

HadCM3 TAR A2(a) (warm/wet)

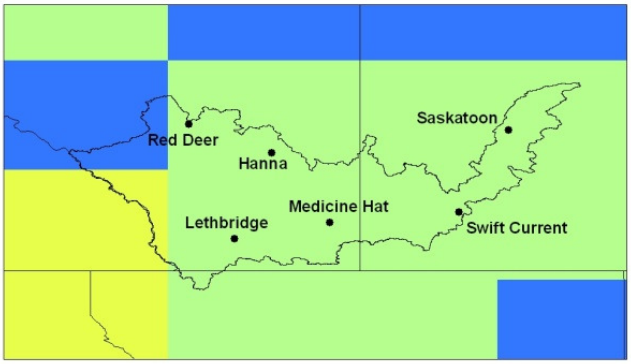

CGCM3.1/T47 B1(1) (cool/dry)

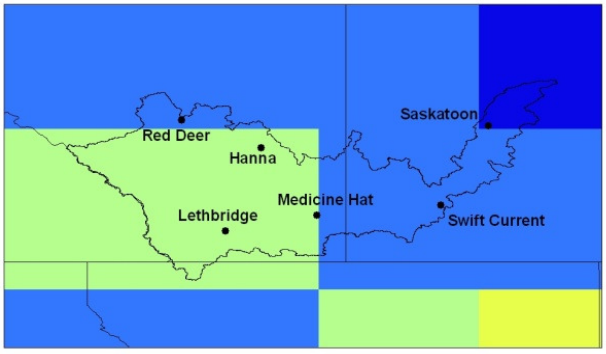

CSIRO MK3.0 A1B(1) (cool/wet)

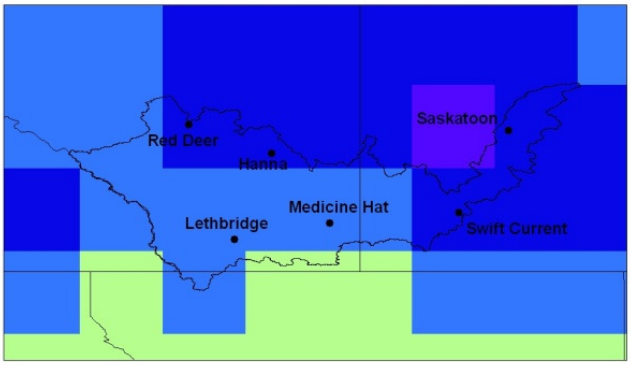

CSIRO MK3.0 A1B(1) (cool/wet)

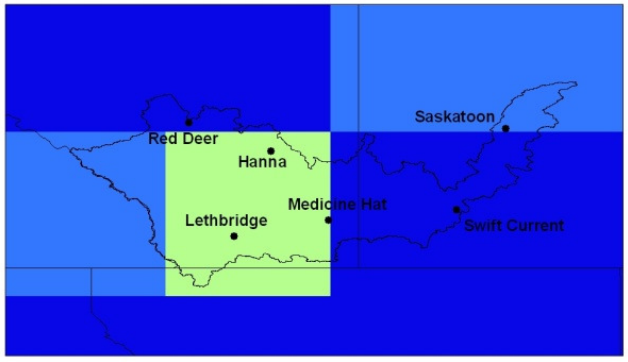

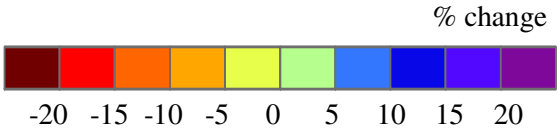

Figure 13. Annual precipitation (% change) climate change scenario for the 2050s.

MIROC3.2 MEDRES A2(1) (warm/dry)

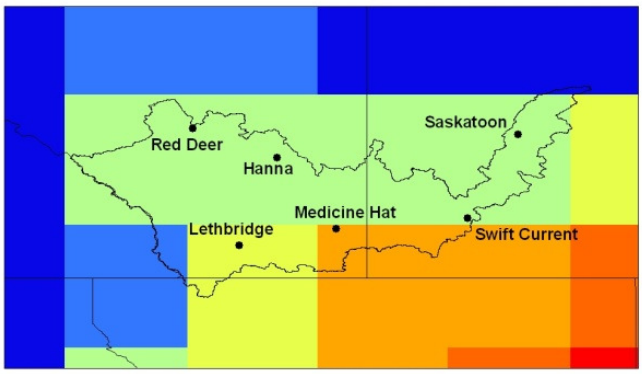

HadCM3 TAR A2(a) (warm/wet)

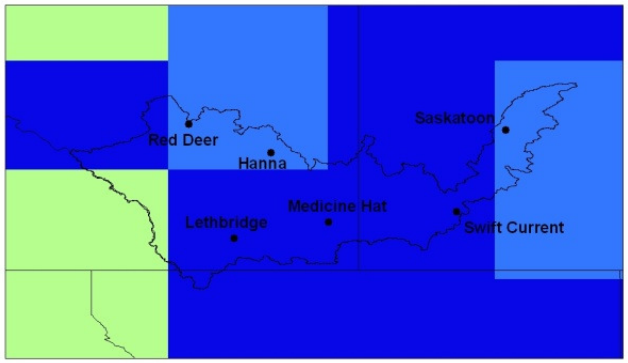

CGCM3.1/T47 B1(1) (cool/dry)

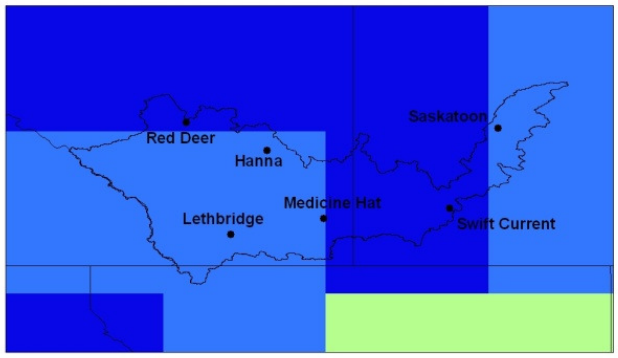

CSIRO MK3.0 A1B(1) (cool/wet)

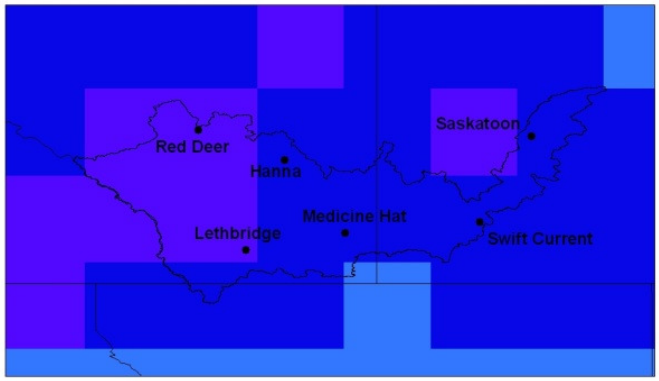

CGCM3.1/T47 B1(2) (median)

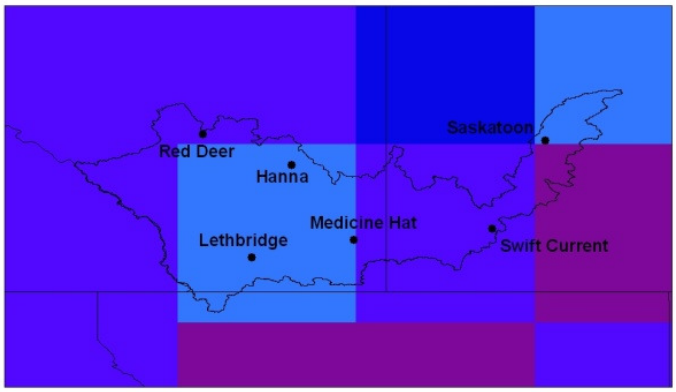

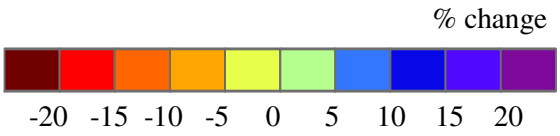

Figure 14. Annual precipitation (% change) climate change scenario for the 2080s.

2050s Seasonal Climate Change Scenarios

This section compares the seasonal changes among the models for mean temperature and precipitation changes for the 2050s period across the study area. By comparing the seasons we are able to understand when the greatest changes are projected and whether they are increases or decreases as compared to the annual average changes.

Figures 15-18 show the mean temperature climate change scenarios for winter (December, January, February: DJF), spring (March, April, May: MAM), summer (June, July, August: JJA) and fall (September, October, November: SON), respectively, for the five scenarios in each season. Figure 15 shows the smallest increase in mean winter temperature changes of between +0.5 to +3^{o}C over the basin for the HadCM3 TAR A2(a) and CSIRO MK3.1 A1B(1) GCMs. CGCM3.1 B1(2) projects an increase of between +3 and +4^{o}C and CGCM3.1 B1(1) gives temperatures that increase by +3 to +5^{o}C over the basin. The greatest increase in temperature is projected by MIROC3.2 MEDRES A2(1) with +4 to +5^{o}C increases.

The spring season (Figure 16) projected temperature increases range between +0.5 to +4^{o}C. CGCM3.1 B1(2) projects the smallest increases over the eastern region of the basin (+0.5^{o}C) and MIROC3.2 MEDRES A2(1) projects the greatest increase over the entire basin of between +3 and +4^{o}C. Increases in summer mean temperature (Figure 17) range between +3 and +5^{o}C; greater warming is projected in the southern and eastern regions of the basin. Fall and spring mean temperature projections are similar with increases ranging between +2 to +5^{o}C (Figure 18).

Figures 19-22 show the percent change in precipitation for each of the seasons, DJF, MAM, JJA, and SON, respectively, for the five scenarios. All the models are projecting an increase in winter precipitation (Figure 19) over the basin. The CSIRO MK3.0 A1B1(1) model projects an increase of 0 to 5% in the eastern half of the basin and a 5 to 10% increase in the western and northern regions. The MIROC MEDRES A2(1) and HadCM3 TAR A2(a) models project precipitation increases between 10 and >25% and the CGCM3 B1(1) and B1(2) models project increases between 5 and 20%.

The spring season (Figure 20) projections are for increased precipitation, but less than for the winter season. CGCM3 B1(1) projects the greatest increase of 10 to >20%. All models suggest greater increases in precipitation over the eastern region of the basin relative to the western regions. This increase in precipitation over this region could be related to the greater increase projected in mean

temperature conditions allowing the atmosphere to hold more water and thus have more precipitable water available. The HadCM3 TAR A2(a) model is projecting a slight decrease in precipitation just south of the study region (0 to -5%).

Figure 21 shows the models' summer projections; the HadCM3 TAR A2(a) and CGCM3 B1(2) project minimal increases over parts of the basin (0 to 5%) but the CSIRO MK3.0 A1B1(1) is the only model projecting major increases in precipitation (5 to 25%). The MIROC MEDRES A2(1) projects the largest decrease of values between <-20 to -10% with the greatest decrease in the southern region of the basin. The HadCM3 TAR A2(a) and CGCM3 B1(1) show similar patterns with the greatest decreases in the western region ranging from -15 to -5%. CGCM3 B1(2) also shows decreased precipitation values for the western region (-15 to -5%) and slight increases in the eastern region (0 to 5%).

The fall precipitation (Figure 22) change projections are for increased precipitation over the basin for the CSIRO MK 3.0 A1B(1), CGCM B1(1) and B1(2) scenarios. MIROC MEDRES A2(1) projects increased precipitation over the northern region and decreased precipitation over the southern region of the basin. The HadCM3 TAR A2(a) model projects increased precipitation over the southern and eastern regions and decreases over the northern and western regions.

Despite discrepancies between the model projections of precipitation within each season, the models tend to agree on increased precipitation in the winter season and decreases during the summer season. These results are similar to other studies conducted in this region (Barrow and Yu 2005; Christensen et al. 2007). This is important when assessing impacts associated with agricultural drought or those land uses relying on summer rainfall, especially those not having access to irrigation for crops and grassland for livestock. This change in seasonal precipitation may also impact communities that rely on surface water for recreation or irrigation, resulting in water shortages sooner. It may also impact those communities that are vulnerable to spring and early summer flooding resulting in more severe floods due to the increased winter/spring precipitation and increased temperatures.

MIROC3.2 MEDRES A2(1) (warm/dry)

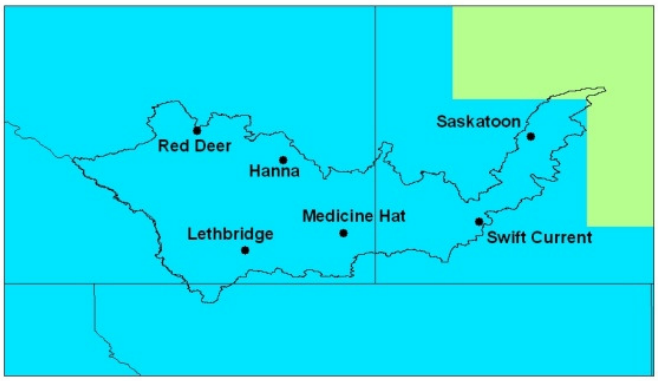

HadCM3 TAR A2(a) (warm/wet)

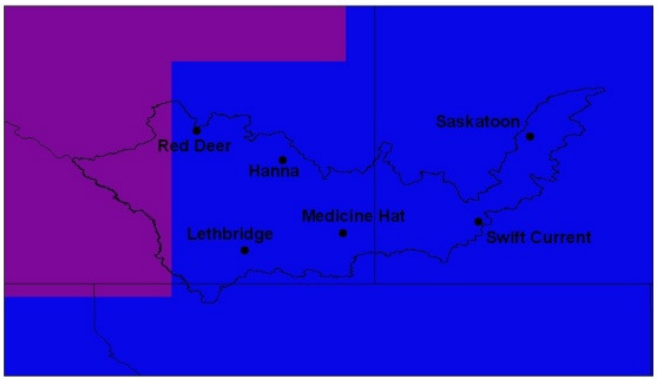

CGCM3.1/T47 B1(1) (cool/dry)

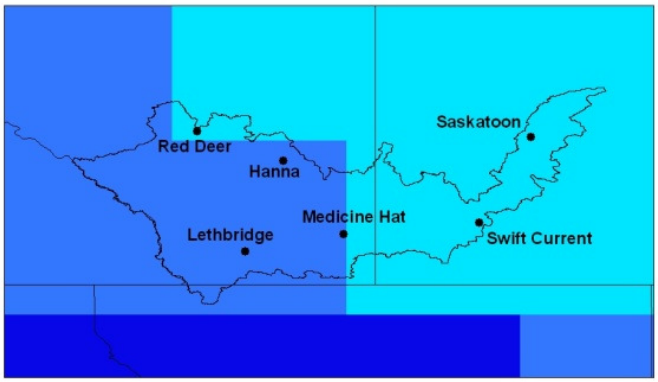

CSIRO MK3.0 A1B(1) (cool/wet)

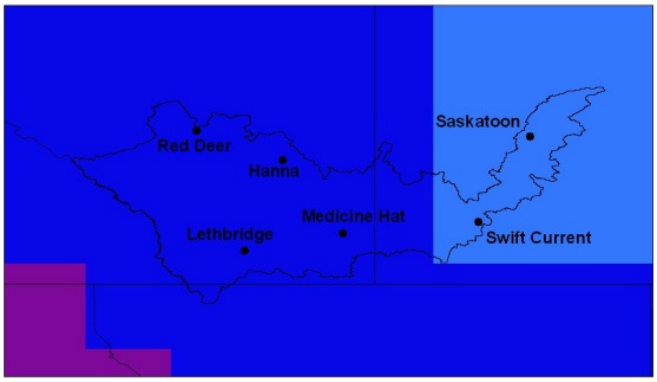

CGCM3.1/T47 B1(2) (median)

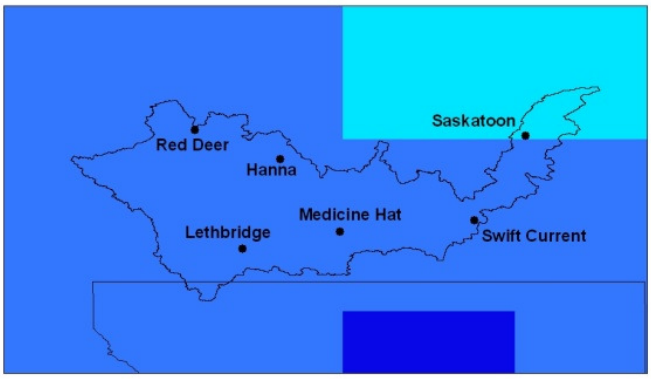

Figure 15. Winter (DJF) mean temperature (°C) climate change scenario for the 2050s.

MIROC3.2 MEDRES A2(1) (warm/dry)

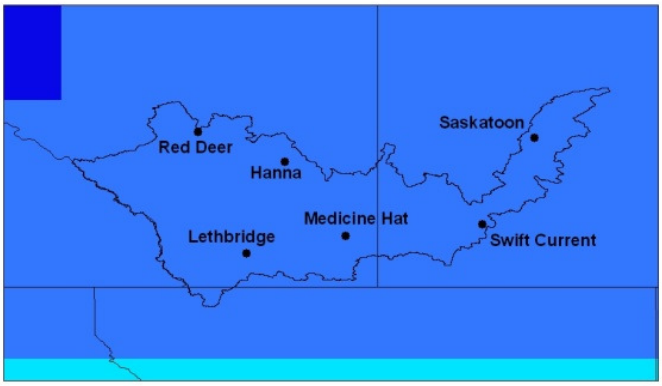

HadCM3 TAR A2(a) (warm/wet)

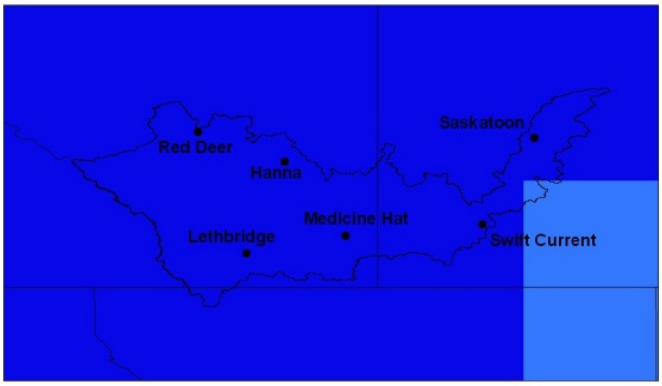

CGCM3.1/T47 B1(1) (cool/dry)

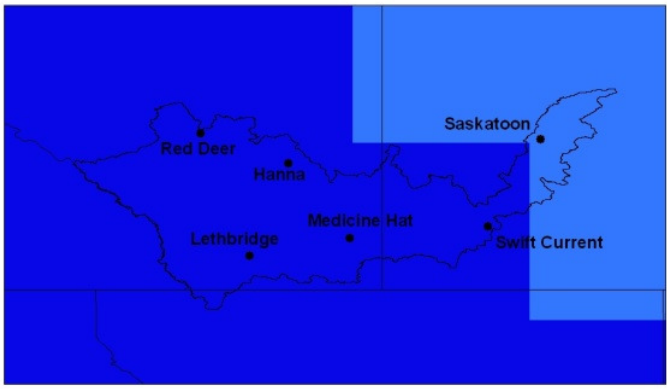

CSIRO MK3.0 A1B(1) (cool/wet)

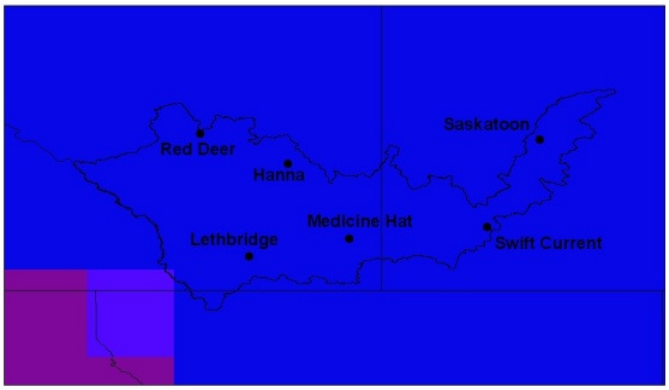

CGCM3.1/T47 B1(2) (median)

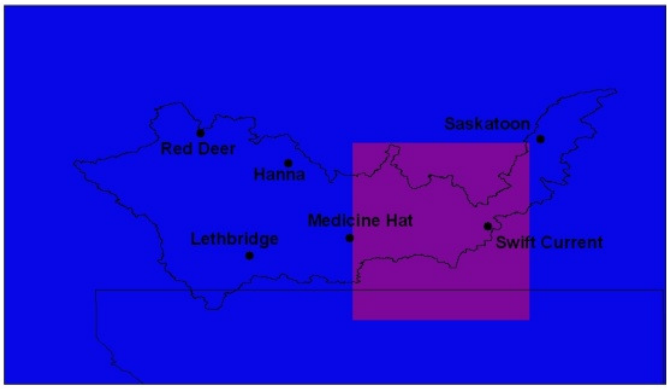

Figure 16. Spring (MAM) mean temperature (°C) climate change scenario for the 2050s.

MIROC3.2 MEDRES A2(1) (warm/dry)

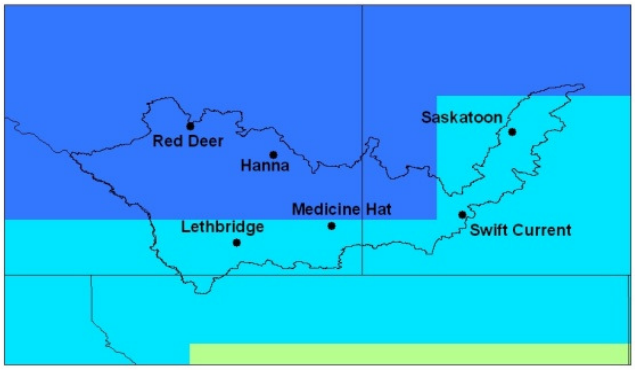

HadCM3 TAR A2(a) (warm/wet)

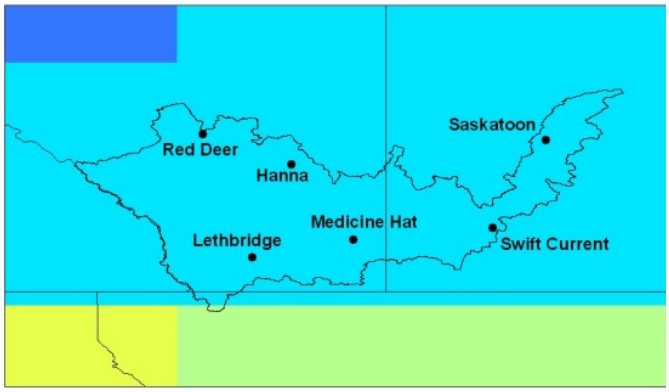

CGCM3.1/T47 B1(1) (cool/dry)

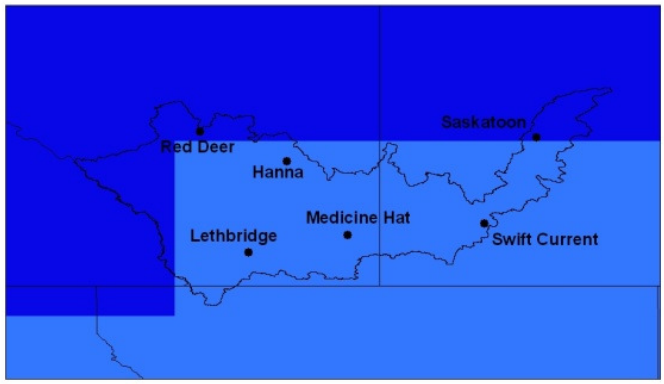

CSIRO MK3.0 A1B(1) (cool/wet)

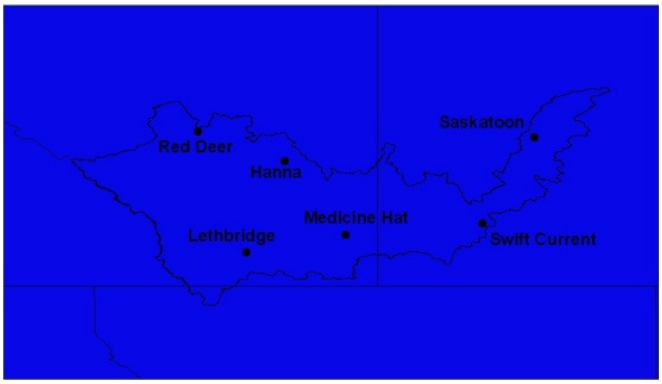

CGCM3.1/T47 B1(2) (median)

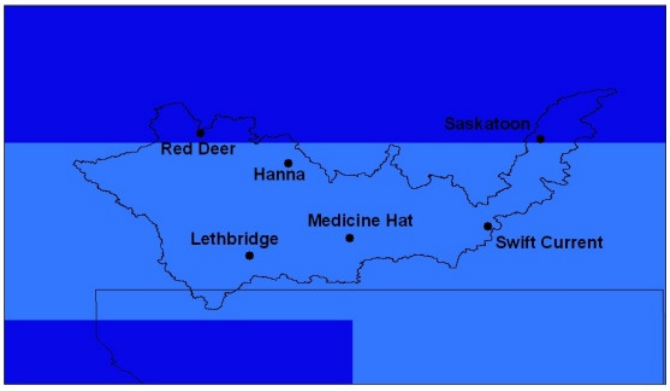

Figure 17. Summer (JJA) mean temperature (°C) climate change scenario for the 2050s.

MIROC3.2 MEDRES A2(1) (warm/dry)

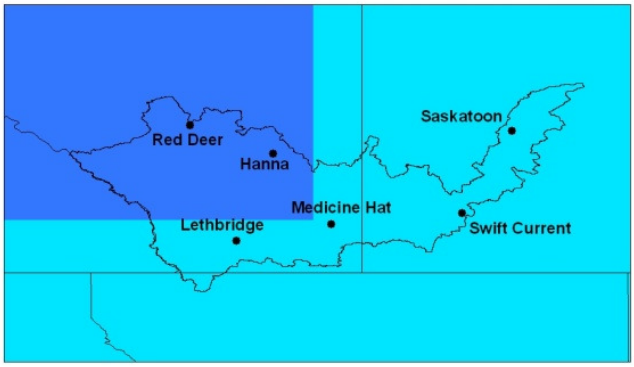

HadCM3 TAR A2(a) (warm/wet)

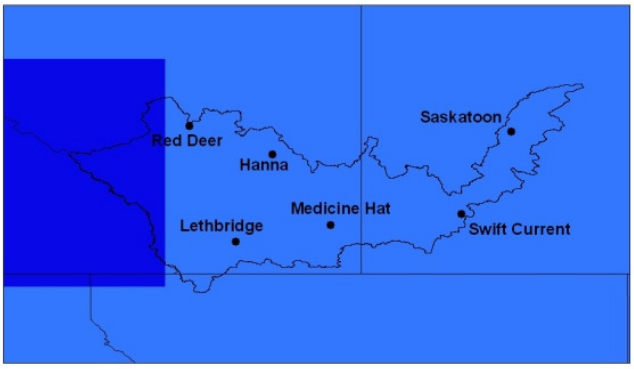

CGCM3.1/T47 B1(1) (cool/dry)

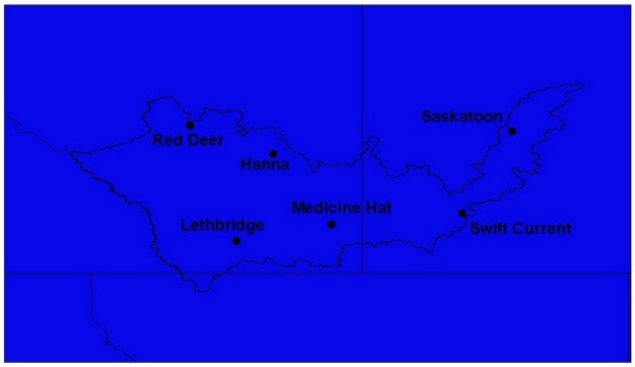

CSIRO MK3.0 A1B(1) (cool/wet)

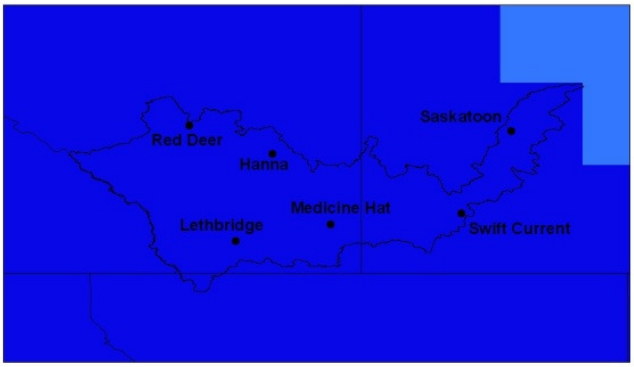

CGCM3.1/T47 B1(2) (median)

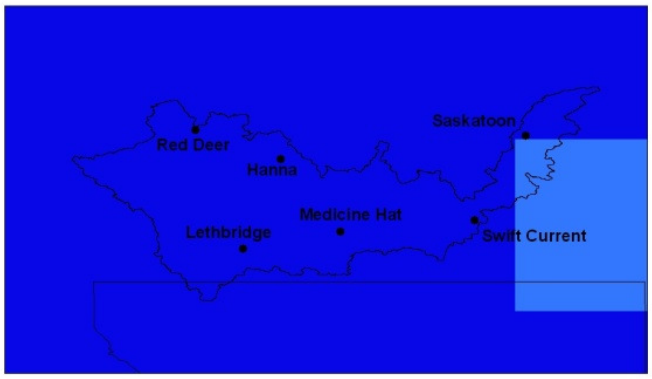

Figure 18. Fall (SON) mean temperature (°C) climate change scenario for the 2050s.

MIROC3.2 MEDRES A2(1) (warm/dry)

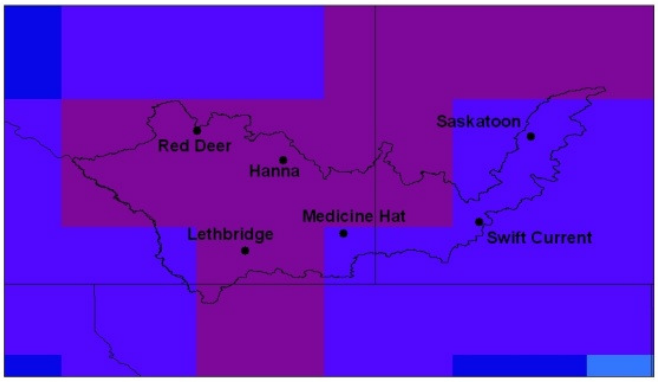

HadCM3 TAR A2(a) (warm/wet)

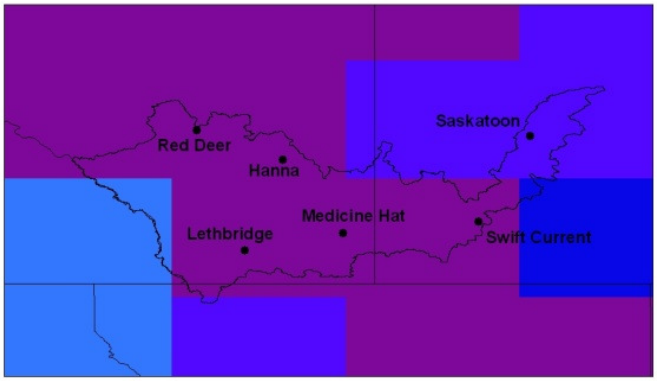

CGCM3.1/T47 B1(1) (cool/dry)

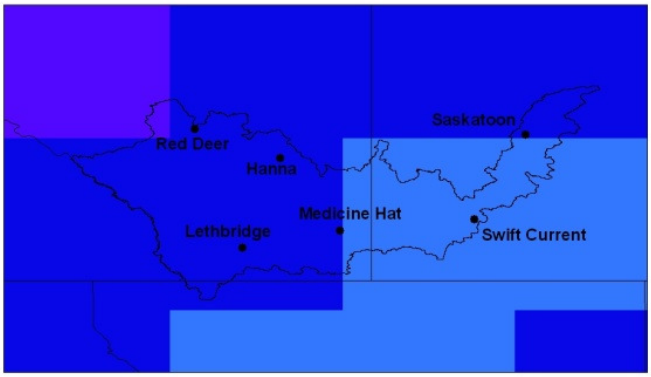

CSIRO MK3.0 A1B(1) (cool/wet)

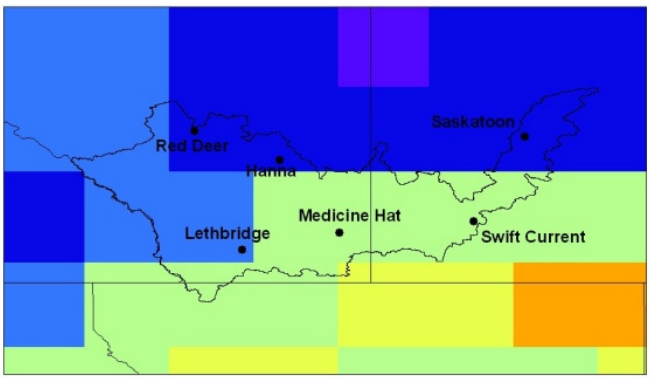

CGCM3.1/T47 B1(2) (median)

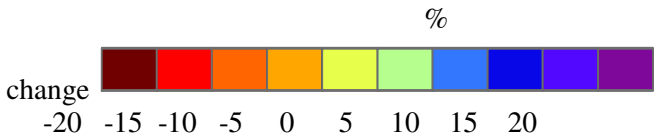

Figure 19. Winter (DJF) precipitation (% change) climate change scenario for the 2050s.

MIROC3.2 MEDRES A2(1) (warm/dry)

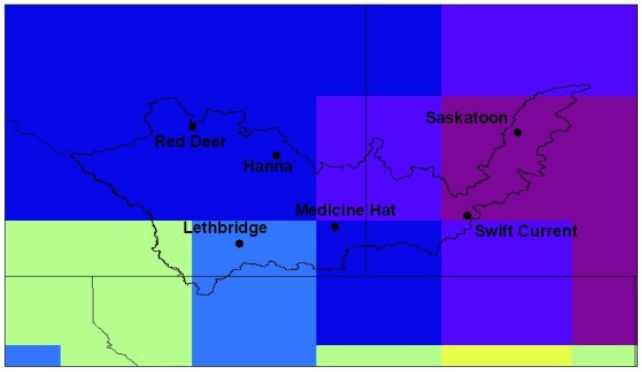

HadCM3 TAR A2(a) (warm/wet)

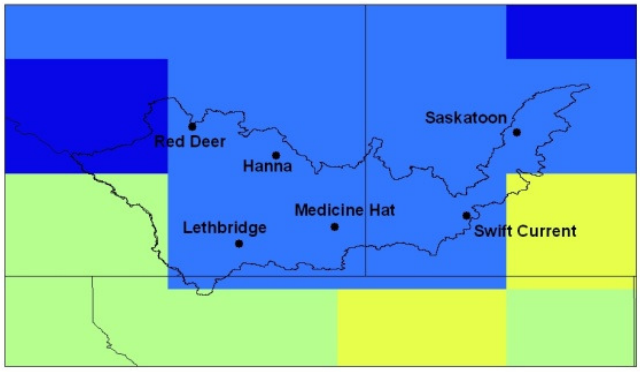

CGCM3.1/T47 B1(1) (cool/dry)

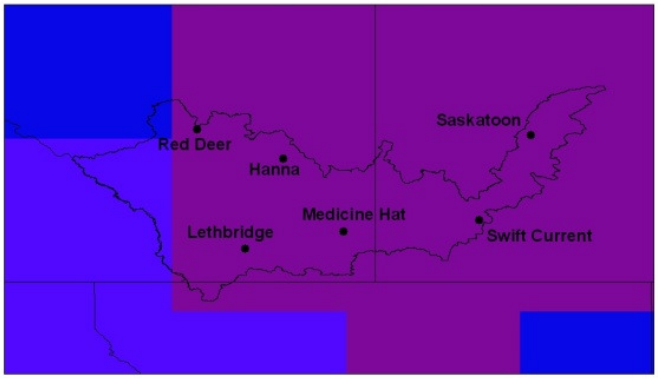

CSIRO MK3.0 A1B(1) (cool/wet)

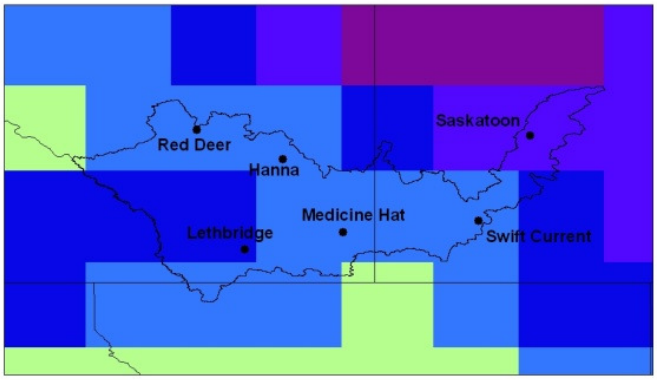

CGCM3.1/T47 B1(2) (median)

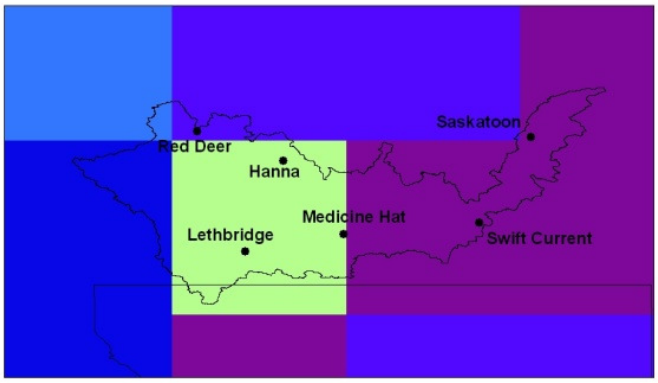

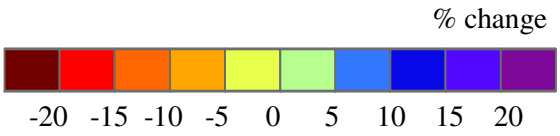

Figure 20. Spring (MAM) precipitation (% change) climate change scenario for the 2050s.

MIROC3.2 MEDRES A2(1) (warm/dry)

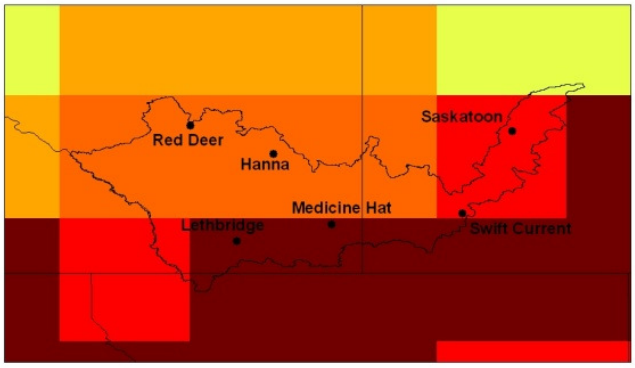

HadCM3 TAR A2(a) (warm/wet)

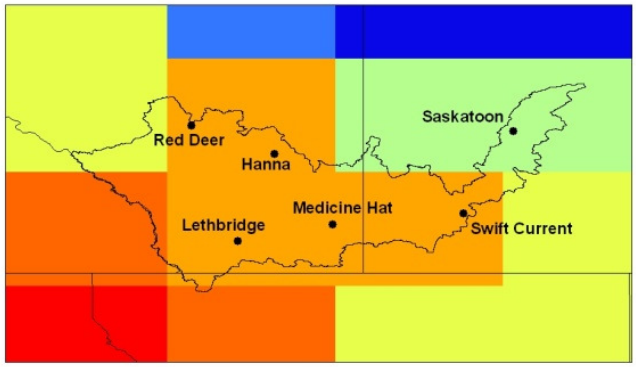

CGCM3.1/T47 B1(1) (cool/dry)

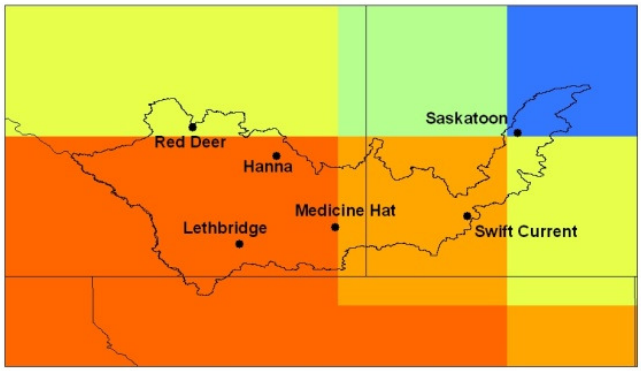

CSIRO MK3.0 A1B(1) (cool/wet)

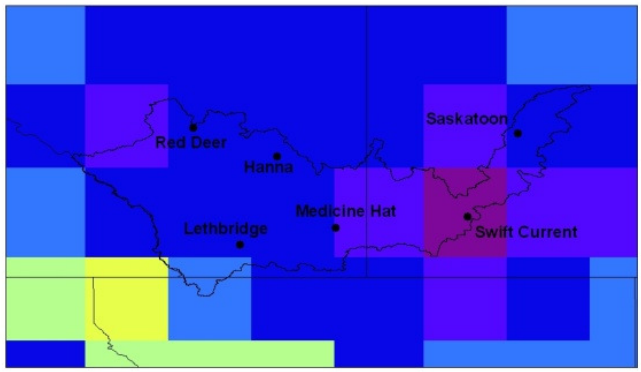

CGCM3.1/T47 B1(2) (median)

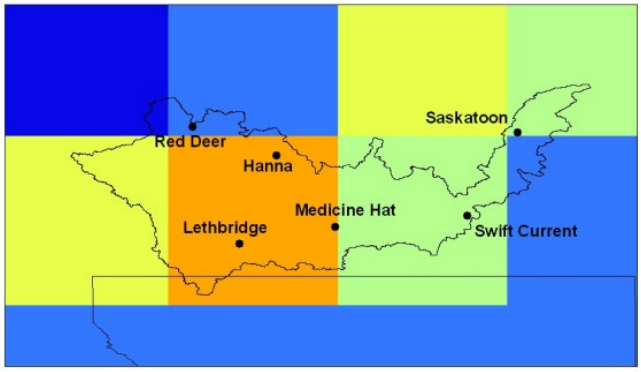

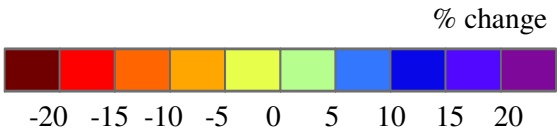

Figure 21. Summer (JJA) precipitation (% change) climate change scenario for the 2050s.

MIROC3.2 MEDRES A2(1) (warm/dry)

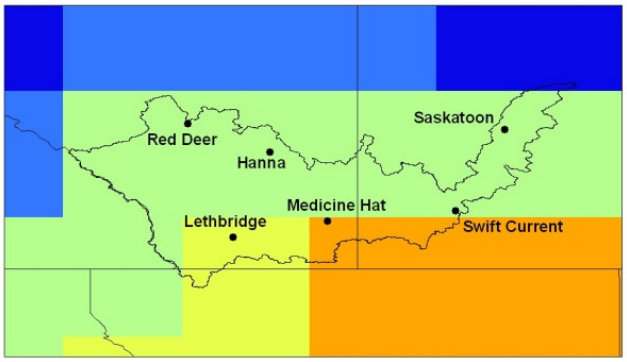

HadCM3 TAR A2(a) (warm/wet)

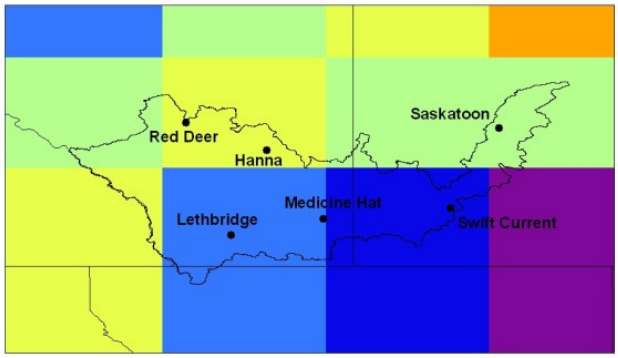

CGCM3.1/T47 B1(1) (cool/dry)

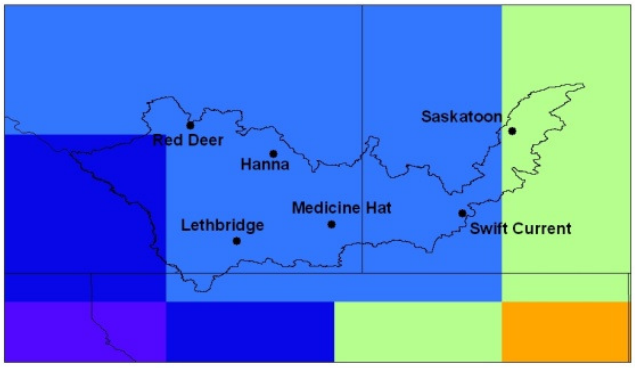

CSIRO MK3.0 A1B(1) (cool/wet)

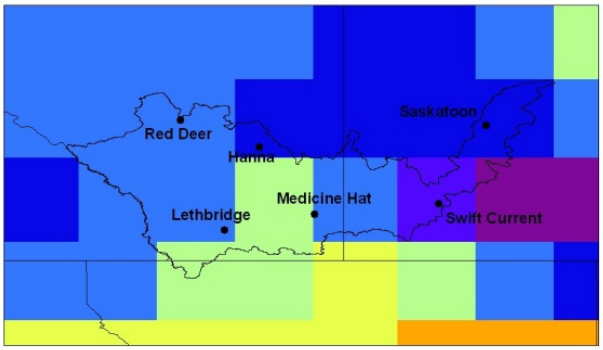

CGCM3.1/T47 B1(2) (median)

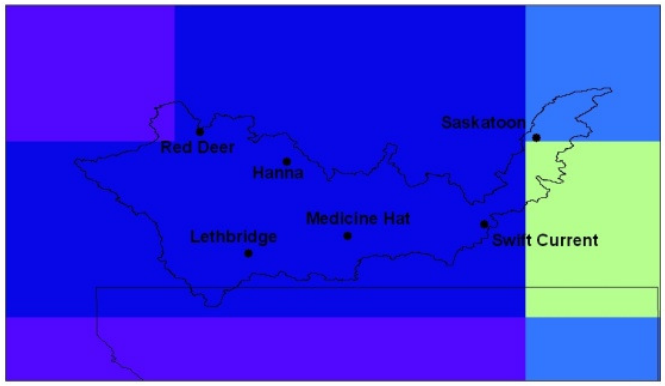

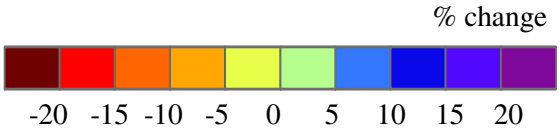

Figure 22. Fall (SON) precipitation (% change) climate change scenario for the 2050s.

Climate Moisture Index (CMI) Scenarios

Figures 23-27 show the 5 climate model CMI projections for 1961-1990, and the 2020s, 2050s and the 2080s for the July-June period. It is important to recognize that the baseline conditions for each model vary, and that they are not directly comparable to the observed baseline conditions, but the changes associated with each future time period can be compared to the projected baseline and put into context.

Figure 23 shows the MIROC MEDRES A2(1) CMI scenarios; there is a slight decrease in CMI over the southeastern region during the 2020s from values ranging from -150 to -100 mm for the baseline to -200 to -150 mm. This spatial pattern of decreased moisture continues through the 2050s and the 2080s with values ranging from <-200 mm to -50 mm relative to the -150 to 0 mm during the baseline period over the eastern region of the basin.

Figure 24 shows the CMI projections for HadCM3 TAR A2(a). This model for the 2020s also projects a decrease in moisture over the eastern region from a positive CMI to a negative CMI. The 2050s and 2080s CMI scenarios are very similar, both showing values in the eastern region of the basin comparable to the baseline and also a small decrease over the central region from 50 to 100 mm for the baseline to 0 to 50 mm.

Figure 25 shows the CGCM3 B1(1) CMI for the future time periods; the only change is over the western region of the basin, with increases in the 2020s and 2050s and then remaining constant throughout the 2080s. The CSIRO MK3.0 A1B(1) (Figure 26) projects increases of CMI during all the future scenarios relative to the baseline conditions. The greatest increase is projected in the western-center region of the basin where the baseline ranges from 0 to 50 mm and by the 2080 ranges from 150 to 200 mm. The CGCM3.1 B1(2) (Figure 27) model projects an increase in CMI over the western region for the 2020s with values ranging from 0 to >250 mm relative to the baseline -50 to 250. The 2050s shows a slight decrease in the central region relative to the 2020s and the 2080s are similar to the 2020s.

The CMI projections for the MJJ period are shown in figures 28-32 for 1961-1990, and the 2020s, 2050s and the 2080s. Climate scenarios for this season are particularly important for dry land farmers who rely on snowmelt as well as spring and summer precipitation as their only source of water.

The MIROC MEDRES A2(1) MJJ CMI scenarios (Figure 28) project a decrease in climate moisture during each of the three future time periods. By the 2020s nearly the entire basin has a decrease of 50 mm. The southern and central regions of the basin have decreases of another 50 mm by the 2050s and by the 2080s there has been a substantial decrease in climate moisture over entire basin of about 100 mm relative to the baseline period.

The HadCM3 TAR A2(a) model also projects a decrease in future moisture availability ; however not as extreme as the MIROC MEDRES A2(1) model (Figure 29). The eastern half of the basin experiences very little change during the 2020s but a depletion of about 50 mm is projected for the 2050s and holds steady through the 2080s. The central half of the basin loses about 50 mm of moisture during the 2020s, and then holds steady during the 2050s with another decrease of 50 mm by the 2080s. The western region of the basin experiences a slight decrease (50 mm) of moisture availability during the 2050s and holds steady during the 2080s.

Figure 30 shows the very little change for the CGCM3.1 B1(1) CMI future scenarios. A small increase is projected during the 2020s for the northwest region of the basin during the 2020s (50 mm) and during the 2080s another moisture decrease is projected for the central region of the basin (50 mm) relative to the baseline conditions.

Figure 31 shows the CMI scenarios for the CSIRO MK3.0 A1B(1) model. This model projects slight increases in moisture availability during the 2020s between Medicine Hat and Lethbridge of about 50mm. The 2050s also projects an increase in moisture for the Swift Current and Saskatoon regions but the 2080s projects similar values as the baseline conditions.

The median CGCM3.1 B1(2) scenario (Figure 32) projects very little change for the future CMI values during the 2020s and 2050s but a decrease during the 2080s of about 50 mm is projected over the central and northern regions of the basin . Overall, with decreased precipitation and increased temperatures in summer, the climate moisture index is decreasing throughout the basin particularly in the central and eastern portions which rely heavier on rainfall for soil moisture compared to irrigated areas. Areas that have access to irrigation or supplementary water may actually benefit from increases in summer temperatures; different crop type choices may be available with a longer growing season and more heat units (Barrow and Yu 2005).

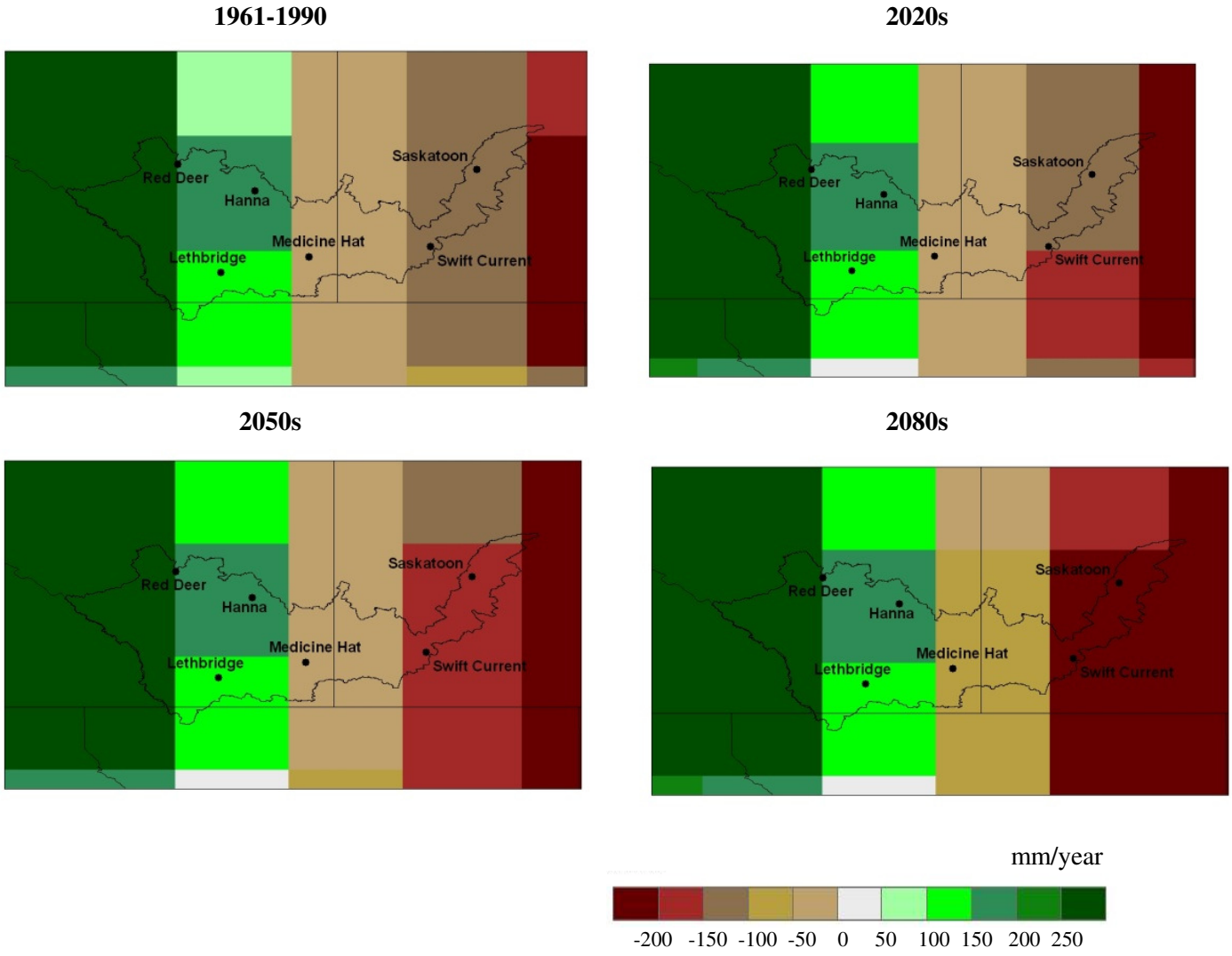

Figure 23. Scenarios of Climate Moisture Index for the 1961-1990, 2020s, 2050s and 2080s, July-June period using the MIROC3.2 MEDRES A2(1) (warm/dry).

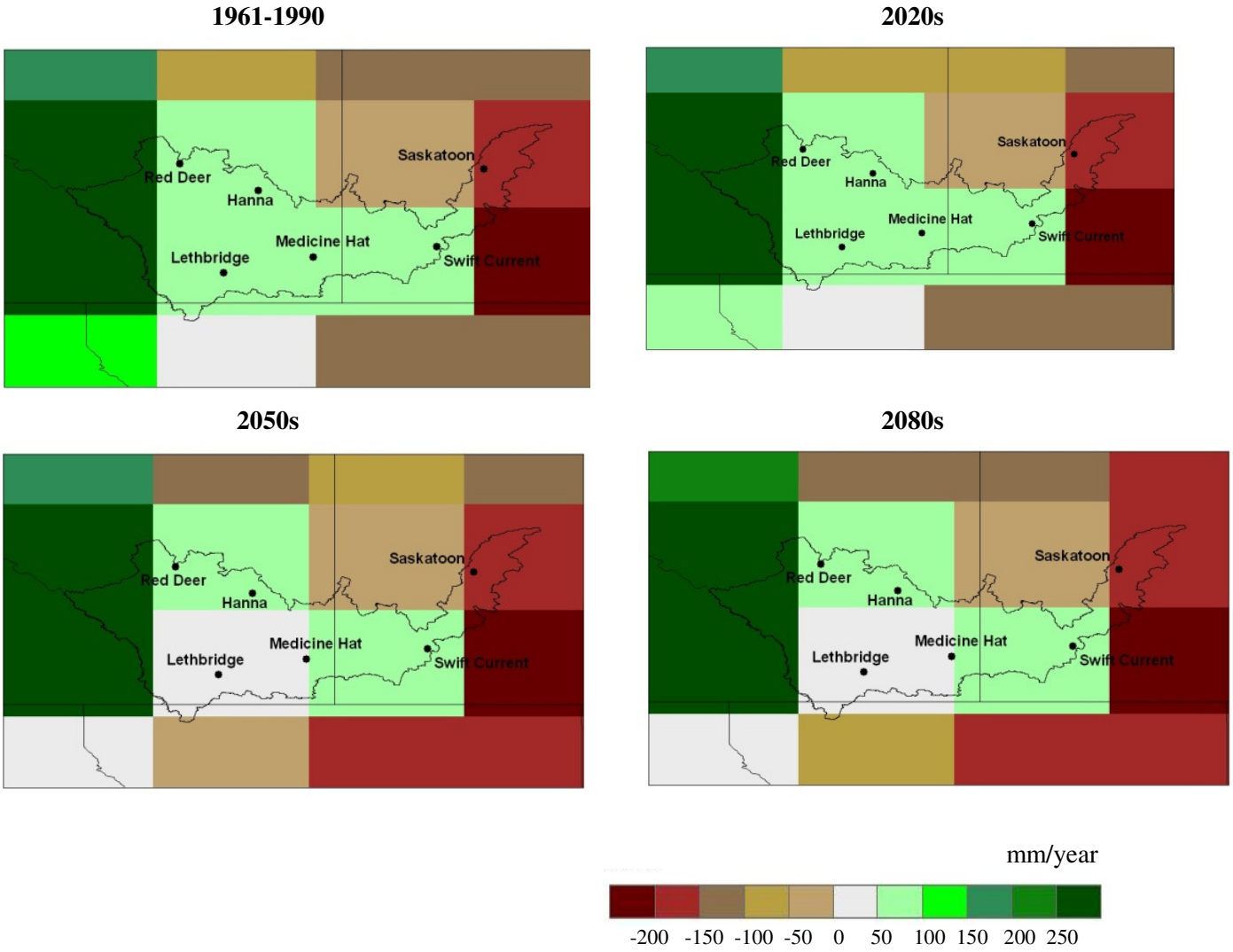

Figure 24. Scenarios of Climate Moisture Index for the 1961-1990, 2020s, 2050s and 2080s, July-June period using the HadCM3 TAR A2(a)(warm/wet).

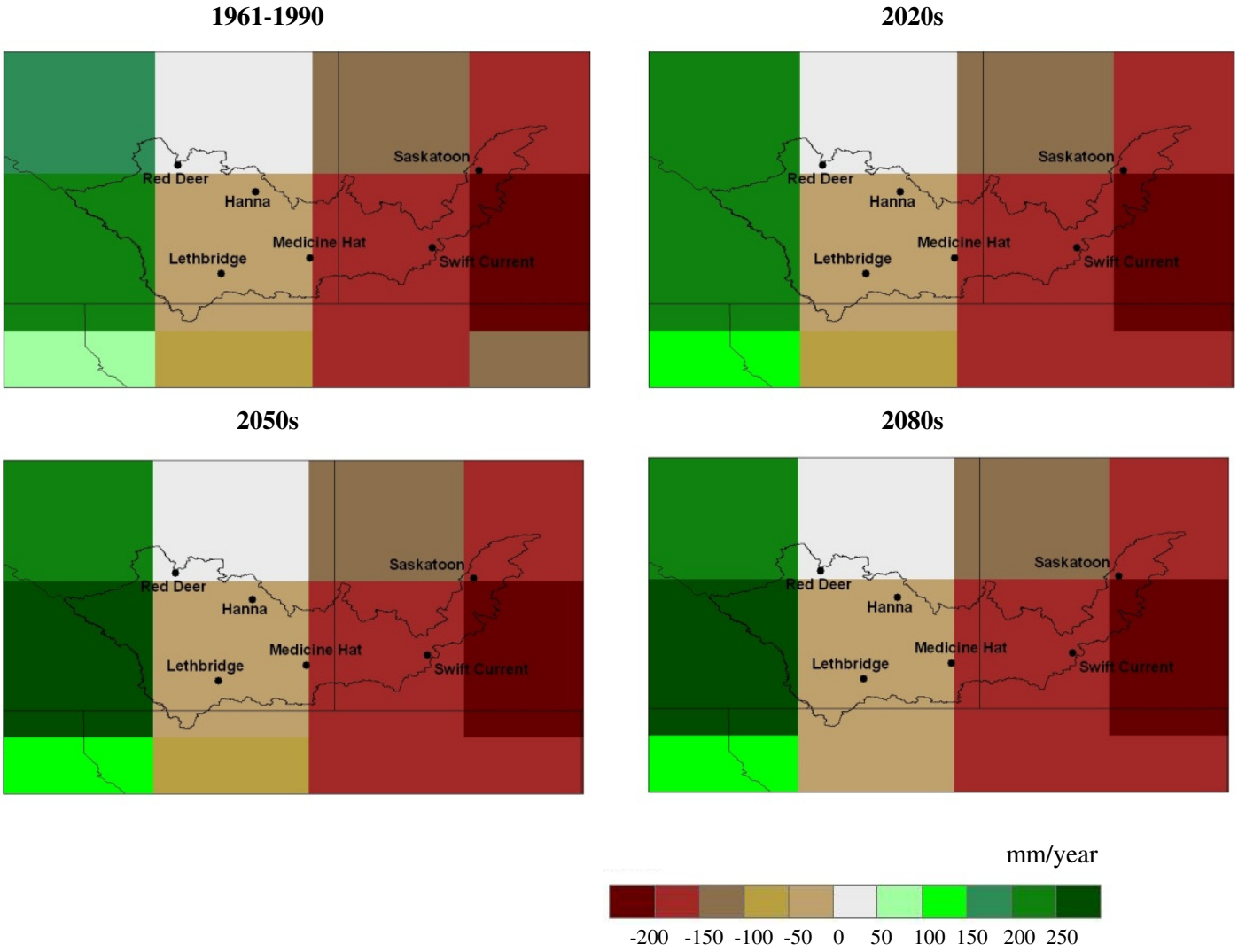

Figure 25. Scenarios of Climate Moisture Index for the 1961-1990, 2020s, 2050s and 2080s, July-June period using the CGCM3.1/T47 B1(1) (cool/dry).

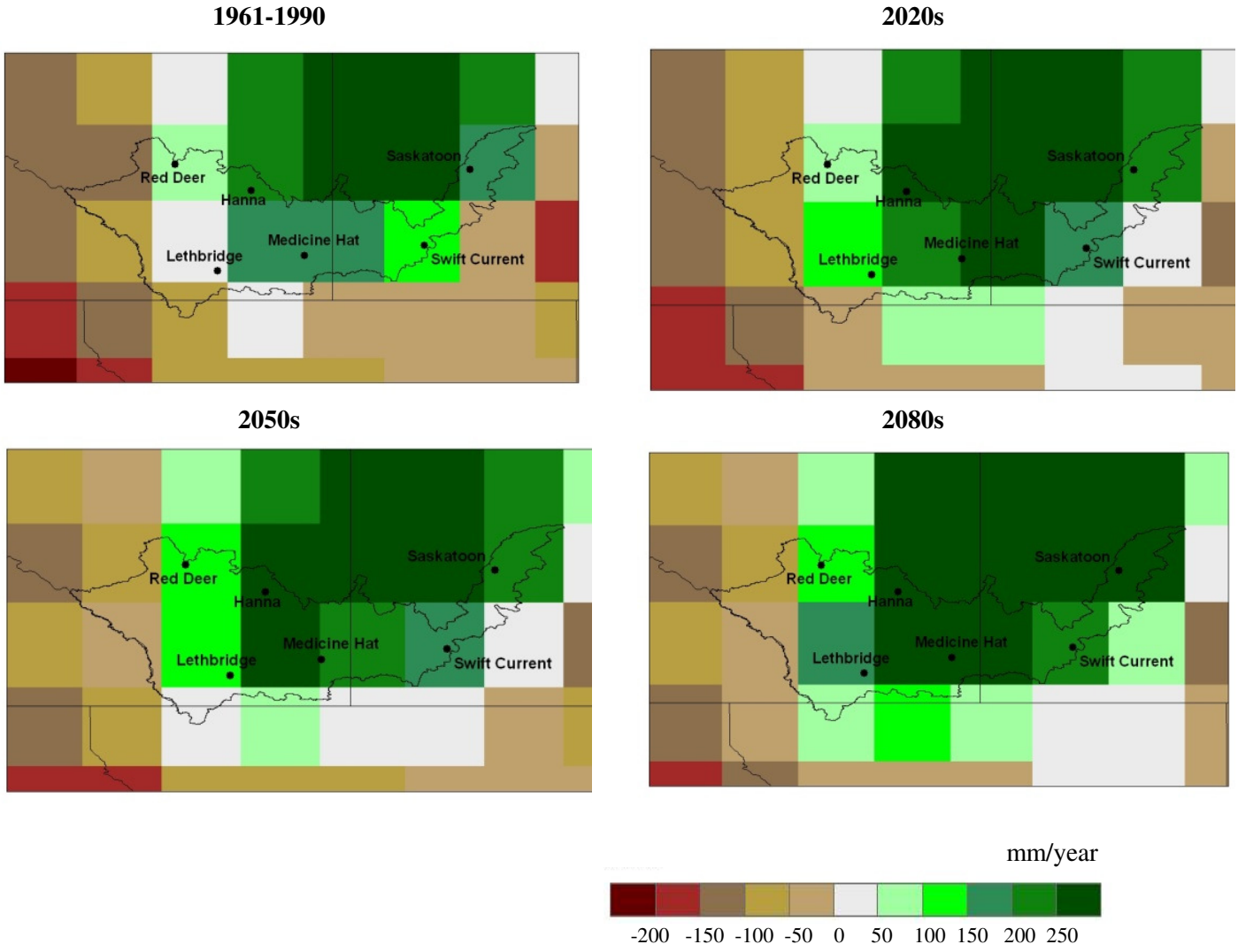

Figure 26. Scenarios of Climate Moisture Index for the 1961-1990, 2020s, 2050s and 2080s, July-June period using the CSIRO MK3.0 A1B(1) (cool/wet).

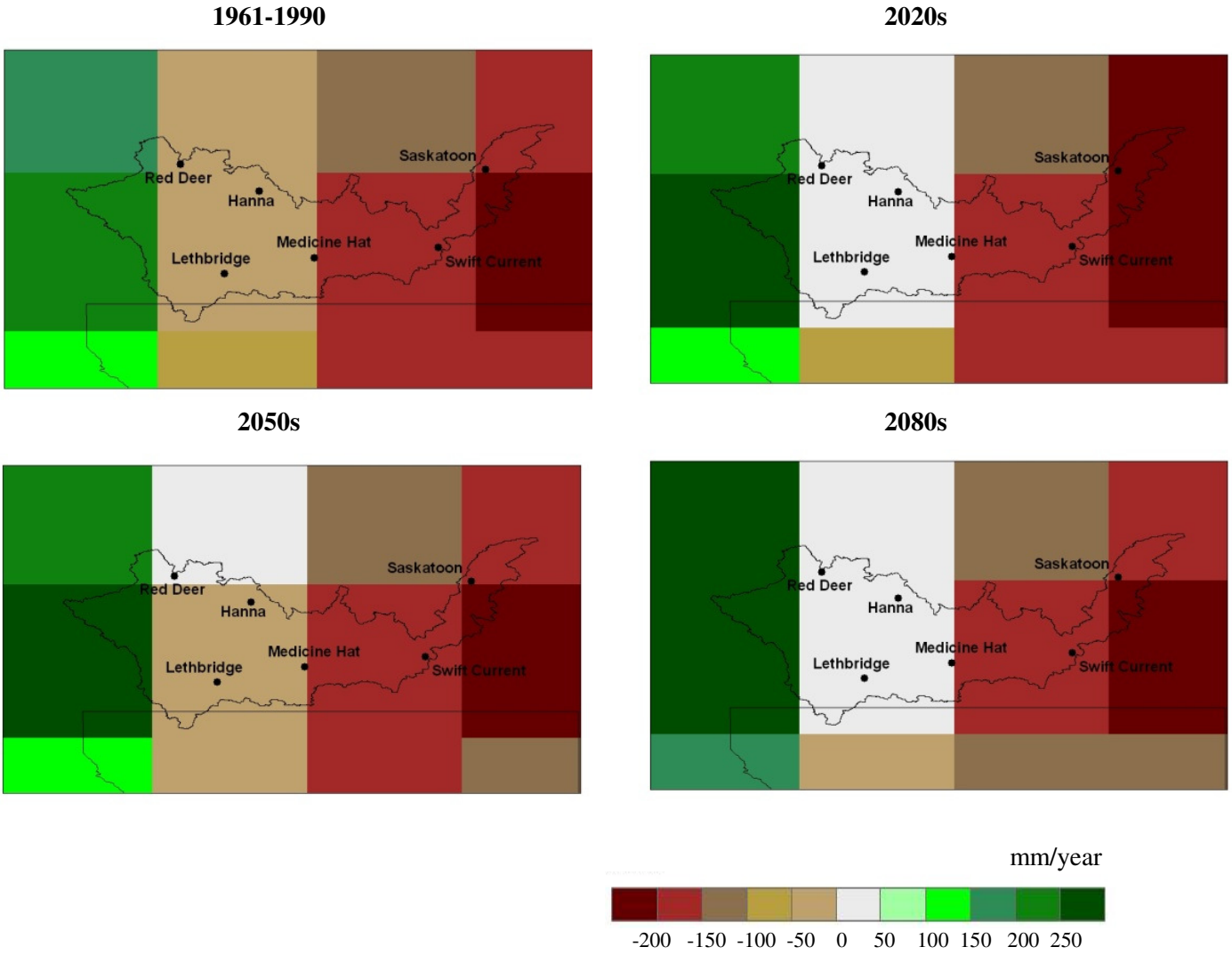

Figure 27. Scenarios of Climate Moisture Index for the 1961-1990, 2020s, 2050s and 2080s, July-June period using the CGCM3.1/T47 B1(2) (median).

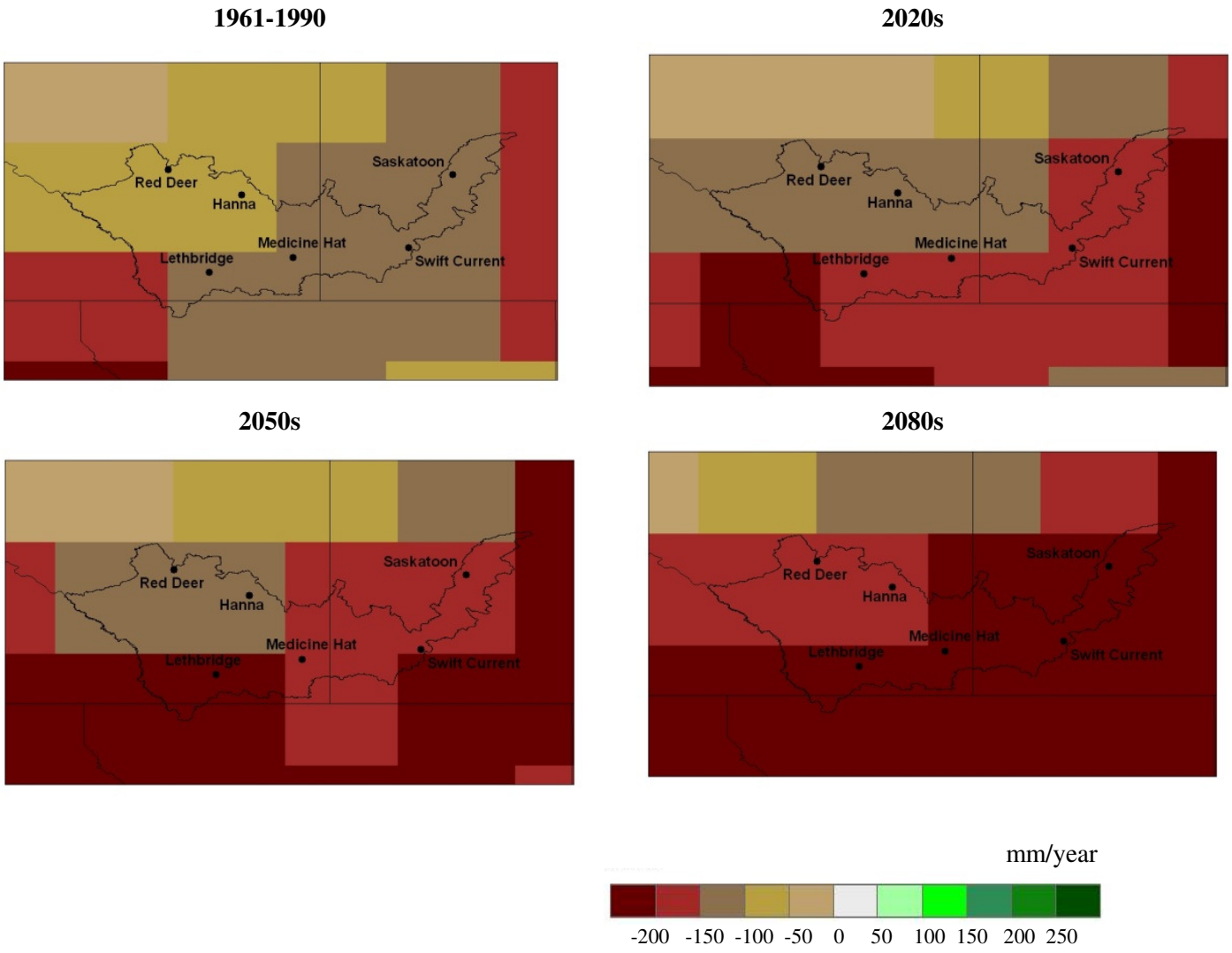

Figure 28. Scenarios of Climate Moisture Index for the 1961-1990, 2020s, 2050s and 2080s, May-June-July period using the MIROC3.2 MEDRES A2(1) (warm/dry) .

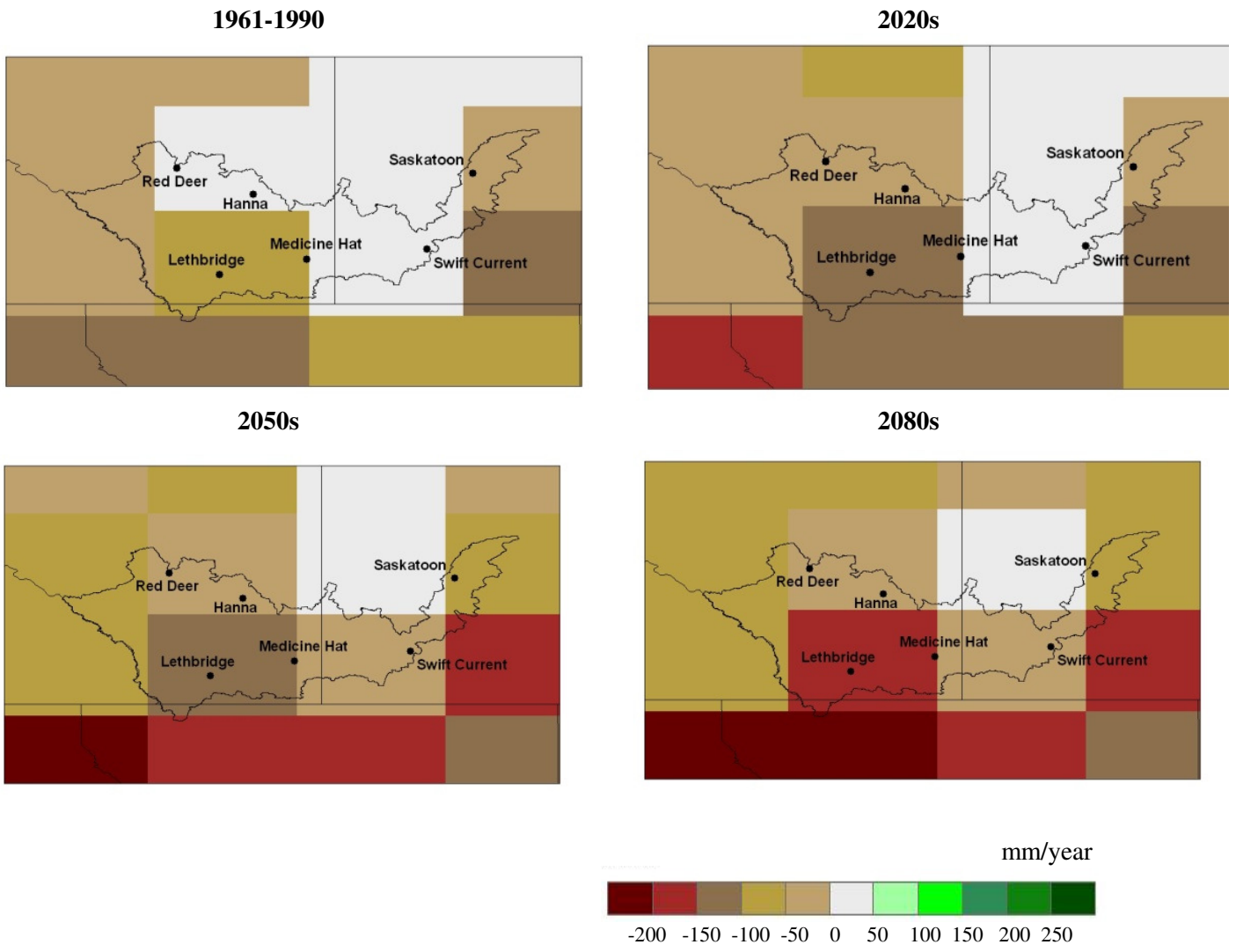

Figure 29. Scenarios of Climate Moisture Index for the 1961-1990, 2020s, 2050s and 2080s, May-June-July period using the HadCM3 TAR A2(a) (warm/wet).

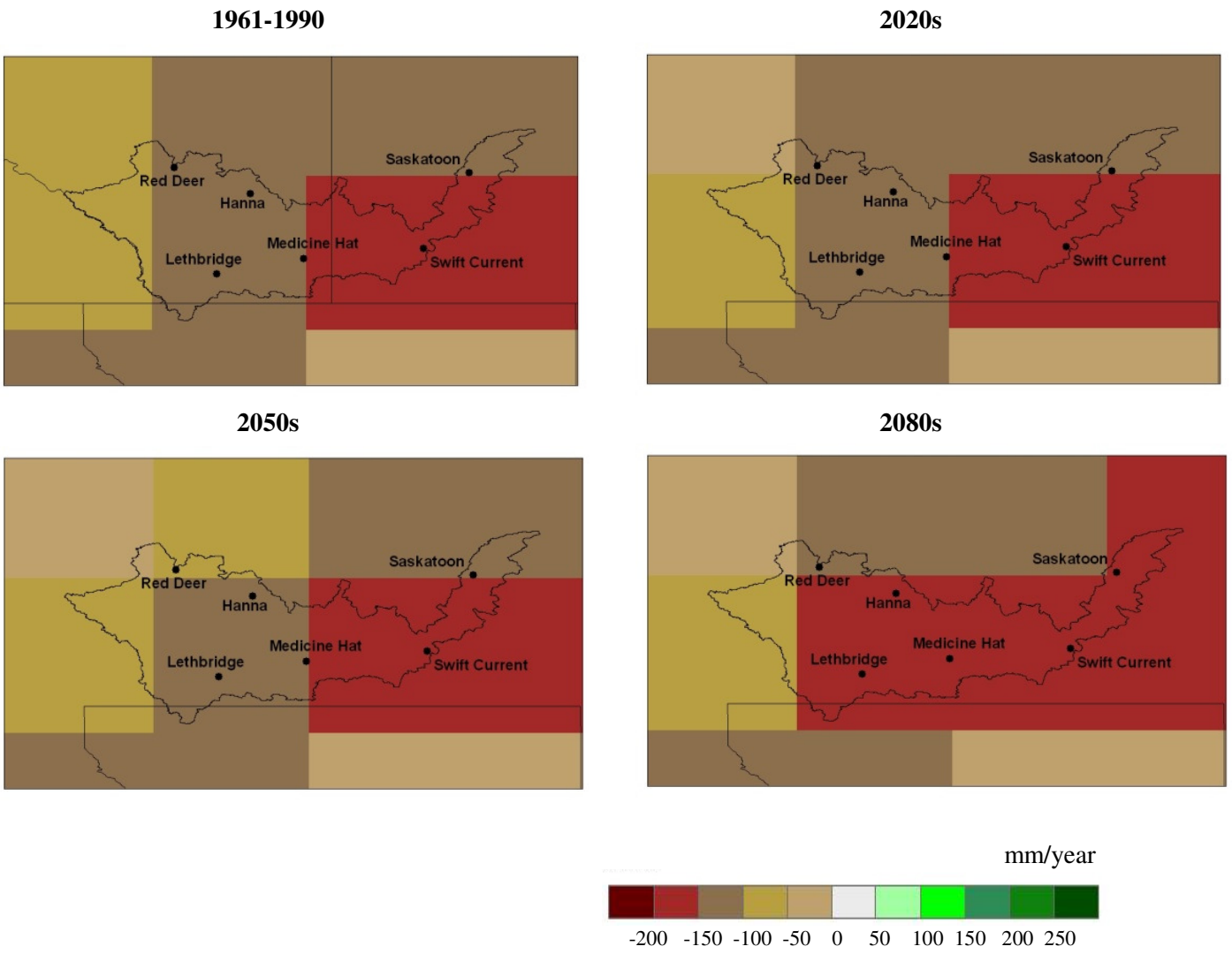

Figure 30. Scenarios of Climate Moisture Index for the 1961-1990, 2020s, 2050s and 2080s, May-June-July period using the CGCM3.1/T47 B1(1) (cool/dry).

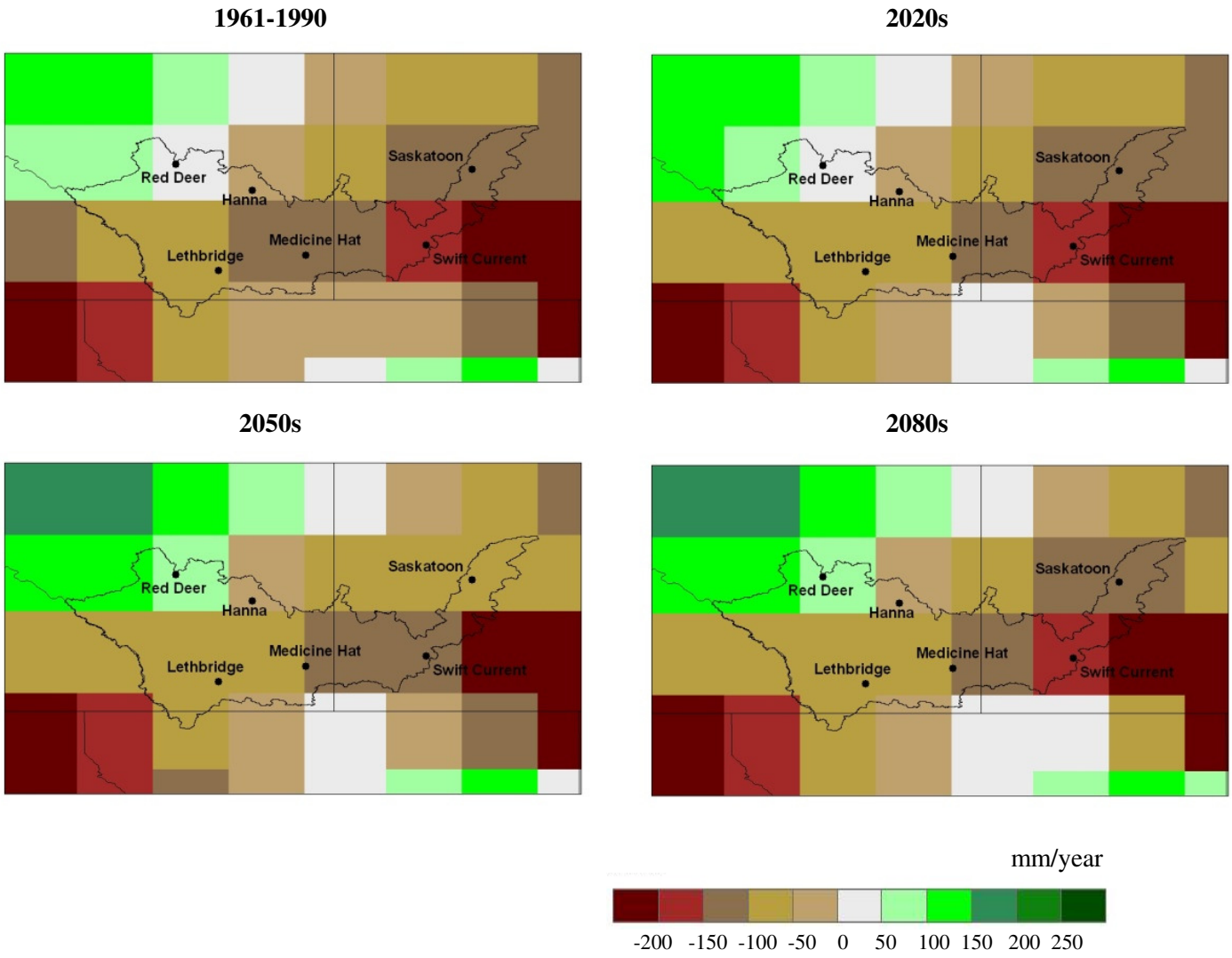

Figure 31. Scenarios of Climate Moisture Index for the 1961-1990, 2020s, 2050s and 2080s, May-June-July period using the CSIRO MK3.0 A1B(1) (cool/wet).

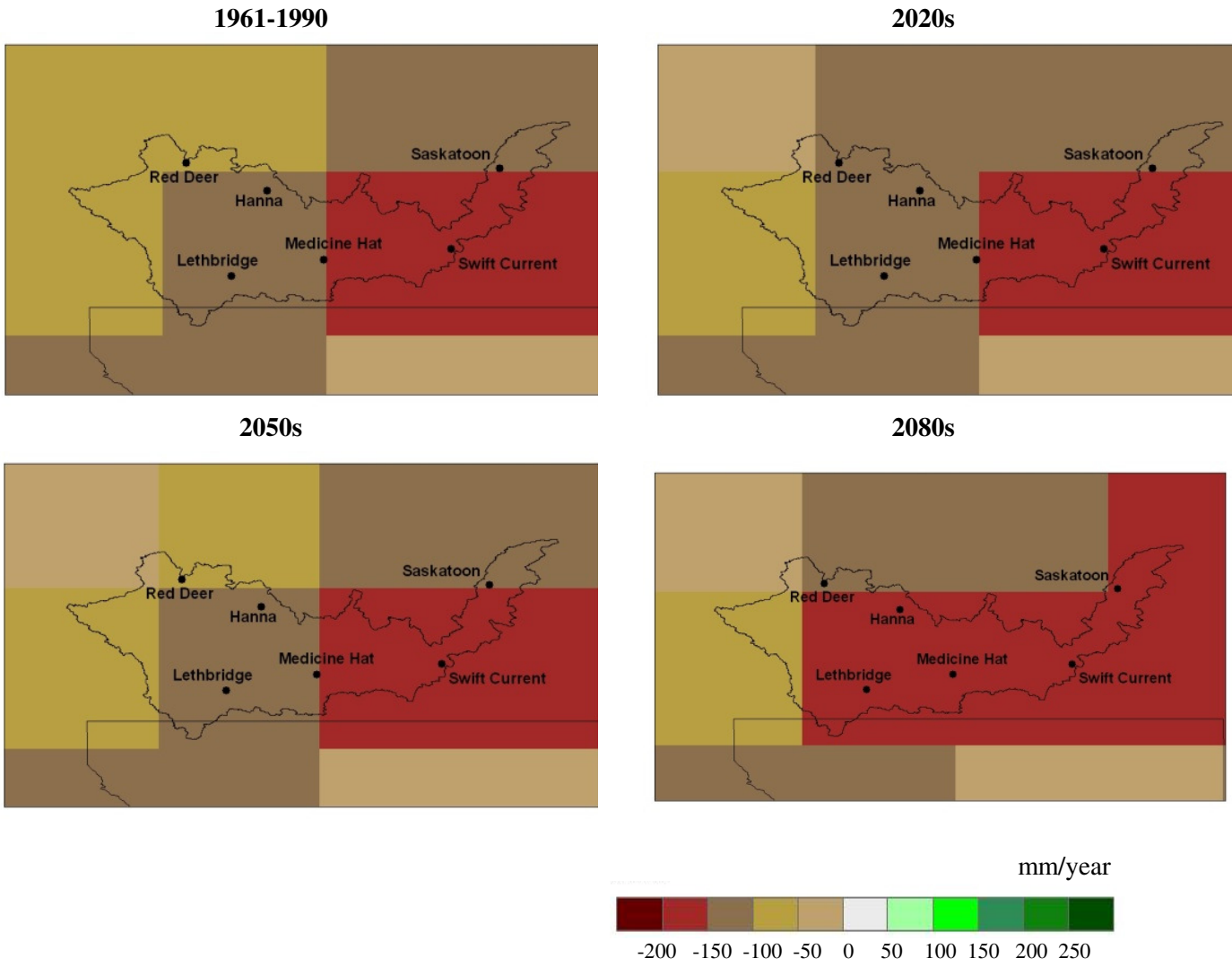

Figure 32. Scenarios of Climate Moisture Index for the 1961-1990, 2020s, 2050s and 2080s, May-June-July period using the CGCM3.1/T47 B1(2) (median).

Future Summer and Annual Drought Scenarios

Drought scenarios were derived for the season of May-June-July (MJJ) and annually for the July-June period (annual growing season) using the Climate Moisture Index. Moderate droughts were defined as events below the 20th percentile using 1961-90 period. The change in total area of land under moderate drought conditions was also analyzed for the future time periods relative to the baseline period. Table 2 shows the percentage of land considered in the moderate drought stage in the SSRB, below the 20th percentile, for the three future time periods and for both seasons. The area of land for the 1961-90 period below moderate drought conditions is not shown as the 20th percentile simply means that 20% (84 000 km^2) of the total area (420 000 km^2) is under drought conditions for this time period. It's important to note that the climate models do not simulate consistent increases or decreases in the total area of land under drought conditions for the three future time periods because they incorporate natural variability of wet and dry cycles and the influence of anthropogenic forcings of climate variability.

For the MJJ season the CSIRO A1B(1) is the only model showing a decrease in the total area of land under moderate drought conditions for the three future time periods. The MIROC A2(1) model shows the most extreme changes; by the 2050's and 2080's almost 50% and 90% of the land, respectively, is in moderate drought conditions . The HadCM3 A2(1) shows the next greatest increases in percent of land in a drought state with the 2020s having 31% and the 2050s and 2080s just over 50% of the total area under moderate drought conditions. CGCM3 b1(1) and CGCM3 b1(2) show similar areas for the 2020s and 2080s with slight increases; however the B1(1) scenarios shows an increase during the 2050s up to 32% of the land compared to the B1(2) scenario which is comparable to the baseline area.

The total area of land below the 20th percentile for the annual (July-June) period and the five scenarios shows similarities and differences relative to the MJJ period. Again the MIROC A2(1) and HadCM3 A2(2) scenarios show increases in total land area for each of the future time periods. The other three models project decreases in the total area of land under moderate drought conditions, except for the 2050s where CGCM3 B1(1) projects the same as for the baseline value. The difference between the annual and seasonal MJJ total land area change relates to the increased winter precipitation offsetting the decreased annual P-PET compared to the MJJ season which is reflecting the increase in temperature and more variable precipitation amounts. It is important to recognize that even though three models are simulating a decrease in total area of land in moderate or less severe than moderate drought conditions,

some of the precipitation that once accumulated as snow throughout the winter season will be received in the form of rain which will impact runoff and availability of water for storage and use through the summer season. The decrease in summer moisture is important for those that rely on natural precipitation not from an irrigation source.

Table 2. Average percent (%) of area below moderate drought conditions (20th) percentile for the MJJ and July-June period for the future time periods in the SSRB.

MJJ

	CGCM3 b11	CGCM3 b12	CSIRO A1B1	HadCM3 A21	Miroc A21
2010-39	24	25	19	31	49
2040-69	32	21	14	51	68
2070-99	25	25	18	55	90

July-June

	CGCM3 b11	CGCM3 b12	CSIRO A1B1	HadCM3 A21	Miroc A21
2010-39	18	15	12	25	50
2040-69	22	14	14	43	62
2070-99	17	12	16	51	89

Climate Scenarios for the SSRB

Temperature and Precipitation

Future scenarios of seasonal and annual temperature and precipitation were also derived from each the five climate models and regridded to the 0.5 ^{o} x 0.5^{o} grid for the 2050s. Figures 33-37 shows the winter, spring, summer, fall and annual temperature (^{o}C) for the 2050s and the observed baseline conditions, respectively and Figures 38-42 show the projected precipitation for the same time and period. These climate scenarios were derived by simply adding (ratio) the climate change scenario to the observed baseline conditions to give a range of future projected temperatures (precipitation) for the 2050s season. These climate scenarios allow us to assign to the future climate temperature or precipitation values rather than just changes relative to each model. For example the MIROC MEDRES A2(a) and HadCM3 TAR A2(2) are the warm scenarios and are distinguishable from the cool CGCM3.1/T47 B1(1) and CSIRO MK3.0 A1B(1) climate models simply based on the colour schemes. Similar differences in projections are evident in Figure 40 between the dry CGCM3.1/T47 B1(1) and wet CSIRO MK3.0 A1B(1) for the summer season.

MIROC3.2 MEDRES A2(1) (warm/dry)

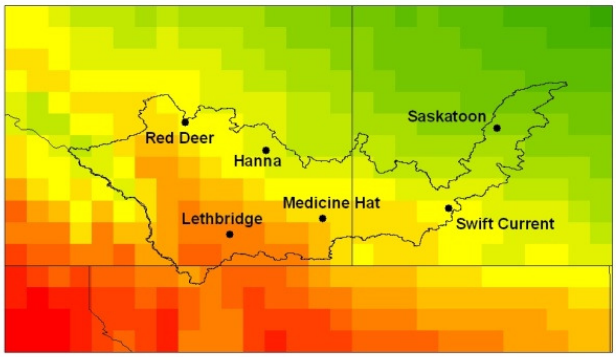

HadCM3 TAR A2(a) (warm/wet)

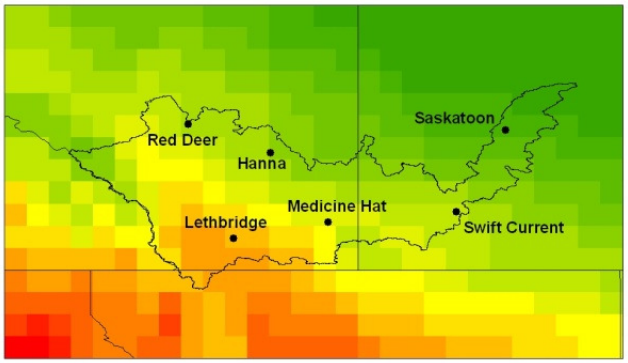

CGCM3.1/T47 B1(1) (cool/dry)

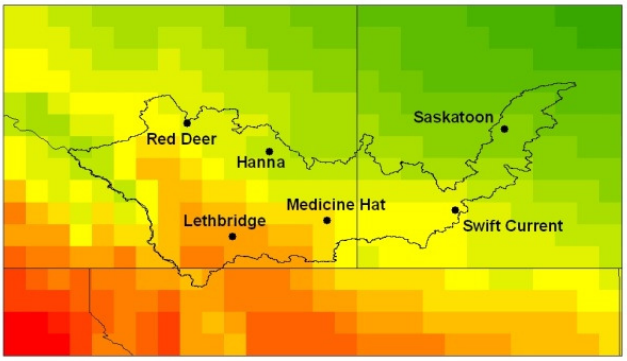

CSIRO MK3.0 A1B(1) (cool/wet)

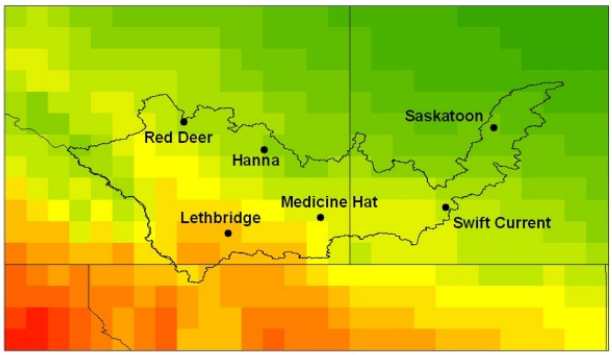

CGCM3.1/T47 B1(2) (median)

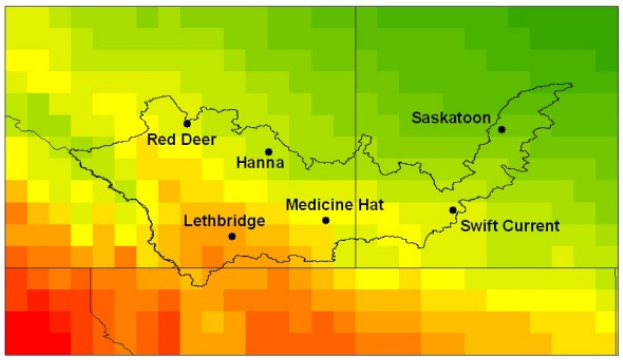

1961-1990

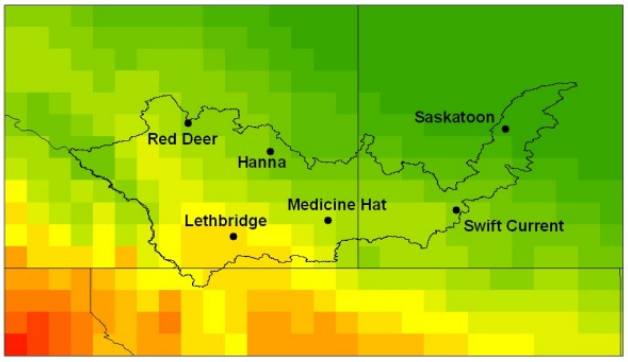

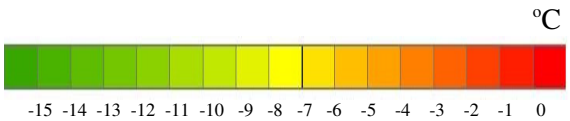

Figure 33. Winter (DJF) mean temperature (°C) scenario for the 2050s.

MIROC3.2 MEDRES A2(1) (warm/dry)

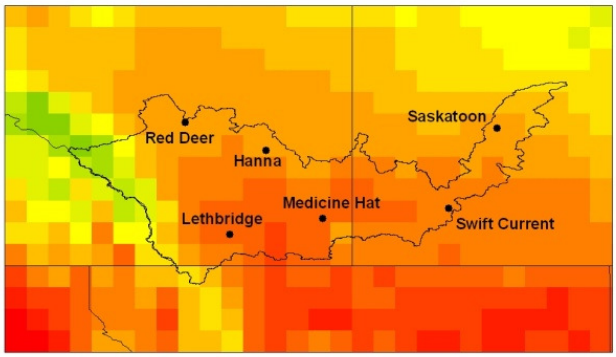

HadCM3 TAR A2(a) (warm/wet)

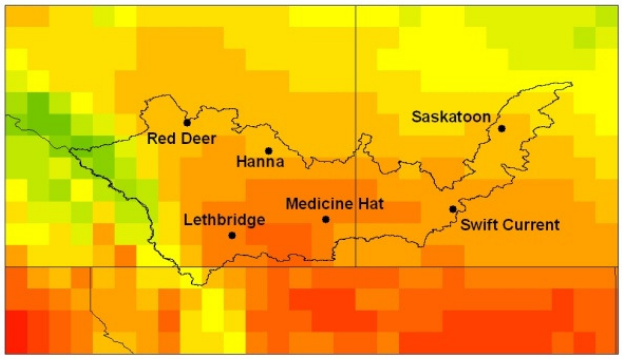

CGCM3.1/T47 B1(1) (cool/dry)

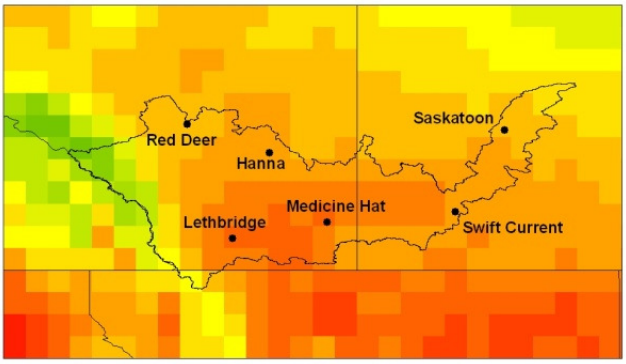

CSIRO MK3.0 A1B(1) (cool/wet)

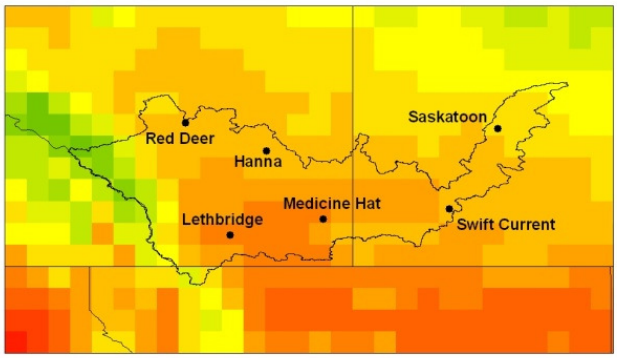

CGCM3.1/T47 B1(2) (median)

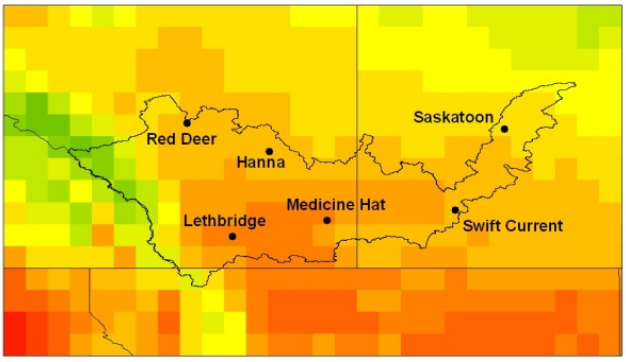

1961-1990

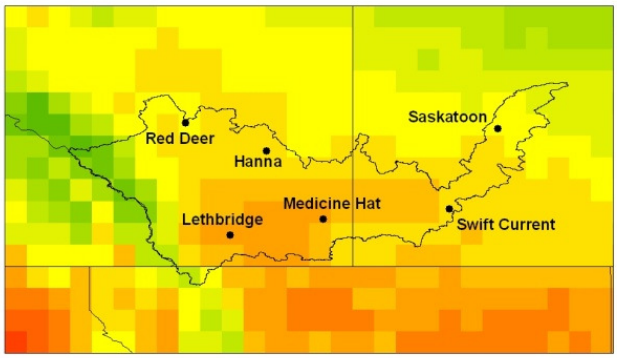

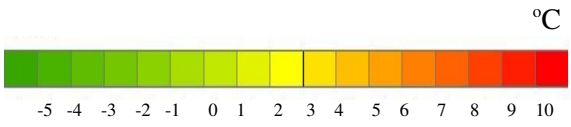

Figure 34. Spring (MAM) mean temperature (°C) scenario for the 2050s.

MIROC3.2 MEDRES A2(1) (warm/dry)

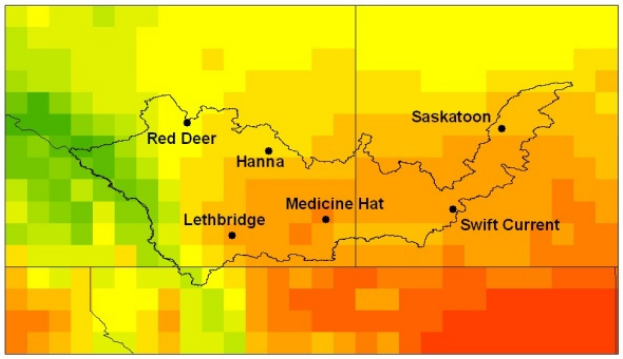

HadCM3 TAR A2(a) (warm/wet)

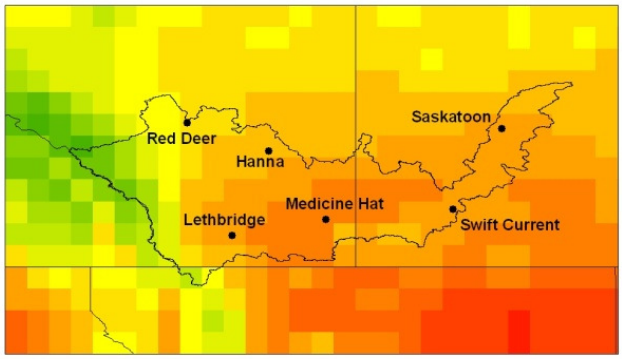

CGCM3.1/T47 B1(1) (cool/dry)

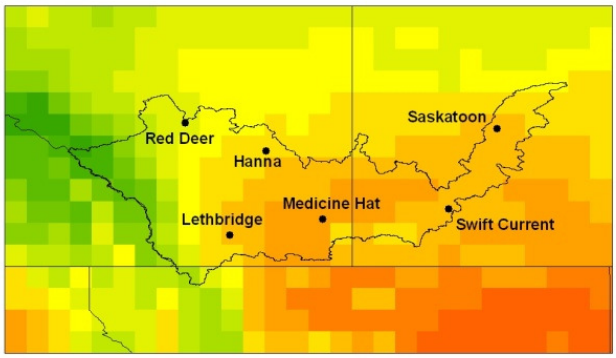

CSIRO MK3.0 A1B(1) (cool/wet)

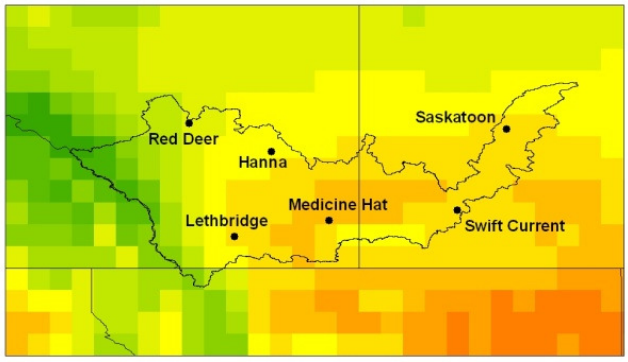

CGCM3.1/T47 B1(2) (median)

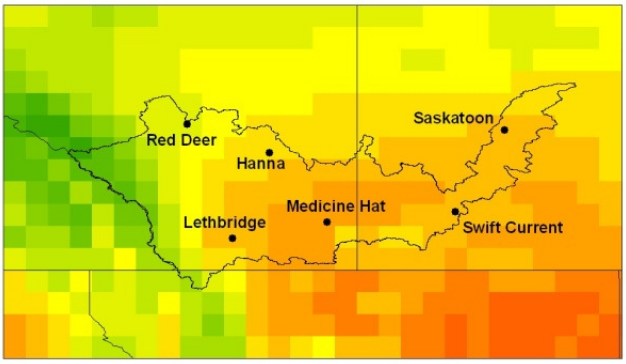

1961-1990

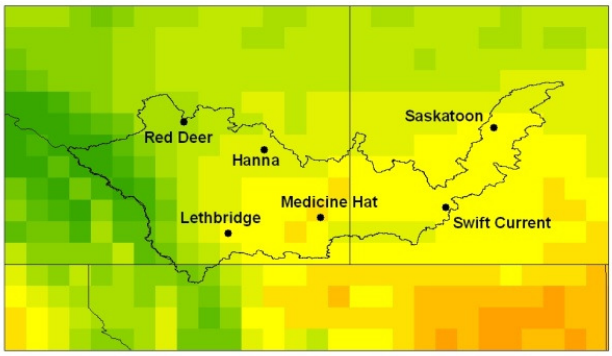

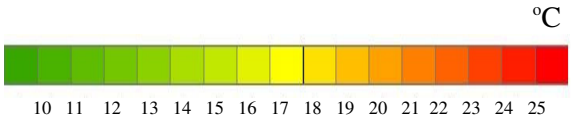

Figure 35. Summer (JJA) mean temperature (°C) scenario for the 2050s.

MIROC3.2 MEDRES A2(1) (warm/dry)

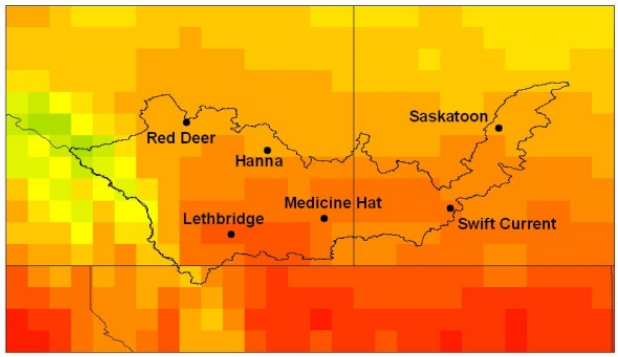

HadCM3 TAR A2(a) (warm/wet)

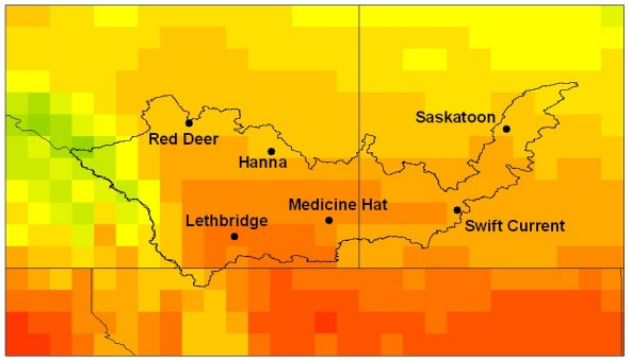

CGCM3.1/T47 B1(1) (cool/dry)

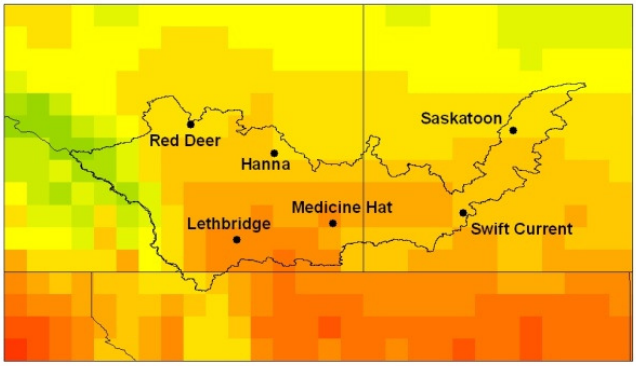

CSIRO MK3.0 A1B(1) (cool/wet)

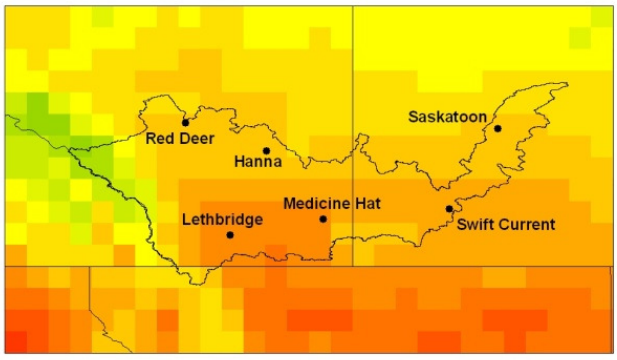

CGCM3.1/T47 B1(2) (median)

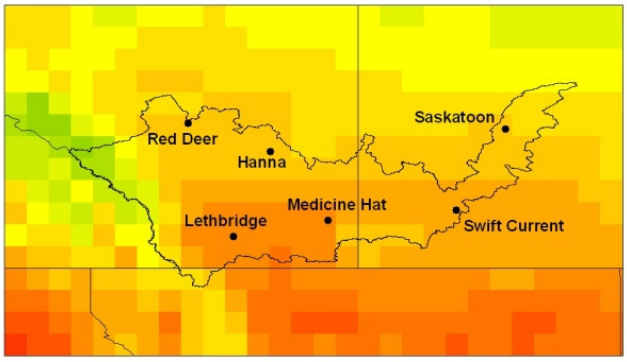

1961-1990

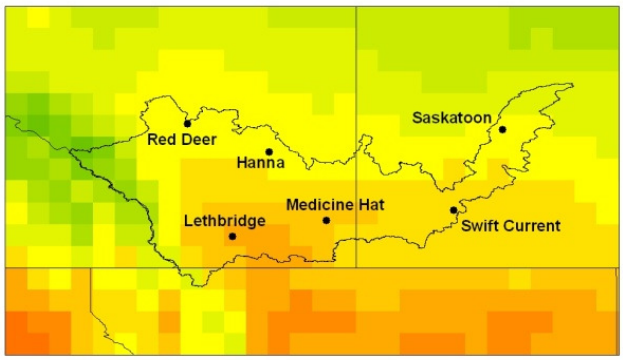

Figure 36. Fall (SON) mean temperature (°C) scenario for the 2050s.

MIROC3.2 MEDRES A2(1) (warm/dry)

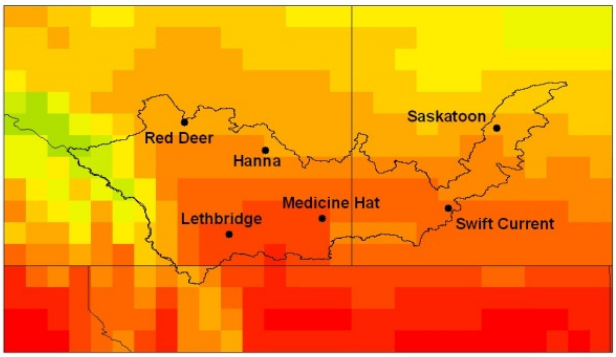

HadCM3 TAR A2(a) (warm/wet)

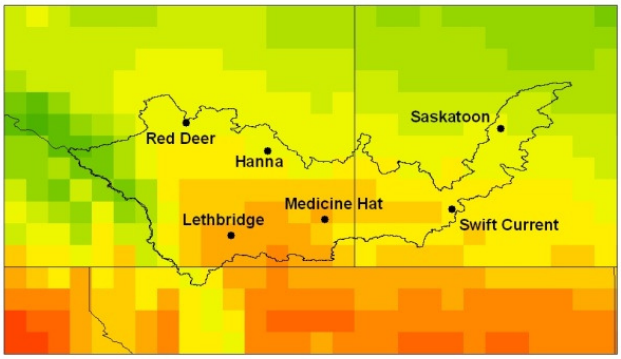

CGCM3.1/T47 B1(1) (cool/dry)

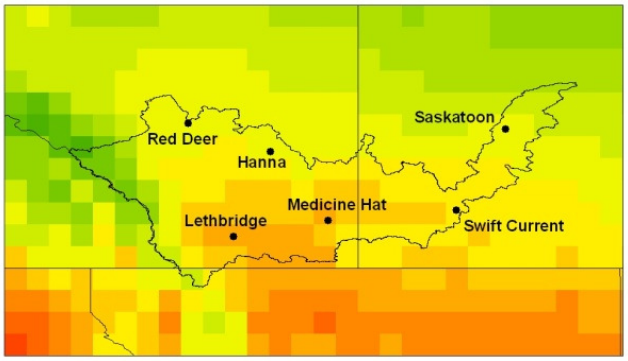

CSIRO MK3.0 A1B(1) (cool/wet)

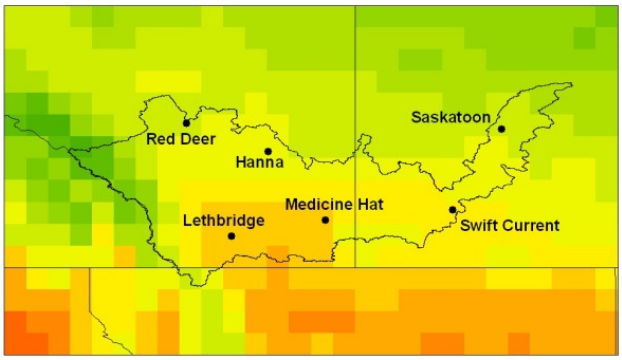

CGCM3.1/T47 B1(2) (median)

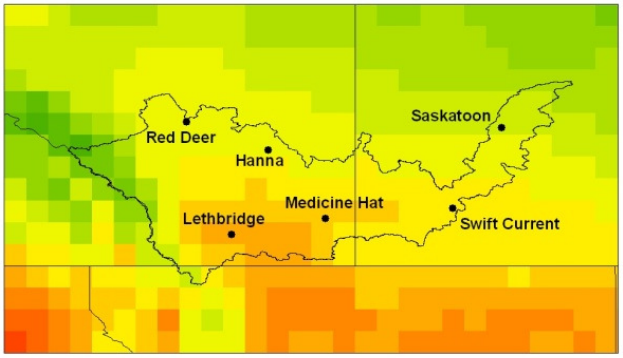

1961-1990

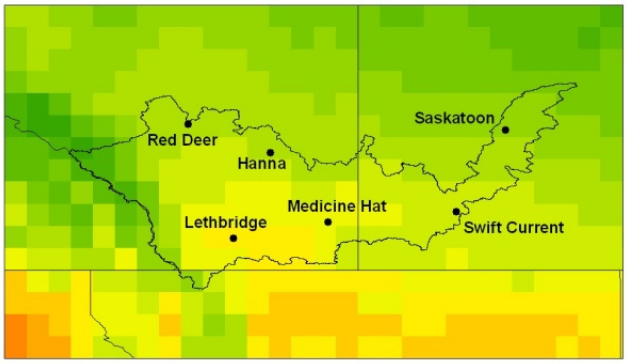

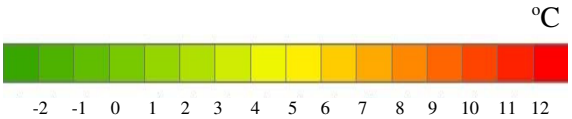

Figure 37. Annual mean temperature (°C) scenario for the 2050s.

MIROC3.2 MEDRES A2(1) (warm/dry)

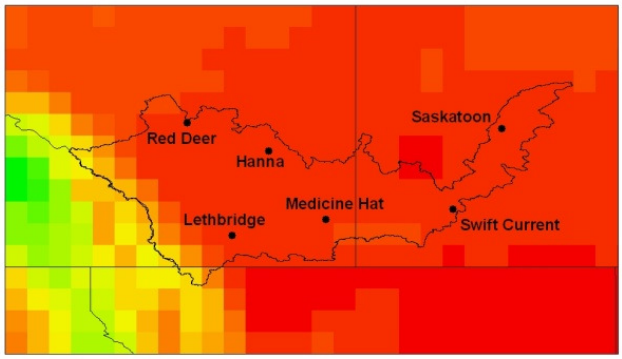

HadCM3 TAR A2(a) (warm/wet)

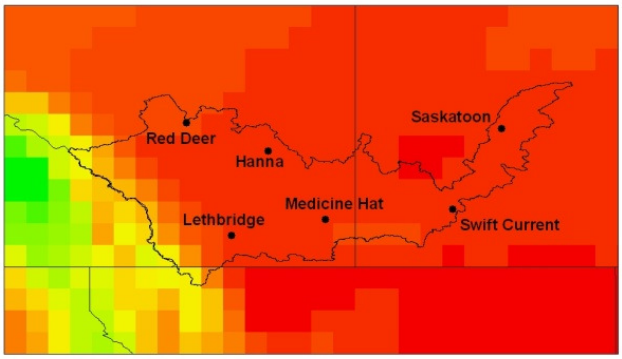

CGCM3.1/T47 B1(1) (cool/dry)

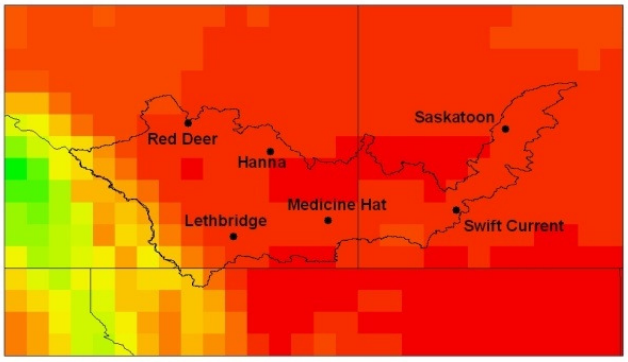

CSIRO MK3.0 A1B(1) (cool/wet)

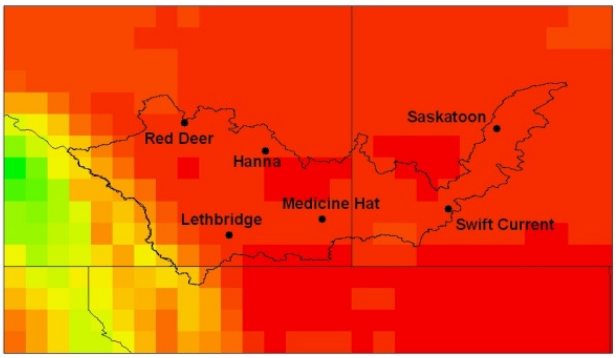

CGCM3.1/T47 B1(2) (median)

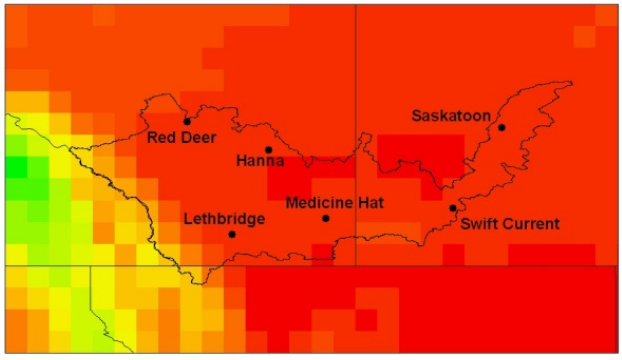

1961-1990

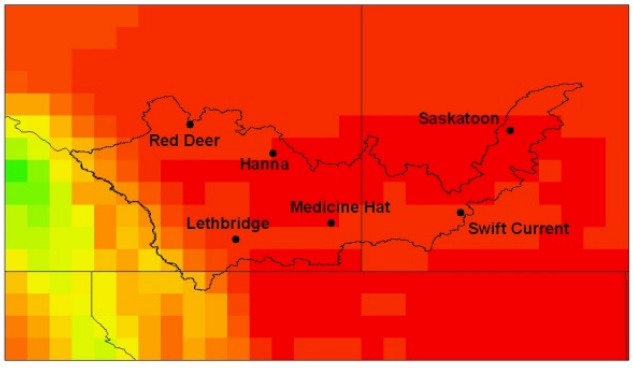

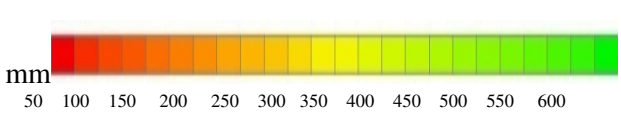

Figure 38. Winter (DJF) precipitation (mm) scenario for the 2050s.

MIROC3.2 MEDRES A2(1) (warm/dry)

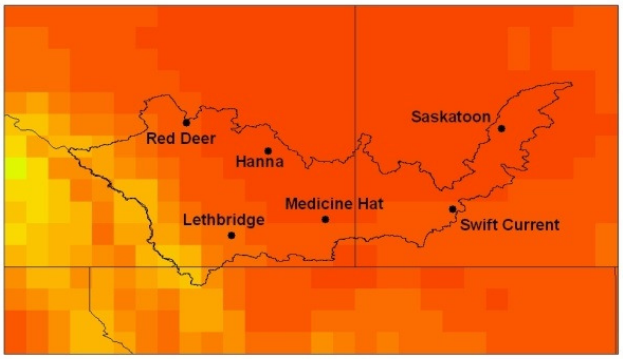

HadCM3 TAR A2(a) (warm/wet)

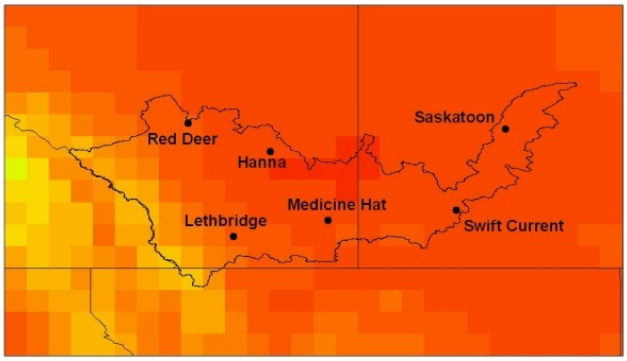

CGCM3.1/T47 B1(1) (cool/dry)

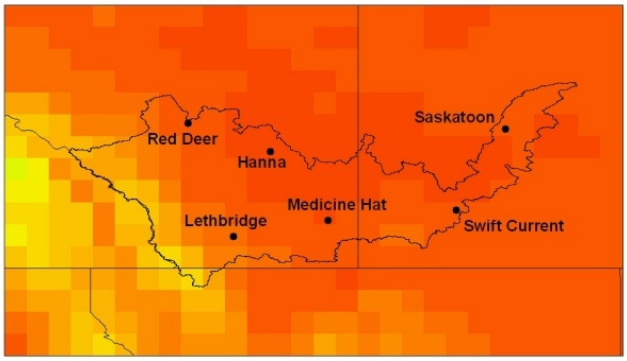

CSIRO MK3.0 A1B(1) (cool/wet)

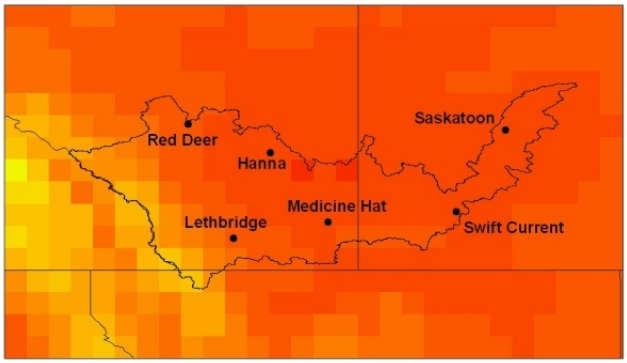

CGCM3.1/T47 B1(2) (median)

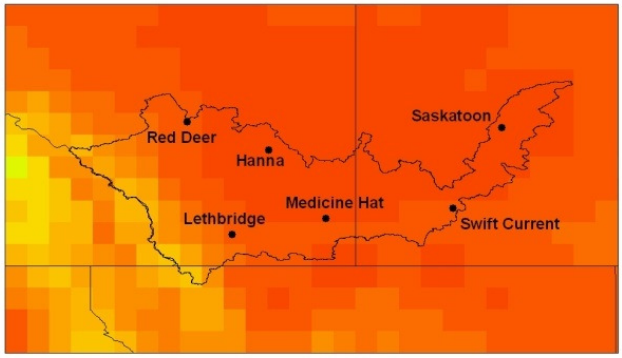

1961-1990

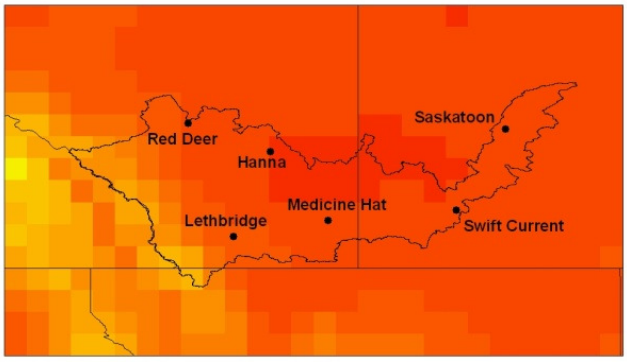

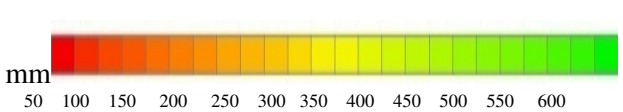

Figure 39. Spring (MAM) precipitation (mm) scenario for the 2050s.

MIROC3.2 MEDRES A2(1) (warm/dry)

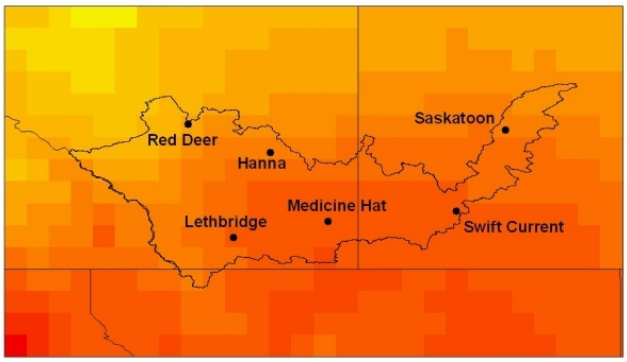

HadCM3 TAR A2(a) (warm/wet)

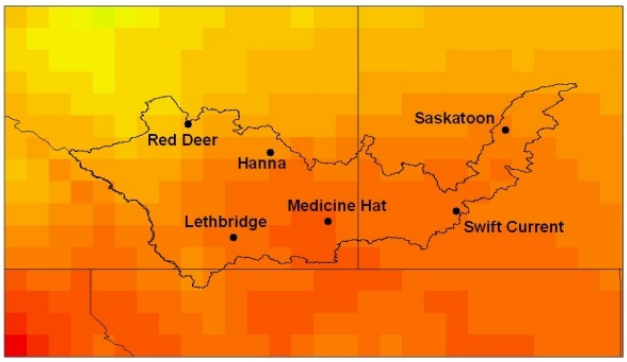

CGCM3.1/T47 B1(1) (cool/dry)

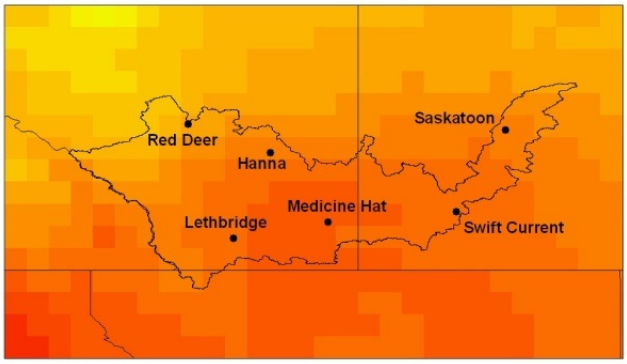

CSIRO MK3.0 A1B(1) (cool/wet)

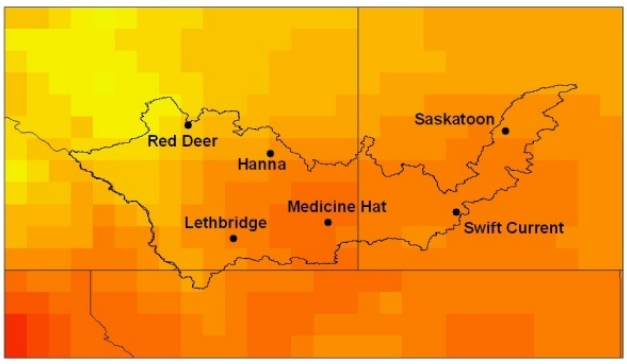

CGCM3.1/T47 B1(2) (median)

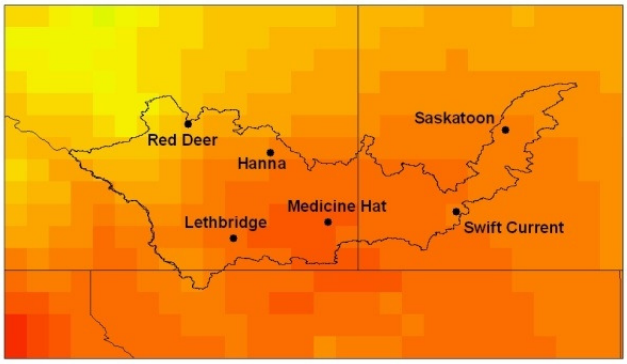

1961-1990

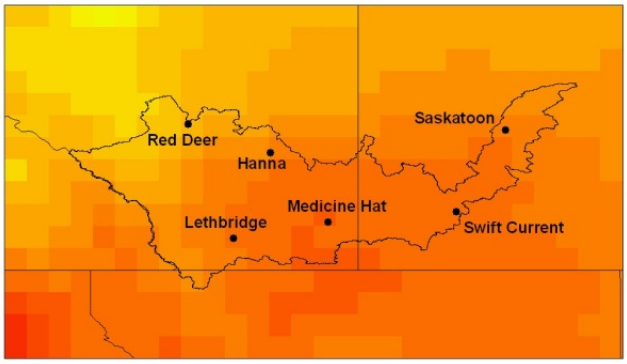

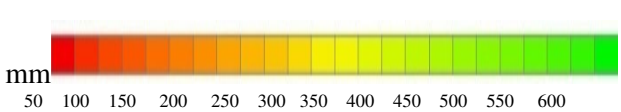

Figure 40. Summer (JJA) precipitation (mm) scenario for the 2050s.

MIROC3.2 MEDRES A2(1) (warm/dry)

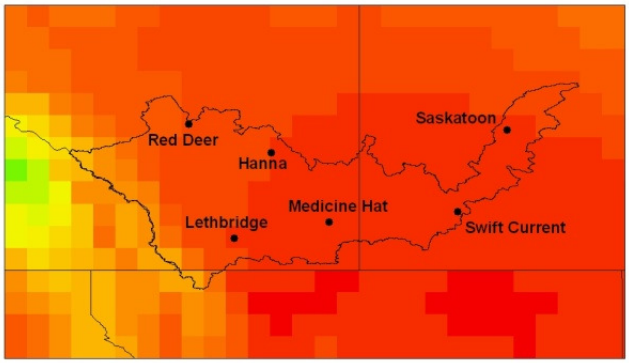

HadCM3 TAR A2(a) (warm/wet)

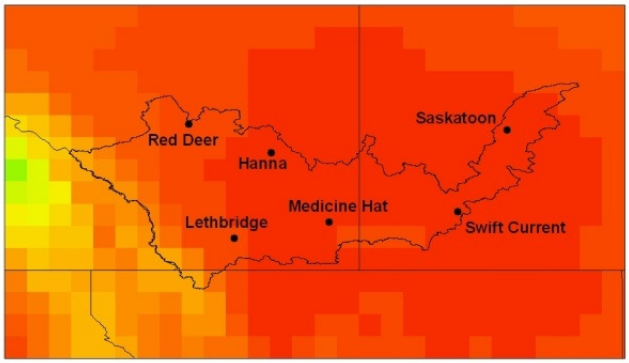

CGCM3.1/T47 B1(1) (cool/dry)

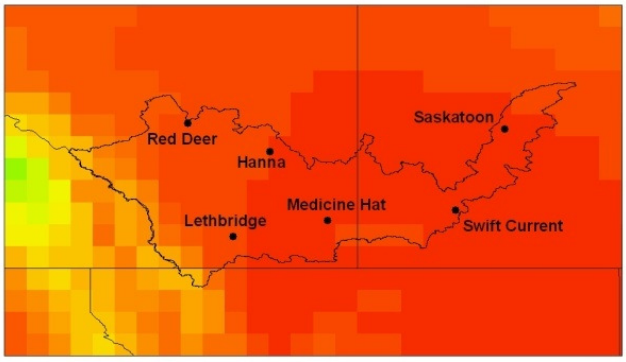

CSIRO MK3.0 A1B(1) (cool/wet)

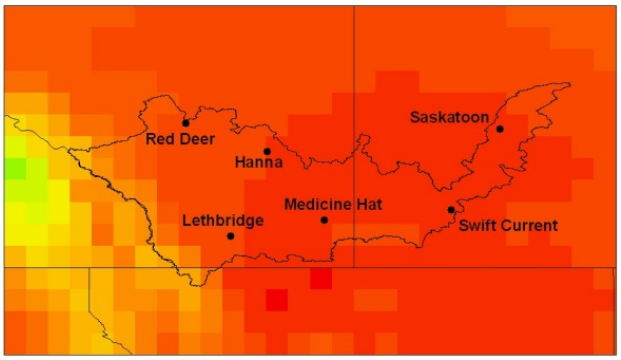

CGCM3.1/T47 B1(2) (median)

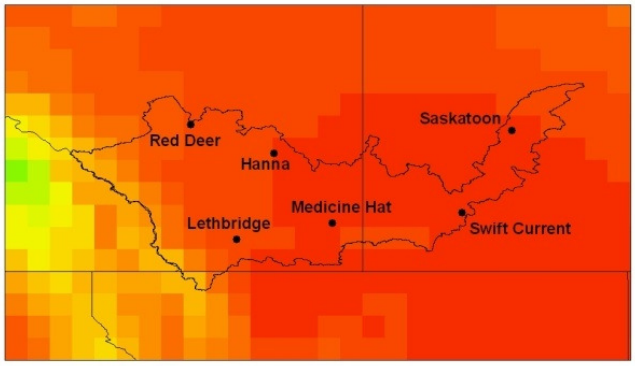

1961-1990

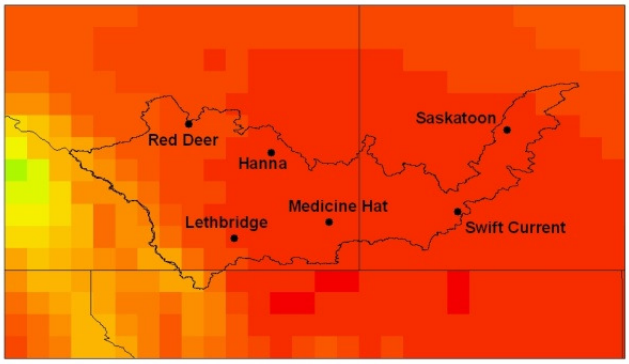

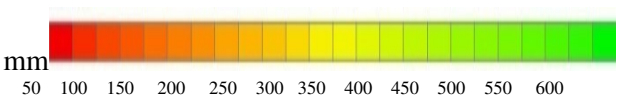

Figure 41. Fall (SON) precipitation (mm) scenario for the 2050s.

MIROC3.2 MEDRES A2(1) (warm/dry)

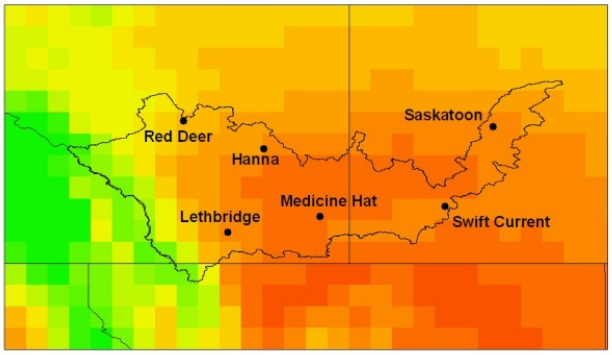

HadCM3 TAR A2(a) (warm/wet)

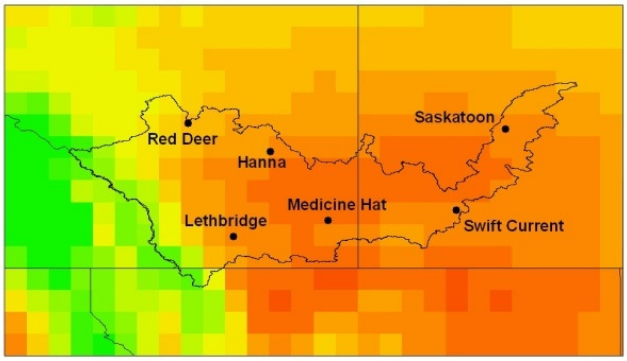

CGCM3.1/T47 B1(1) (cool/dry)

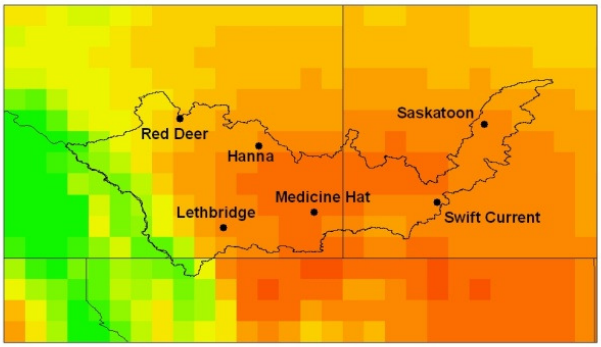

CSIRO MK3.0 A1B(1) (cool/wet)

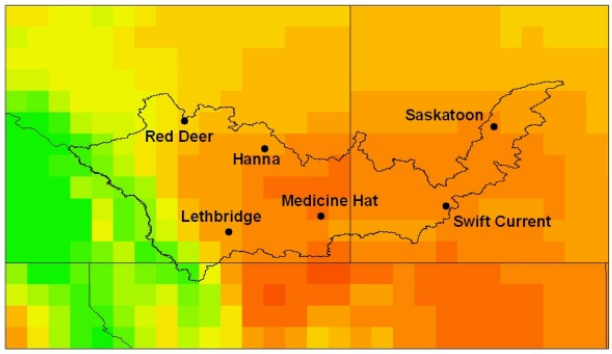

CGCM3.1/T47 B1(2) (median)

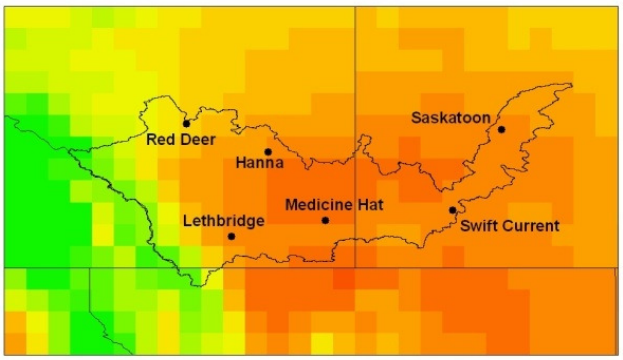

1961-1990

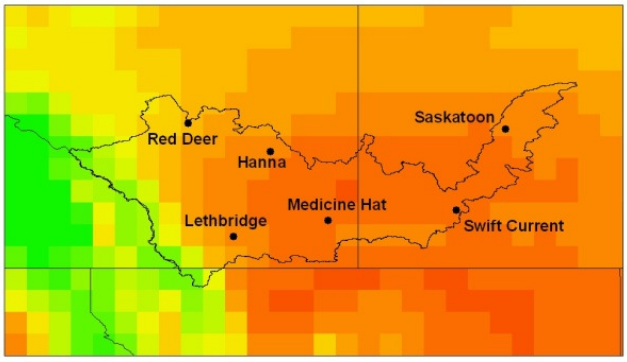

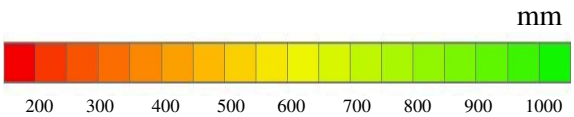

Figure 42. Annual precipitation (mm) scenario for the 2050s.

Five Study Site Climate Scenarios

Climate scenarios were also derived for the five studied communities using the local station or from one nearby that accurately represented the community. This allows for a more detailed analysis at the site level compared to the climate scenarios of the entire SSRB.

The GCM grid cells centered on Lethbridge, Red Deer and Medicine in Alberta and Swift Current and Saskatoon in Saskatchewan were selected for a more detailed analysis of future seasonal/annual minimum/maximum/mean temperature and precipitation scenarios (Figures 43-47, respectively) for the three future time periods. All of the stations have similar seasonal precipitation and temperature distribution, with summer having the greatest amount of precipitation and warmest temperatures; however the absolute values range with the southern stations receiving less precipitation and experiencing warmer temperatures overall. During winter and spring, increases in minimum temperature are greater than increases in maximum temperature. The southern stations (Medicine Hat, Swift Current and Lethbridge) experience the greatest increase in temperature both on a seasonal and annual basis but the northern stations (Red Deer and Saskatoon) have the greatest increase in annual precipitation relative to the southern stations.

Monthly scenarios of future precipitation show large changes in seasonal distributions at all sites projected by most models resulting in higher winter and lower summer precipitation and increased annual total precipitation. Future monthly uncertainty is highest during the late spring through summer and into early fall which is when most of the annual precipitation falls. This summer/fall extreme variability relative to winter is likely related to the weaknesses of the models' ability to simulate convective precipitation rather than frontal (Lin et al. 2008).

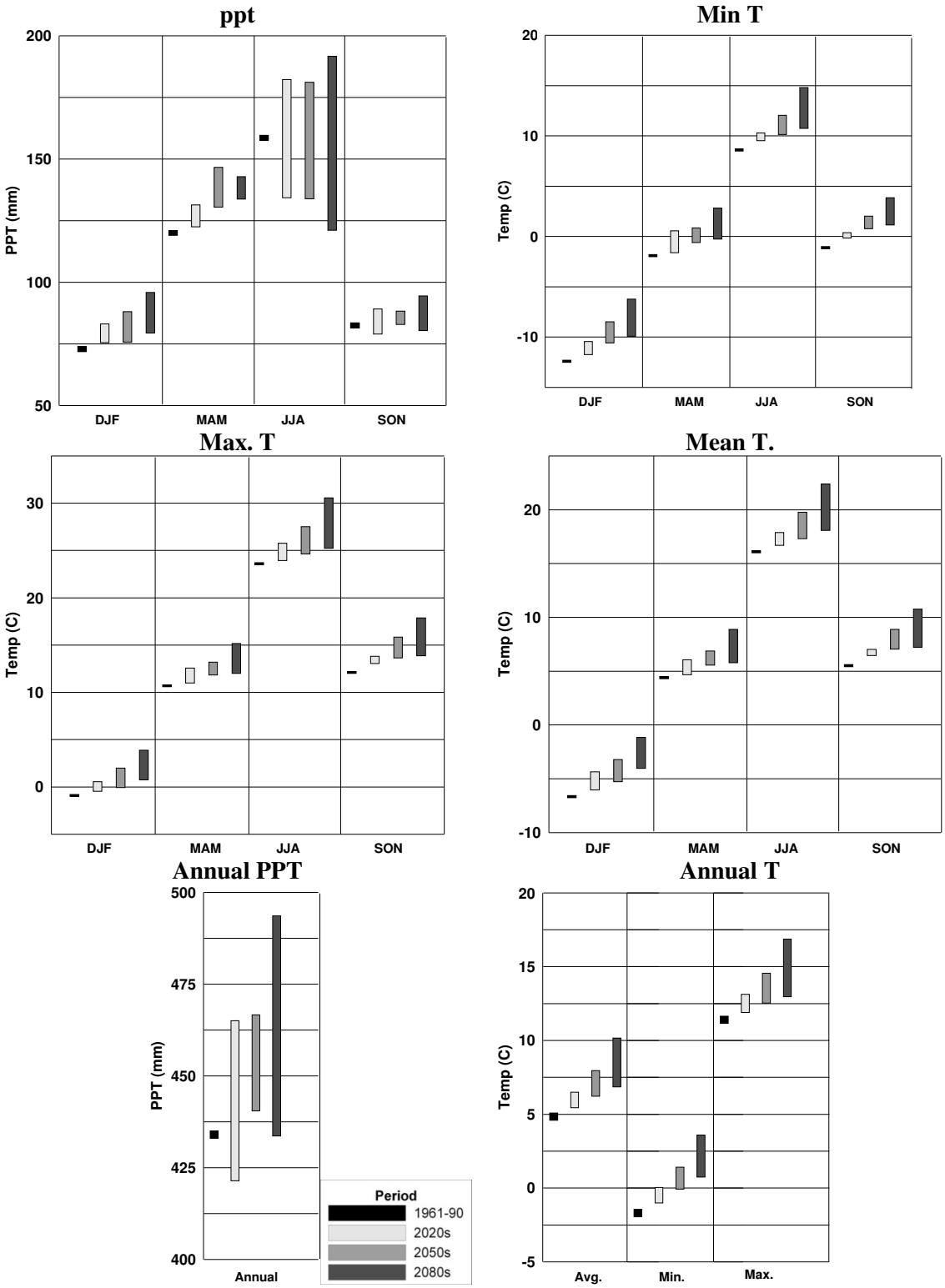

Figure 43. Lethbridge future climate scenarios based on 5 scenarios for each season, 2020s, 2050s and 2080s.

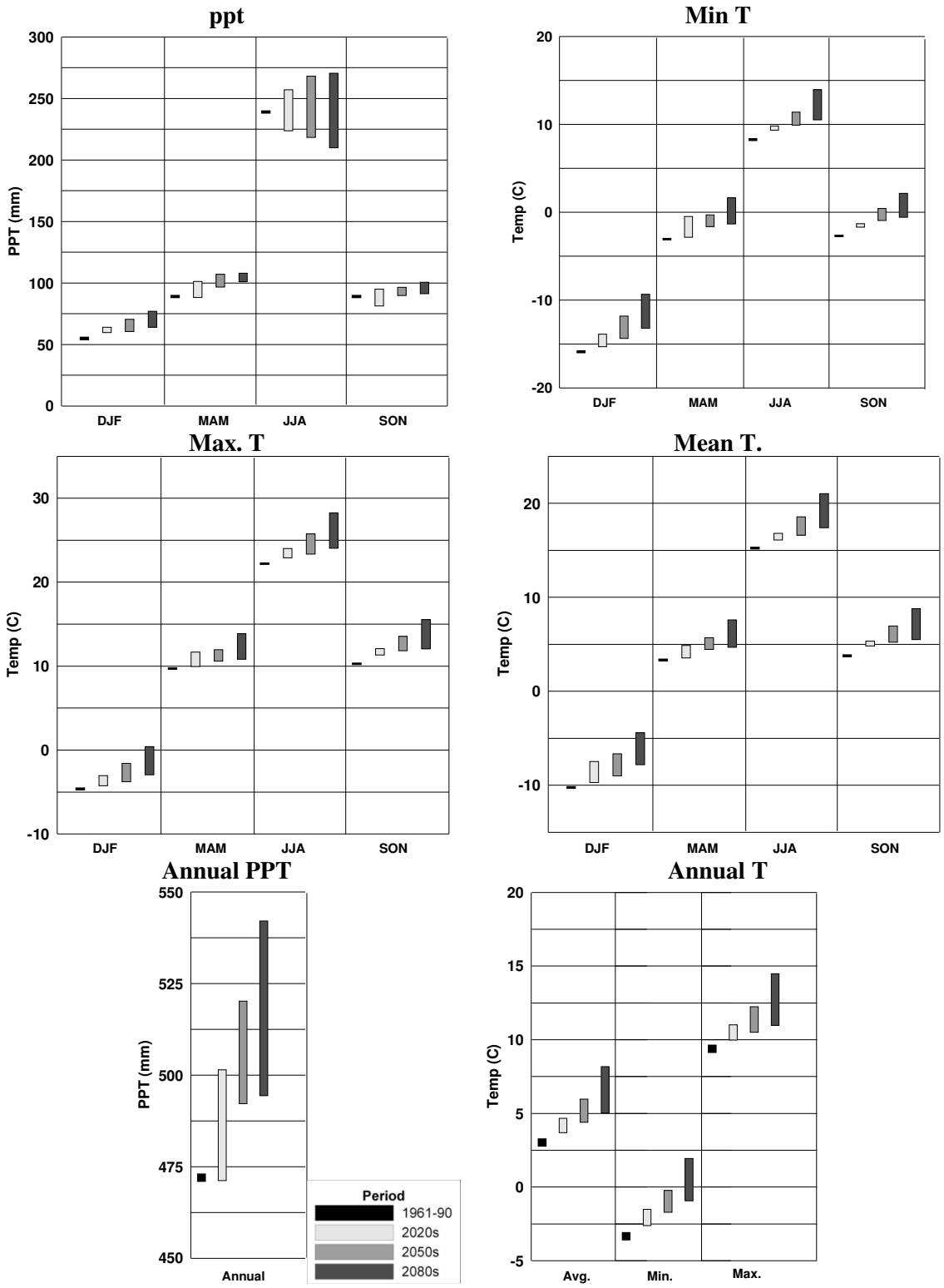

Figure 44. Red Deer future climate scenarios based on 5 scenarios for each season, 2020s, 2050s and 2080s.

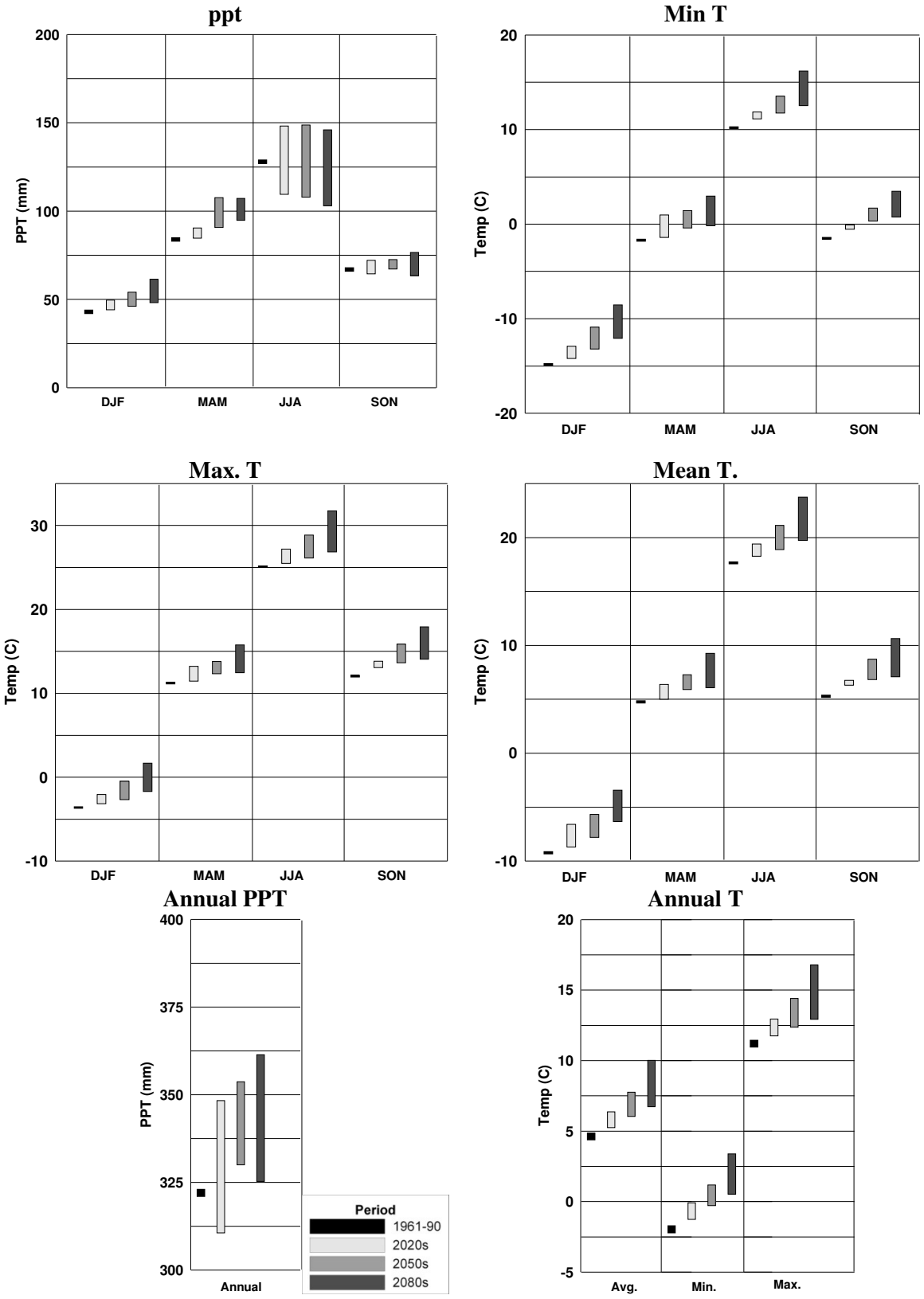

Figure 45. Medicine Hat future climate scenarios based on 5 scenarios for each season, 2020s, 2050s and 2080s.

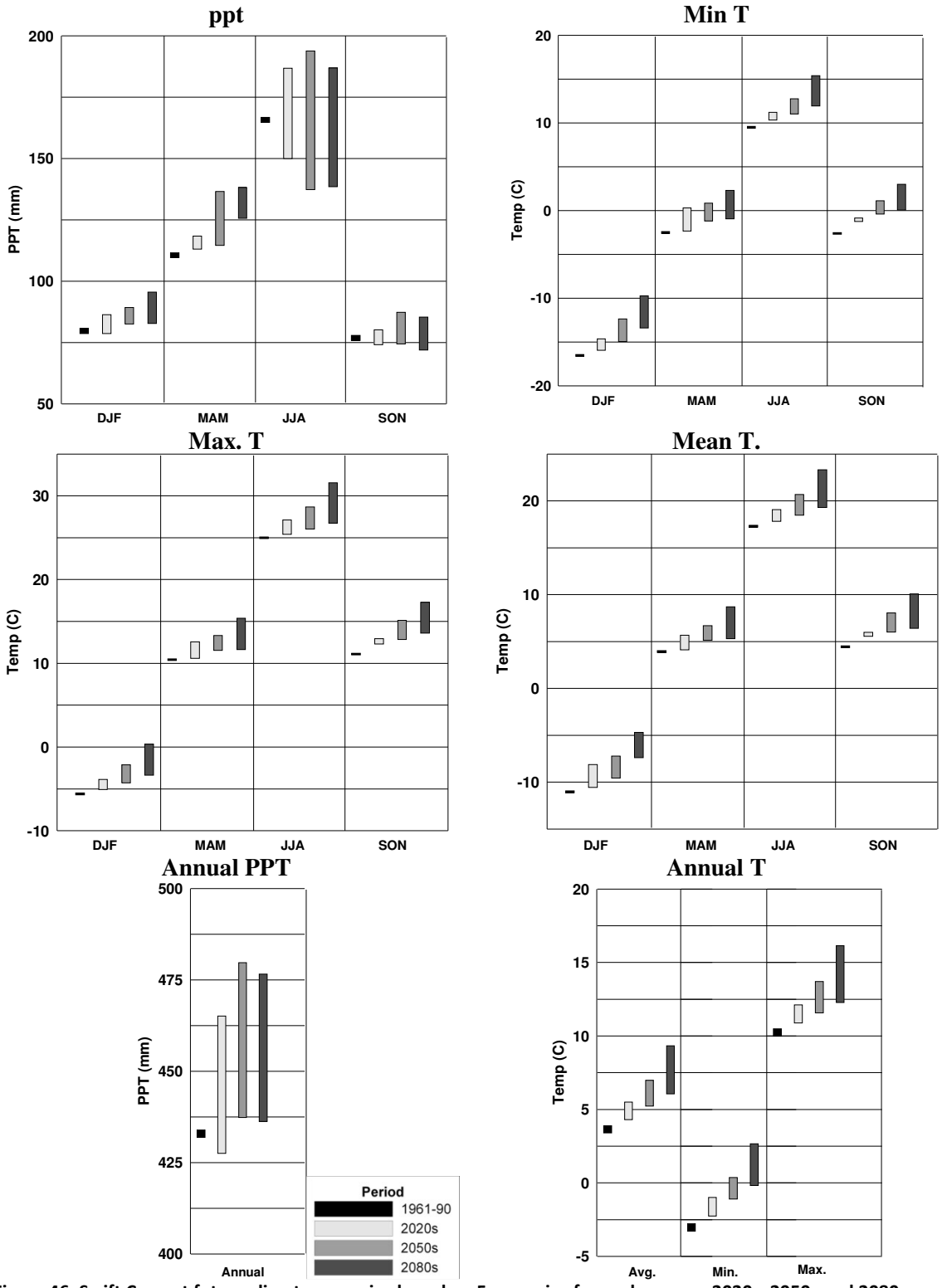

Figure 46. Swift Current future climate scenarios based on 5 scenarios for each season, 2020s, 2050s and 2080s.

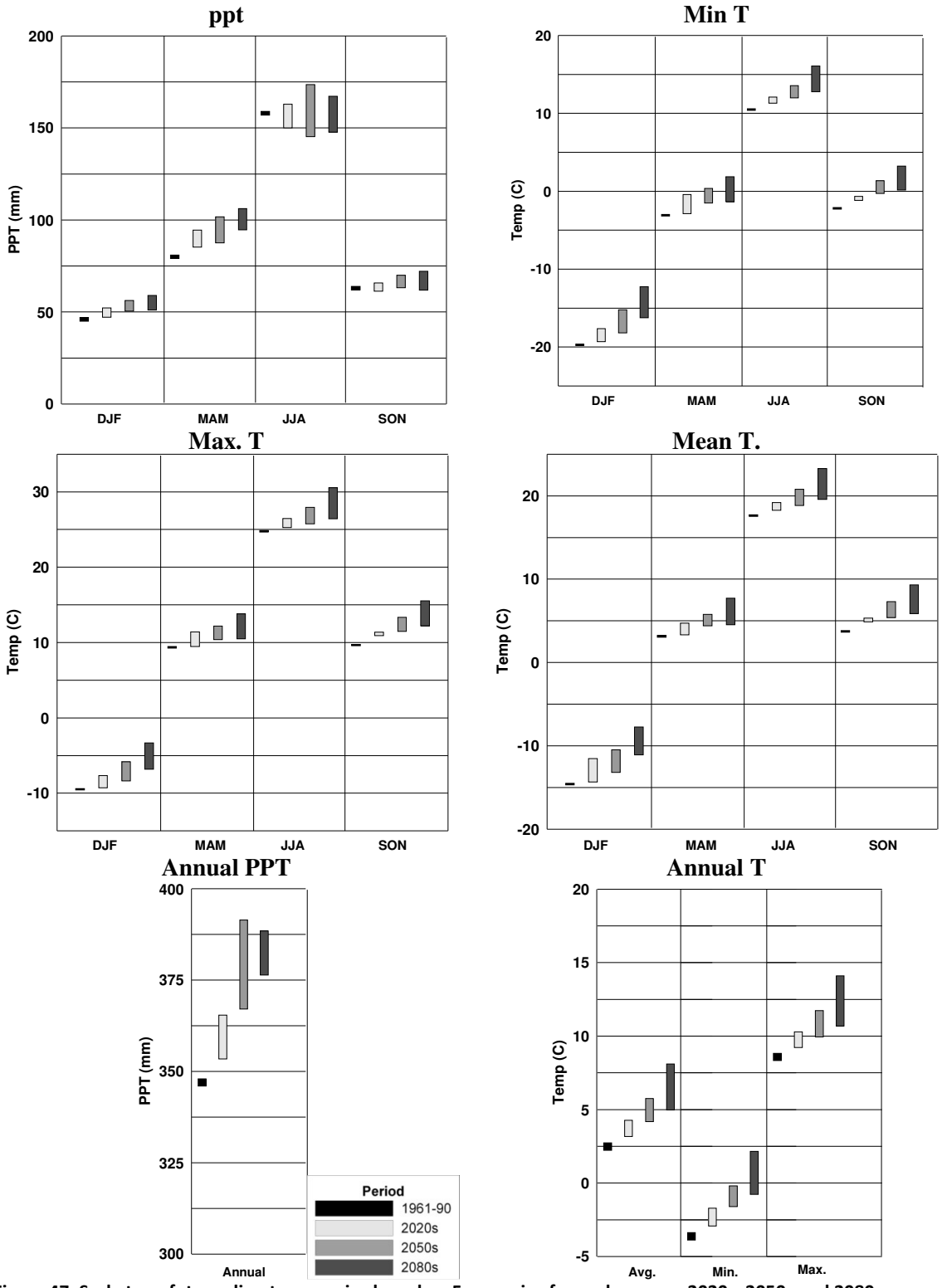

Figure 47. Saskatoon future climate scenarios based on 5 scenarios for each season, 2020s, 2050s and 2080s.

Downscaled Future Climate Scenarios: Lethbridge and Swift Current

Here we provide future downscaled scenarios for Lethbridge and Swift Current using the LARS-Weather Generator and ask does "downscaling" provide better results than climate scenarios derived from GCMs?

Future climate change scenarios were derived for the 2050s at Lethbridge and Swift Current using the five GCMs to adjust the LARS-WG parameters. Monthly-observed homogenized precipitation and minimum/maximum temperature datasets, used to calibrate the model, were obtained for the entire study area for 1961-90 from Environment Canada (Mekis and Hogg 1999; Vincent et al. 2002). Figure 48 compares the future monthly minimum/maximum and precipitation climate scenarios between those derived using GCMs and downscaled with LARS-WG at the two stations. Overall the results of the downscaled monthly station data are very similar to those derived of using GCMs. The principal difference between the two scales of climate scenarios is the monthly precipitation variability. At Lethbridge LARS-WG shows greater variability for the months of February, June, August, November and December. At Swift Current March, April and August have greater precipitation variability that those derived using GCMs. The scenarios derived using the coarse resolution GCMs are not substantially different than those derived using downscaling. Downscaling is more labour intensive, leaving the question, "Does downscaling provide better results"?

LARS-WG also generates a series of wet and dry days and the agriculturally important extreme events of frost and high temperature. At both stations there is a decreased number of days below freezing ($<0^{o}C$) and increased number of high temperature days ($>30^{o}C$) in the summer months that extends from late spring and into early fall (Figure 49). In July and August the models project that the number of days $>30^{o}C$ could double by the 2050s. Changes to the length of wet (>0mm) and dry (0mm) spell length are variable and fluctuate around the 1961-90 average monthly number of days; therefore it is difficult to draw any conclusions. On average the majority of the models favour increasing wet spell length for the winter months and increasing dry spell length for the late summer months. The increased winter wet spell length and increased precipitation may help offset the drought impacts in dryland regions that rely on spring and summer moisture to sustain agriculture and may also help fill storage ponds.

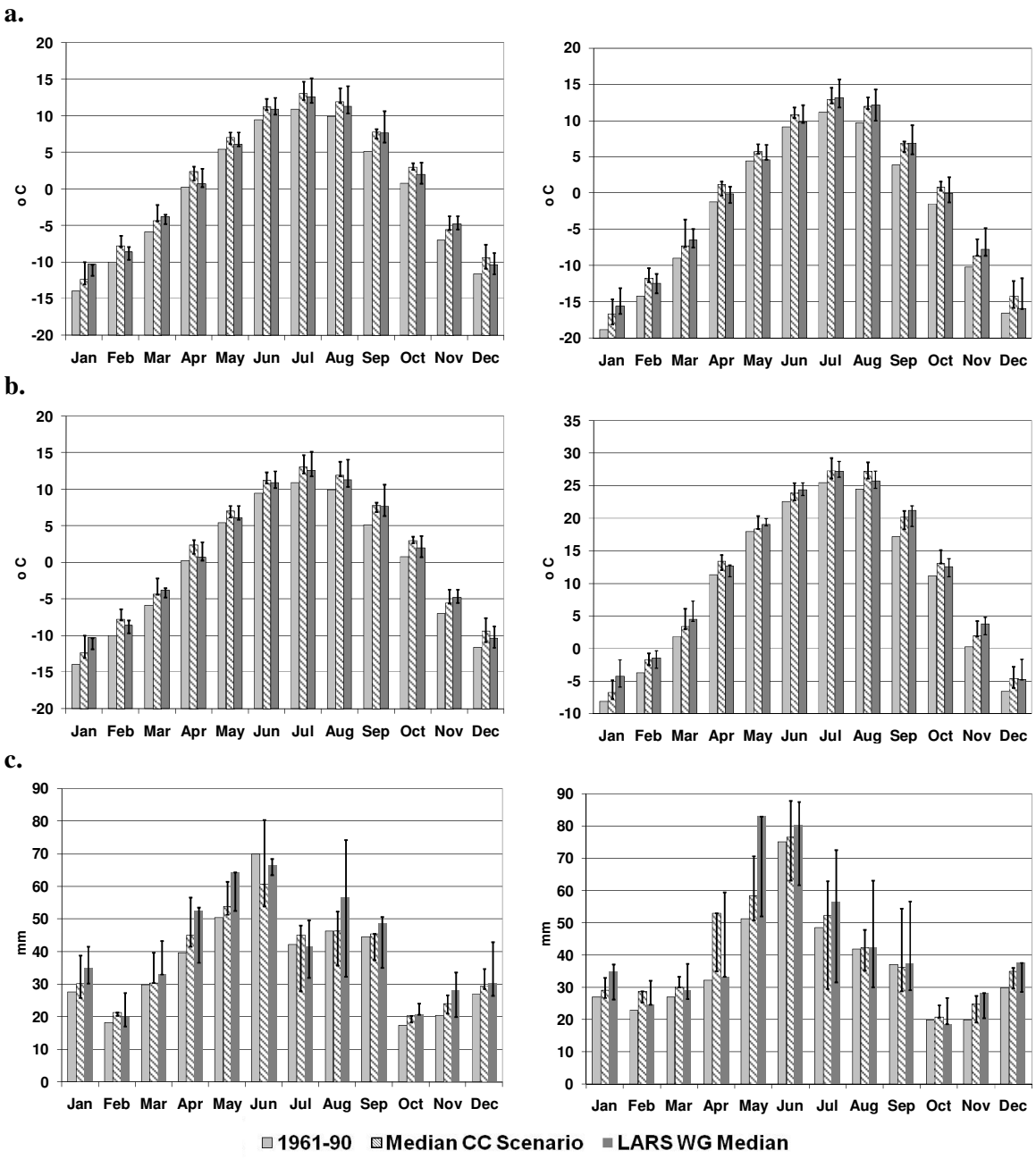

Figure 48. Lethbridge, AB (left side) and Swift Current, SK (right side) future climate scenarios: Solid grey bars represent the monthly averages for the baseline 1961-90 period and the hatched bars represent the median (CGCM3 B1(2)) scenario for the 2040-2069 period, deriving climate change scenarios from GCMs and LARS-WG. The error bars represent the full range of values from 5 GCMs. (a) minimum temperature (b) maximum temperature (c) precipitation.

a. Lethbridge

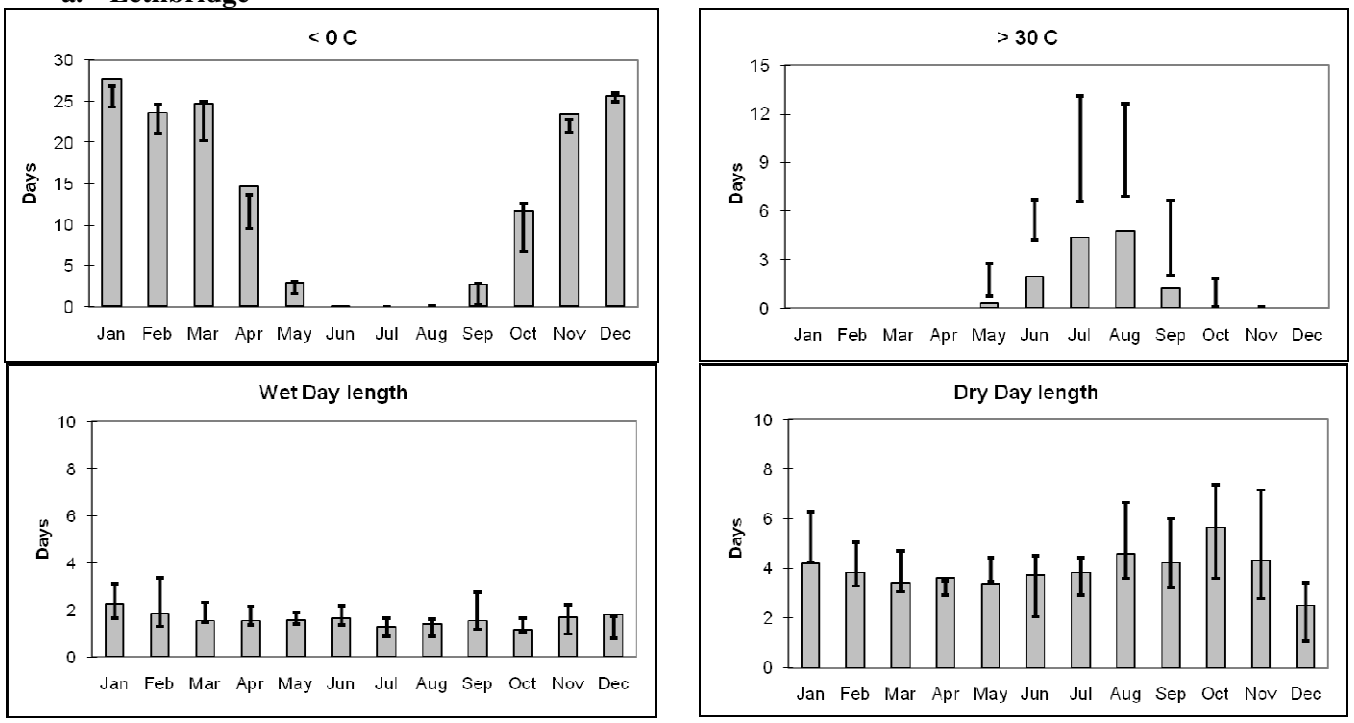

b. Swift Current

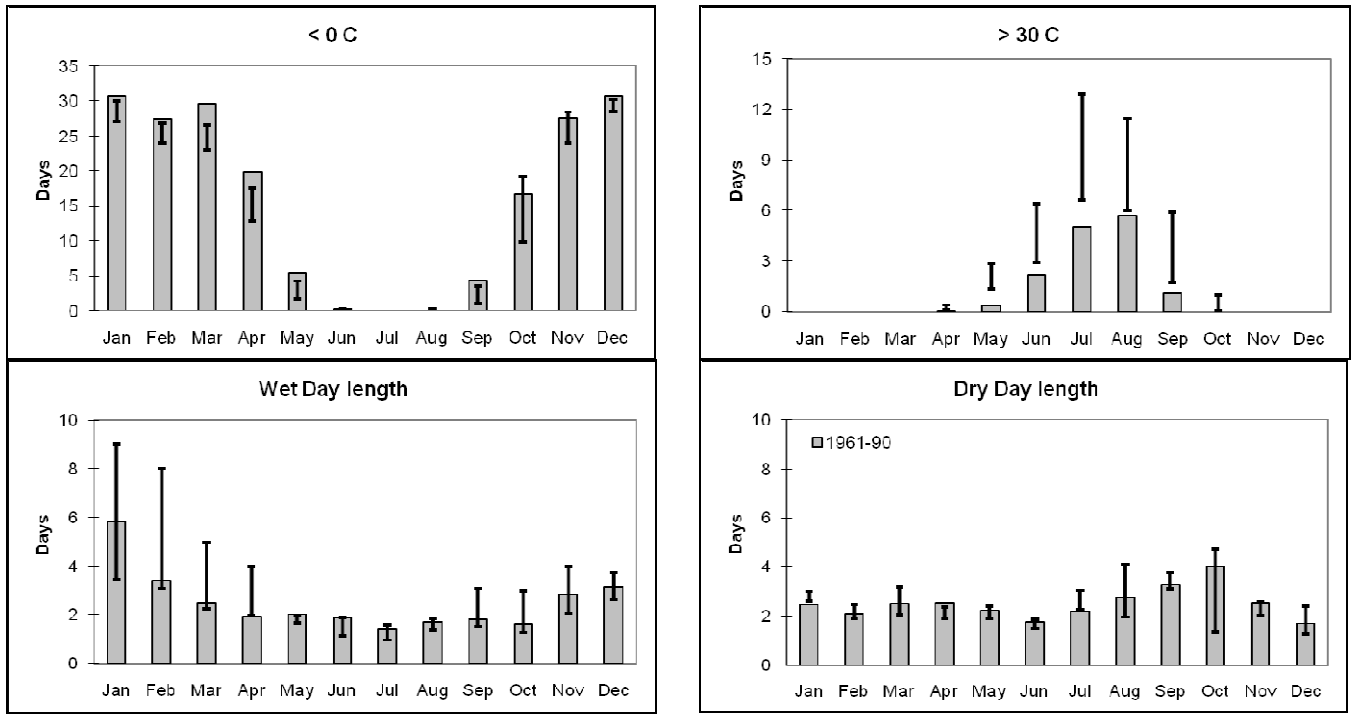

Figure 49. Results from LARS-WG at (a) Lethbridge and (b) Swift Current; grey bars represent the monthly values for the 1961-90 baseline period and std. dev. bars represent the 2050s period range for the five GCMs. Variables compared are for the length of temperature spells below 0°C and above 30°C, and monthly dry-day and wet-day lengths.

Future Climate Variability Scenarios

Because GCMs simulate atmospheric and oceanic states and processes at global scale, the most robust projections are for the largest areas and for multi-decadal means. Thus the IPCC-TGICA (2007) places highest confidence in the projections of global temperature trends expressed as the difference between a baseline of 30 years and a future 30-year time slice. The GCM projections have decreasing reliability for progressively smaller areas and time periods, and for water-related variables versus temperature. Here we are interested in a single watershed, and water-related extreme events. Thus the coarse resolution is a constraint, although the SSRB spans 5-11 GCM cells (depending upon the grid cell size of the GCM), but more problematic is the greater sensitivity of the communities to climate variability, departures from mean conditions, than climate change, shifts in the mean. Most of the climate risks identified by the communities are departures from mean conditions (e.g., droughts, floods, frost) and not a shift in mean conditions as projected by GCMs. Data on future extremes and variability have been extracted from GCMs for large regions, but once again, the reliability declines as the regions of interest decrease in size.

Despite these constraints, we derived, with caution, some scenarios on the degree of variability that might be expected under the climate change scenarios presented above. This analysis is a preliminary step to investigating long-term trends and variability of future climate scenarios using the Climate Moisture Index of P-PET, as modeled by the CGCM3.1/T67 covering the total Prairie Provinces area. This model was chosen for this analysis since it is the latest version of the Canadian Model and is run at a finer spatial resolution than the T47 model. The methods used for this variability analysis are similar to those presented by Burke et al. (2006) where they presented PDSI (Palmer Drought Severity Index) variability on a global scale. An 8-year low pass digital filter was used to smooth the annual P-PET for each grid cell to retain information that was coarser than the frequency of eight years to remove the variability associated with ENSO (El Niño-Southern Oscillation). Principle Component (PC) analysis was used capture the greatest variance of all grid cells to analyze and compare trends between the observed 1961-90 and 20th Century modeled P-PET and future SRES (A1B, A2, and B1) P-PET experiments. The B1 scenario is close to the median and the A2/A1B scenarios tend to be warmer/drier scenarios (Figure 2) relative to all the models tested.

Figure 50 shows the standardized first principle component (PC1) for the change in P-PET over the Prairie Provinces; negative/positive values represent drier/wetter conditions. There is a strong Pacific

Decadal Oscillation (PDO) pattern evident, switching from a positive phase in 1947 to negative and again positive in 1977. During negative PDO phases the sea surface temperature is warmer in the North Pacific and cooler along the west coast of North America bringing generally cooler wet conditions to the Prairies (Bonsal and Lawford 1999), the opposite pattern exists for positive PDO phases and we expect drier conditions. The negative PDO pattern dominates during 1947-1976 but positive PDO indices occur in 1957-58 and 1969-1970 and are observed in observed P-PET PC1 as negative values during these periods. During the 1977-78 "regime shift" (Mantau et al., 1997) when the PDO shifted from a negative to positive phase (Figure 51), the P-PET for the observed PC1 values also became negative (Figure 50a). This teleconnection between positive PDO phases and dry periods on the prairies has been well documented. Preliminarily results indicate that at timescales great than eight years, the 20th Century experiment reproduces a similar pattern to the observed data (see Figure 50a), placing increased confidence in the GCMs ability to produce future climate scenarios.

Future P-PET scenario based on the standardized PC1 and SRES experiments also maintains similar natural variability as the observed and modeled P-PET (Figure 50b), but a declining trend in P-PET is projected by the three experiments extending to the end of this century. This decline in moisture is associated with decreasing precipitation and increased temperatures during the spring/summer period.

a.

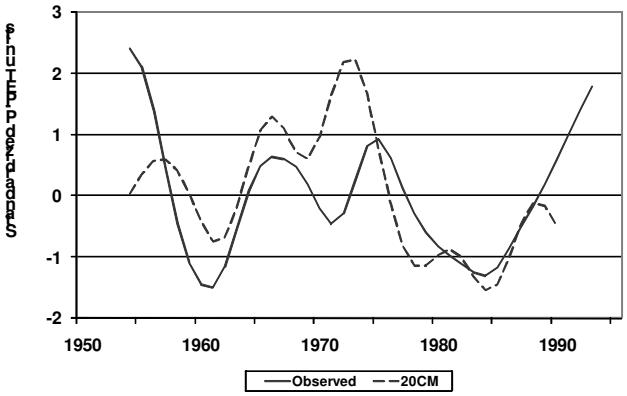

b.

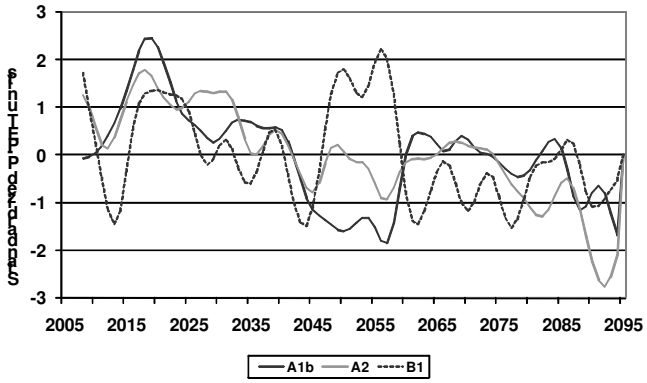

Figure 50. The first principal component on annual P-PET values for timescales greater than 8 years. a. Compares the observed and 20CM timescales trends. b. Compares the future scenarios. The first eigenvalue explains 86% of observed and over 95% of the GCM annual P-PET values for the 1961-90 period.

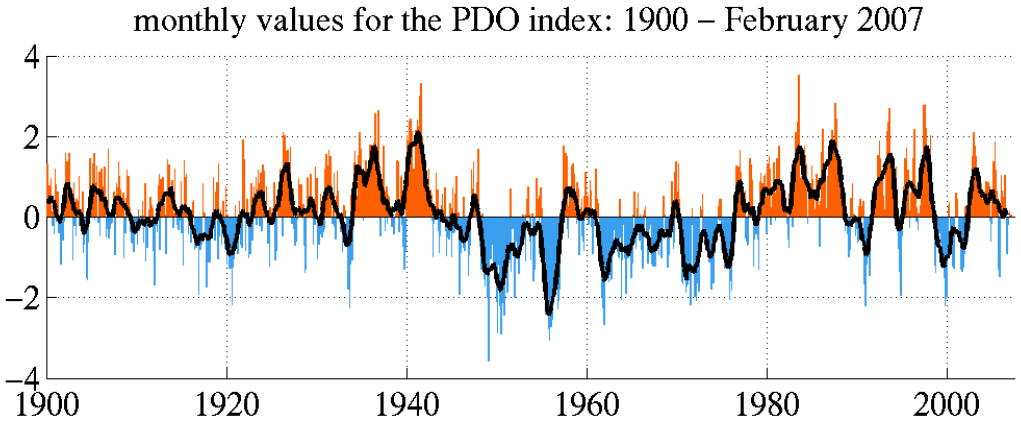

Figure 51. Monthly values for the PDO index: 1900 – February 2007. (Mantau et al., 1997) http://jisao.washington.edu/pdo/

Conclusions

Output is available from various GCMs to develop scenarios of the future climate of the SSRB, and thereby assess future vulnerabilities and climate risks. However, application of these scenarios to vulnerability assessment requires an understanding the source, derivation and limitations of the scenarios because model projections are only simulations of possibilities. Some climate risks cannot be properly evaluated because current models and methods do not provide reliable information at the relevant spatial and temporal scale for the variables identified by stakeholders. For example, one important variable that hasn't been accounted for in this study is the change in wind occurrence and speed, which can have dramatic effects on snow sublimation and evaporation of water from soil and storage ponds.

GCM scenarios suggest the SSRB will experience an increase in both temperature and precipitation by 2050. More precipitation is expected in winter, in the form of rainfall due to rising temperatures, and less in summer. Warmer temperatures imply there will be a longer growing season, but there will also be less precipitation in summer, and therefore less available soil moisture. The projected changes in temperature will influence snow accumulation in the mountains, which feeds the rivers that communities depend on for their water supply. Decreases in river flows and changes in the dominant flow season shifting from summer to spring will cause river flows to decrease in throughout the summer and fall months. Increased temperatures will result in increased evaporation from soil and storage dugouts, rivers, lakes and reservoirs. In addition, droughts are expected to become more frequent and prolonged.

These new scenarios of the future climate and surface water supplies of the SSRB represent the shift in average conditions that communities and institutions can expect. This is critical information in anticipation of the impacts of climate change, but not necessarily the most relevant information for the rural communities, or at least those studied by IACC project researchers. The major climate risks (drought, flooding, storms) and vulnerabilities identified through the community assessments are departures from mean conditions and sensitivities to this climate variability and extreme events. Therefore, this report supplements the conventional GCM scenarios of climate change with sources of hydroclimatic data at finer scales: downscaled GCM output, annual Climate Moisture Index (CMI) data from a GCM, and proxy climate (tree-ring) records that capture the natural hydroclimatic variability that underlies the trends imposed by global warming. These approaches and information are necessitated by the nature of vulnerability to climate change on the Canadian plains as revealed through the "bottom

up" approach to vulnerability assessment undertaken in the IACC project. The "top down" approach of providing conventional GCM-base scenarios of shifts in mean conditions also is useful in terms of informing stakeholders about the directions of climate change, whether or not they perceive these trends as immediate climate risks.

Recommendations

These scenarios of the mean conditions and variability of future climate and water resources have considerable implications for economic, environmental and social processes within the SSRB. The forces driving the Prairies' climate, its variability and its water resources need to be understood in greater depth for society to be better prepared for the future. Planning and implementing adaptation to climate change requires that communities and institutions understand the uncertainty associated with future climate conditions and develop practices and policies that can be implemented to offset this uncertainty based on resources and level of concern. This will require that the scientific community work closer with government and decision makers and properly inform the public.

References

Barrow, E.M. and G.Yu. (2005) "Climate Scenarios for Alberta. A Report Prepared for the Prairie Adaptation Research Collaborative (PARC) in Co-Operation with Alberta Environment." 73: University of Regina, Saskatchewan.

Barrow, E.M., Maxwell B. and P. Gachon. (2004) "Climate Variability and Change in Canada: Past, Present and Future, Climate Change Impacts Scenarios Project, National Report, Environment Canada, Meteorological Service of Canada, Adaptation Impacts Research Group, Atmospheric and Climate Sciences Directorate Publication." pp. 114 Canada.

Beriault, A. and D.J. Sauchyn. (2006) “Tree-ring reconstructions of streamflow in the Churchill River basin, northern Saskatchewan.” Canadian Water Resources Journal, 31(4): pp. 249-262.

Bonsal, B. and R. Lawford. (1999) "Teleconnections between El-Nino and La-Nina Events and Summer Extended Dry Spells on the Canadian Prairies." International Journal of Climatology, no. 19, pp. Bonsal, B.R., T.D. Prowse, and A. Pietroniro. (2003) "An Assessment of GCM-Simulated Climate for the Western Cordillera of Canada (1961-90)." Hydrological Processes, 18: pp. 3703-16.

Bonsal, B. and E. Wheaton. (2005) "Atmospheric Circulation Comparisons between the 2001 and 2002 and the 1961 and 1988 Canadian Prairie Droughts." Atmosphere-Ocean 43(2), pp. 163-72.

Bonsal, B. and T.D. Prowse. (2006) "Regional Assessment of GCM-Simulated Current Climate over Northern Canada." Arctic, 59(2), pp. 115-28.

Bonsal B. and M. Regier (2007) “Historical comparison of the 2001/2002 drought in the Canadian Prairies.” Climate Research 33: pp.229-242

Burke E.J., Brown S.J., Christidis N. 2006. Modeling the recent evolution of global drought and projections for the Twenty-First Century with the Hadley Centre Climate Model. *J. of Hydrometeorology* **7**: pp.1113-1125.

Christensen, J.H., B. Hewitson, A. Busuioc, A. Chen, X. Gao, I. Held, R. Jones, R.K. Kolli, W.-T. Kwon, R. Laprise, V. Magaña Rueda, L. Mearns, C.G. Menéndez, J. Räisänen, A. Rinke, A. Sarr and P. Whetton. (2007) “Regional Climate Projections. In: Climate Change 2007: The Physical Science Basis. Contribution of Working Group I to the Fourth Assessment Report of the Intergovernmental Panel on Climate Change” [Solomon, S., D. Qin, M. Manning, Z. Chen, M. Marquis, K.B. Averyt, M. Tignor and H.L. Miller (eds.)]. Cambridge University Press, Cambridge, United Kingdom and New York, NY, USA.

Girardin, M.P., and D. Sauchyn. 2008. Three centuries of annual area burned variability in northwestern North America inferred from tree rings. *The Holocene*, 18: pp.205-214

Hay, L. E. and M. P. Clark. (2003) "Use of Statistically and Dynamically Downscaled Atmospheric Model Output for Hydrologic Simulations in Three Mountainous Basins in the Western United States." Journal of Hydrology. 282(1-4): pp. 56-75.

Hogg, E.H. (1997) "Temporal Scaling of Moisture and the Forest-Grassland Boundary in Western Canada." Agricultural Forest Meteorolology. 84: pp. 115-22.

Hulme, M., E.M. Barrow, N. Arnell, P.A. Harrison, T.E. Downing, and T.C. Johns. (1999) "Relative Impacts of Human-Induced Climate Change and Natural Climate Variability." Nature, 397: pp. 688-91.

IPCC ."Climate Change 2007: The Physical Science Basis. Contribution of Working Group I to the Fourth Assessment Report of the Intergovernmental Panel on Climate Change." edited by S. Solomon, D. Qin, M. Manning, Z. Chen, M. Marquis, K.B. Averyt, M. Tignor and H.L. Miller, 996. Cambridge, United Kingdom and New York, NY, USA: Cambridge University Press, 2007.

IPCC. "Climate Change 2001: The Scientific Basis." In Contribution of Working Group I to the Third Assessment Report of Intergovernmental Panel on Climate Change, edited by J.T. Houghton, Y. Ding, D.J. Griggs, M. Noguer, P.J. van der Linde, X. Dai, K. Maskell and C.A. Johnson, 881. Cambridge, U.K. and New York, N.Y., U.S.A.: Cambridge University Press, 2001a.

IPCC. "Technical Summary. In: Climate Change 2001." In The Scientific Basis Contribution of Working Group I to the Third Assessment Report of the Intergovernmental Panel on Climate Change, edited by J.T. Houghton, Y. Ding, D. J. Griggs, M. Noguer, P. J. van der Linden, X. Dai, K. Maskell and C.A. Johnson, 62: Cambridge University Press, Cambridge and New York, 2001b.

IPCC-TGCIA. (2007) "General Guidelines on the Use of Scenario Data for Climate Impact and Adaptation Assessment. Version 2.Prepared by T.R. Carter on Behalf of the Intergovernmental Panel on Climate Change, Task Group on Data and Scenario Support for Impact and Climate Assessment." pp. 66.

Jensen, M.E., R.D. Burman, and R.G. Allen. (1990) “Evapotranspiration and Irrigation Water Requirements”. American Society of Civil Engineers.

Keyantash J. and J. Dracup. (2002) “The Quantification of Drought: An Evaluation of Drought Indices.” American Meteorological Society (BAMS) August: 1167-1180

Lin, H., G. Brunet, and J. Derome (2008) “Seasonal Forecasts of Canadian Winter Precipitation by Postprocessing GCM Integrations.” Monthly Weather Review, 136(3): pp. 769-783.

Magzul, L. (2007) “Report on the Blood Tribe (Kainai Nation): community vulnerabilities”, pp.32.

Mantua, Nathan J. and Steven R. Hare. (2002) "The Pacific Decadal Oscillation" Journal of Oceanography, 58(1): pp. 35-44.

Matlock, B. (2007) “Report on the Community Vulnerability of Cabri and Stewart Valley”, pp. 34.

McKenney, D.W., J.H. Pedlar, P. Papadopol, and M.F. Hutchinson. (2006) "The Development of 1901-2000 Historical Monthly Climate Models for Canada and the United States." Agricultural and Forest Meteorology, 138: pp. 69-81.

Mekis, É. and W.D. Hogg. (1999) "Rehabilitation and Analysis of Canadian Daily Precipitation Time Series." Atmosphere-Ocean, 37(1): pp. 53-85.

Meinert, A., B. Bonsal and E. Wheaton. (2008) “Characterizing the Climatological Nature of the 1999-2005 Drought in the Canadian Prairies: Data Sources and Issues”. DRI Workshop, Calgary, AB, January 17-19, 2008, presentation.

Nakicenovic, N., J. Alcamo, G. Davis, B. de Vries, J. Fenhann, S. Gaffin, K. Gregory, A. Grübler, T.Y. Jung, T. Kram, E.L. La Rovere, L. Michaelis, S. Mori, T. Morita, W. Pepper, H. Pitcher, L. Price, K.Riahi, A. Roehrl, H.H. Rogner, A. Sankovski, M. Schlesinger, P.Shukla, S. Smith, R. Swart, S. van Rooijen, N. Victor, and Z. Dadi. " IPCC Special Report on Emissions Scenarios." 599. Cambridge University Press, Cambridge, United Kingdom and New York, NY, USA, 2000.

Parry, M.L. and T.R. Carter. (1998) “Climate Impact and Adaptation Assessment: A Guide to the IPCC Approach”. London: Earthscan.

Pittman, J. (2008) “Report on the Community Vulnerability of Outlook”, pp. 35.

Prado, S. (2008) “Report on the Community Vulnerability of Taber”, pp. 42.

Randall, D.A., R.A. Wood, S. Bony, R. Colman, T. Fichefet, J. Fyfe, V. Kattsov, A. Pitman, J. Shukla, J. Srinivasan, R.J. Stouffer, A. Sumi, and K.E. Taylor. (2007) "Climate Models and Their Evaluation, in Climate Change 2007: The Physical Science Basis." In Contribution of Working Group I to the Fourth Assessment Report of the Intergovernmental Panel on Climate Change, edited by S. Solomon, D. Qin, M. Manning, Z. Chen, M. Marquis, K.B. Averyt, M. Tignor and H.L. Miller. Cambridge, UK and New York, NY, USA: Cambridge University Press.

Sauchyn, D.J., Stroich, J. and A. Beriault. (2003) “A paleoclimatic context for the drought of 1999- 2001 in the northern Great Plains.” The Geographical Journal, 169(2): 158-167.

Schoney, R.A., W.J. Brown, and S.N. Kulshreshtha (1990). “Dyanimcs of Simulated Effects of Irrigation over Dryland Farming in Saskatchewan.” Journal of the American Water Resources Association, 26(3): pp. 509-517.

Semenov, M. A. and E. Barrow (1997). "Use of a Stochastic Weather Generator in the Development of Climate Change Scenarios." Climatic Change, 35: pp. 397-414.

Semenov, M.A. and E.M. Barrow. (2002) "Lars-WG a Stochastic Weather Generator for Use in Climate Impact Studies. Version 3.0. User Manual.

Smith, J.B. and M. Hulme. (1998) "Climate Change Scenarios." In Hanbook on Methods of Climate Change Impacts Assessment and Adaptation Strategies.Version 2.0, edited by J. Feenstra, I. Burton, J.B. Smith and R.S.J. Tol, 3-1 to 3-40. Vrije Universiteit, Amsterdam: United Nations Environment Programme and Institute for Environmental Studies.

Thornthwaite CW (1948) An approach toward a rational classification of climate. Geogr. Rev Jan. :55-94

Venugopal, V., G.E. Foufoula, and V. Sapozhinikov. (1999) "A Space-Time Downscaling Model for Rainfall." Journal of Geophysical Research: Atmospheres, 104(16): pp. 19-705.

Vincent, L.A., X. Zhang, B.R. Bonsal, and W.D. Hogg. (2002) "Homogenization of Daily Temperatures over Canada." Journal of Climate, 15: pp.1322-34.

Wilby, R. H. L. (1994). "Stochastic weather type simulation for regional climate change impact assessment." Water Resour. Res, 30: pp. 3395-3403.

Wilby, R. L. (1997). "Non-stationarity in daily precipitation series: Implications for GCM down-scaling using atmospheric circulation indices." International Journal of Climatology, 17: pp. 439-454.

Wilby, R.L., C.W. Dawson, and E.M. Barrow. (2002) "SDSM - a Decision Support Tool for the Assessment of Regional Climate Change Impacts." Environmental Modelling and Software, 17: pp. 147-59.

Willmott, C.J. and J.J. Feddema. (1992) "A More Rational Climatic Moisture Index." Professional Geographer, 44: pp. 84-87.

Wittrock, V., E. Wheaton and S. Kulshreshtha. (2005) “Climate Change, Ecosystem and Water Resources: Modeling and Impact Scenarios for the South Saskatchewan River Basin, Canada: A Working Paper”. University of Regina, June, IACC Project Working Paper No. 25: pp. 61.

Young, G. and J. Wandel. (2007) “Hanna Community Vulnerability Assessment”, pp.22.